Delays in relativistic and non-relativistic scattering studied by means of quantum measurement theory

Xabier Gutiérrez

Supervisors:

Prof. Dmitri Sokolovski
Prof. Marisa Pons

Departamento de Química Física
UPV/EHU
Noviembre 2023

Memoria presentada para optar al Grado de Doctor Internacional

eman ta zabal zazu

Universidad del País Vasco
Euskal Herriko Unibertsitatea

Delays in relativistic and non-relativistic scattering studied by means of quantum measurement theory

Author:
Xabier Gutiérrez

Supervisors:
Prof. D. Sokolovski
Prof. M. Pons

Departamento de Química-Física
Facultad de Ciencia y Tecnología
Universidad del País Vasco/Euskal Herriko Unibertsitatea
(UPV/EHU)

Bilbao, 2023

Acknowledgements

First of all, I would like to thank my supervisors, Prof. Dmitri Sokolovski and Prof. Marisa Pons for guiding me through this project, introducing me to all the topics and ideas discussed in the Thesis, and for expanding my knowledge and curiosity. I am also grateful to Sofía, my office mate during most of the Thesis, and to Antón for all the discussions and needed coffees we have had since he arrived.

I would also like to thank Prof. Alexandre Matzkin, for hosting me in my short time in Cergy, and to all the wonderful people I met there for the time we spent wandering through Paris or around the piano.

Me gustaría agradecer también a mi familia por apoyarme, en estos cuatro años de tesis, y en todos los anteriores, por el tiempo que he estado lejos y por el tiempo que he estado en casa.

A Denisse, te agradezco todos estos años de paciencia, de calma, de aprendizaje y de tiempo.

This thesis has been supported (2ps) by the Ministerio de Ciencia y Tecnología, through the Predoctoral Grant PRE2019-090105 associated with the project PGC2018-101355-B-I00.

Contents

List of publications

I) **The results of this Thesis are based on the following articles**

Published Articles

1. M. Alkhateeb, X. Gutiérrez de la Cal, M. Pons, D. Sokolovski & A. Matzkin
   Relativistic time-dependent quantum dynamics across supercritical barriers for Klein-Gordon and Dirac particles
   Phys. Rev. A **103**, 042203 (2021).

2. X. Gutiérrez de la Cal, M. Alkhateeb, M. Pons, A. Matzkin & D. Sokolovski
   Klein paradox for bosons, wave packets and negative tunnelling times
   Scientific Reports **10**, 19225 (2020).

3. X. Gutiérrez de la Cal, M. Pons & D. Sokolovski
   Speed-up and slow-down of a quantum particle
   Scientific Reports **12**, 3842 (2022).

Pre-Print Articles

4. X. Gutiérrez de la Cal, M. Pons & D. Sokolovski
   Quantum measurements and delays in scattering by zero-range potentials
   arXiv:2309.06289.

II) **Other articles produced during the Thesis period**

Published Articles not included in this Thesis

5. Dmitri Sokolovski, Xabier Gutiérrez de la Cal & Marisa Pons

   Collective tunnelling of strongly interacting cold atoms in a double well potential

   Annalen der Physik, **532**(3), 1900462. (2020).

6. Xabier Gutiérrez & Alex Matzkin

   Beyond the light-cone propagation of relativistic wavefunctions: numerical results

   Dynamics, **3**(1), 60-70 (2023).

Resumen

Un problema de dipersión clásico puede caracterizarse por el tiempo de recorrido. Para una partícula incidente en un potencial, este tiempo se define como el que tarda la partícula en cruzar el potencial. La definición del tiempo de recorrido clásico se basa en la existencia de una trayectoria dentro del potencial. Hay varias formas de medir experimentalmente este tiempo. Por ejemplo, podemos medir la distancia, o demora espacial, entre el centro de masas (CM) de la partícula transmitida con el de una partícula libre, y asociar esta demora espacial con el tiempo de recorrido.

Alternativamente, se puede usar un reloj para medir la duración. Físicamente, consideramos como un reloj un puntero acoplado a la partícula, en el que algún parámetro del puntero cambia mientras la partícula se encuentra dentro del potencial. Por ejemplo, un espín que rota en la presencia de un campo magnético, de forma que, midiendo la rotación del espín podemos calcular la duración del recorrido. Este es el método de Larmor. En una transición clásicamente permitida, ambas definiciones del tiempo de recorrido coinciden.

En el caso del efecto túnel no está claro cómo definir tal trayectoria, y por tanto cómo definir el tiempo de recorrido. Cuando extendemos estas mediciones a un caso cuántico los resultados obtenidos difieren. El debate alrededor del tiempo de túnel continúa hoy en día, alentado por avances recientes en técnicas de attosegundo, que permiten medirlo experimentalmente.

Cualquier medición en mecánica cuántica está normalmente relacionada con un operador autoadjunto. El problema es que, como Pauli señaló en 1933, no hay un

operador autoadjunto para el tiempo. Por el contrario, el tiempo en mecánica cuántica es un parámetro. En los dos experimentos mencionados, la duración no se mide directamente. Lo que se mide realmente es la demora espacial en el primer caso, o la rotación del espín en el segundo. Los tiempos de recorrido son diferentes y solo coinciden en el límite clásico.

Ha habido numerosos intentos de definir un tiempo de recorrido en mecánica cuántica. Una de las primeras propuestas se debe a Eisenbud, Wigner y Smith, que estudiaron la evolución de un paquete de ondas (PO) transmitido. En el caso de dispersión unidimensional, como la que consideraremos en esta Tesis, este enfoque consiste en medir la distancia entre los CMs del PO transmitido y un PO libre. Cuando se produce una dispersión de un PO ancho, éste adquiere una fase (Φ), relacionada con la demora espacial del PO a través de su derivada respecto de la energía ($\partial_E \Phi$). Este es el tiempo de fase, también llamado tiempo de Eisenbud-Wigner-Smith (EWS), y se aplica a procesos de dispersión que hayan sido completados.

En los años 30 se observó por primera vez que, en el caso del efecto túnel, *no hay una demora apreciable en la transmisión del paquete a través de la barrera*. Si se aplica el método de EWS al efecto túnel, parece que la transmisión es instantánea. Para una dispersión unidimensional en una barrera de anchura d y potencial máximo $V_0 > E$, donde E es la energía de la partícula incidente, el CM del PO transmitido está por delante del CM del libre, aproximadamente, una distancia d. Aparentemente, la velocidad del PO en el potencial es superluminal, ya que parece exceder la velocidad de la luz. Esto estaría en contradicción con la relatividad especial de Einstein.

Esta transmisión superluminal no es el resultado de usar una ecuación no relativista, como la ecuación de Schrödinger, ya que persiste si consideramos partículas relativistas. Además, este resultado ha sido obtenido experimentalmente. La explicación reside entonces en otro lugar.

Un aspecto fundamental de la teoría cuántica estándar es que no hay trayectorias bien definidas asociadas con el efecto túnel, como sí las hay en una dispersión

clásicamente permitida. En el caso del efecto túnel, la demora espacial de la partícula transmitida es el resultado de que la interferencia entre trayectorias alternativas se mantiene intacta. De esta manera, el Principio de Incertidumbre nos prohibe saber qué camino ha tomado la partícula, de forma que la demora espacial no puede asociarse a un "tiempo en la barrera". En general, se considera que el PO se remodela en la barrera, aunque la naturaleza exacta de esta remodelación está todavía bajo debate. Nuestra intención en esta Tesis es estudiar cómo interfieren las amplitudes de trayectorias alternativas, y cómo por ello surge, en el caso del efecto túnel, una demora superluminal.

Esta Tesis está dividida en dos partes principales. La primera considera dispersión no relativista, mientras que la segunda analiza la dispersión relativista.

En la primera parte de esta Tesis nos centramos principalmente en el enfoque de EWS, y analizamos el mecanismo de remodelación del PO a través del efecto túnel. Veremos que el PO no es una copia avanzada del incidente, sino que es el resultado de la interferencia de copias, cada una con su demora espacial. El tiempo de recorrido clásico, asociado a una única trayectoria, puede obtenerse para transmisiones clásicamente permitidas.

El problema del tiempo en una transición cuántica está íntimamente relacionado con las mediciones cuánticas. Las distintas definiciones del tiempo del efecto túnel, o de la duración de una transición cuántica, son realmente descripciones de *cómo* efectuar la medición. Es la diferencia entre experimentos la que conduce a distintas medidas.

En esta Tesis veremos cómo la teoría de medidas cuánticas nos ayuda a interpretar los resultados obtenidos para el tiempo del efecto túnel. Los tiempos que estudiaremos en esta Tesis pueden expresarse como una convolución entre amplitudes complejas y una función "aparato" acoplada a la partícula. Esta convolución toma diferentes formas para los métodos de EWS o del reloj de Larmor, los dos métodos que consideraremos en la primera parte de la Tesis. En general,

en mecánica cuántica una medición afecta la interferencia. En los diferentes escenarios que estudiaremos en esta Tesis veremos que la precisión con la que midamos un tiempo o una demora espacial cambia el resultado de la medida.

El efecto túnel cuántico es un ejemplo de un problema de dispersión para el cual un enfoque puramente cuántico es necesario, ya que una extensión directa del análisis clásico lleva a resultados contradictorios. Además de éste, hay otras situaciones de dispersión para los que el análisis clásico falla, como es la dispersión a bajas energías en barreras bajas o pozos poco profundos. Aplicaremos este análisis cuántico a un potencial de Eckart para estudiar el tiempo superluminal y el efecto que las singularidades, o polos, de la amplitud de transmisión tienen sobre las demoras espaciales de los POs transmitidos. Estos polos están asociados con estados ligados o resonantes, y determinan las interferencias entre las demoras alternativos que el PO transmitido puede adquirir en el potencial.

A pesar de que la mayoría de la Tesis se centra en las demoras de EWS, también estudiaremos la diferencia entre éstos y el tiempo de túnel obtenido con un reloj de Larmor. Este último usa la rotación del espín de la partícula en presencia de un campo magnético para medir el tiempo que la partícula pasa en una región del espacio. Consideraremos el caso de un potencial de rango cero. Éste es un caso ultra cuántico, para el cual la diferencia entre ambas medidas es máxima.

En el caso de dispersión relativista, el efecto superluminal no solo no desaparece, sino que encontramos más resultados anómalos. En la segunda parte de la Tesis consideraremos un tratamiento relativista y de *single-particle* de la dispersión. Con este enfoque, estudiaremos la dispersión de bosones y fermiones a través de barreras supercríticas, esto es, barreras suficientemente altas como para unir la brecha entre los continuos negativo y positivo de energía. Los POs pueden propagarse libremente por estas barreras, para las que no hay supresión de la transmisión. Esto es conocido como la paradoja de Klein.

Nuestro interés en este tipo de barreras reside de nuevo en los tiempos de recorrido aparentemente paradójicos que pueden obtenerse siguiendo el CM de los POs. Para ello consideramos la transmisión de un PO bosónico de energía E,

que satisface la ecuación de Klein-Gordon, a través de una barrera supercrítica de anchura d y altura máxima $V_0 = E/2$. En esta situación, podemos encontrar soluciones en las que la parte transmitida del PO está avanzado $2d$ respecto a un PO libre, *dos veces* la anchura de la barrera. Si utilizasemos este resultado para calcular una duración en la barrera, de la misma manera que podemos hacer en la dispersión clásica, el resultado es un tiempo de recorrido negativo. Esta conclusión parece contradecir la causalidad de Einstein, a pesar de que, como mostraremos, la obtención de este resultado no requiere de velocidades superluminales.

También estudiaremos cómo la dispersión supercrítica difiere para bosones de Klein-Gordon y fermiones de Dirac, y discutiremos la convergencia y causalidad de cada una de sus respectivas soluciones. Como veremos, los bosones y fermiones se comportan de forma diferente en el régimen supercrítico. Analizaremos estas diferencias y las relacionaremos con la paradoja de Klein.

Esta Tesis está organizada como sigue. La **Parte I** está formada por tres capítulos. En el **Capítulo 1** estudiaremos la transmisión de PO Gaussianos no relativistas en términos de la interferencia entre sus copias desplazadas. Consideraremos los casos de las transmisiones clásicamente permitidas y del efecto túnel. Es en este último caso en el que aparecen las demoras superluminales, cuyo origen discutiremos. En el **Capítulo 2**, aplicaremos el método presentado en el anterior capítulo a un potencial de Eckart. También calcularemos la distribución de las demoras en términos de los polos de la amplitud de transmisión, tanto para barreras como para pozos de Eckart. En el **Capítulo 3** compararemos los resultados de EWS y del reloj de Larmor en el caso de un potencial de rango cero. Ambos enfoques pueden ser entendidos como mediciones cuánticas, aunque de parámetros distintos.

La **Parte II** de esta Tesis analiza la dispersión relativista, y está formada por un único capítulo. En el **Capítulo 4** usaremos una serie de múltiples reflexiones para estudiar la transmisión y reflexión de POs bosónicos y fermiónicos a través de barreras supercríticas. Las soluciones son diferentes para cada tipo de partícula.

Analizaremos cada solución en relación a la creación y aniquilación de pares, y a la paradoja de Klein.

Finalmente, presentaremos las **Conclusiones** de la Tesis, también divididas en dos partes: relativista y no relativista.

Introduction

A classical scattering problem can be characterised by a traversal time. For a particle incident on a potential region, this is the time taken for the particle to pass through the potential. The definition of a classical traversal time relies on the existence of a trajectory inside the potential. There are several ways to experimentally measure the traversal time. We can measure the spatial delay the particle acquires after the transmission, compare its centre of mass (COM) with that of a freely propagating one, and relate this delay to the traversal time.

Alternatively, one can think of using a clock to measure this duration. We can consider the clock as a pointer coupled to the particle, where some parameter of the pointer changes when the particle is inside the potential. For example, a spin that rotates in the presence of a magnetic field, so, measuring the spin precession, it would give us the duration of the passage. This is the Larmor clock approach. In a classically allowed scenario, both definitions of the traversal time coincide.

In the case of tunnelling, it is not clear how to define such a trajectory and how to define the traversal time. Extending these measurements to a quantum case leads to different results. The debate around the tunneling time continues today, encouraged by recent advances in atto-second techniques, that allow it to be measured experimentally [1–3].

In quantum mechanics any measurement is usually related to a self-adjoint operator. The problem is that, as Pauli pointed out in 1933 [4], there is no self-adjoint operator for time. Instead, time is a parameter in quantum mechanics. In the two experiments mentioned above, the duration is not measured directly. What

is actually measured is the spatial delay or the spin precession. Each experiment leads to different results for the traversal time, which only coincide in the classical limit. As stated in [5], *a unique, classical question vercorresponds to different quantum versions*.

Numerous attempts have been made to define a traversal time in quantum mechanics (for a general review, see [6] and for a more recent one, see [7]). An early attempt was made by Eisenbud [8] and Wigner [9], and later generalised by Smith [10], who studied the evolution of the transmitted wave packet (WP). In the one-dimensional scattering scenarios considered in this Thesis, this approach corresponds to measuring the spatial delay between the COMs of the tunnelled WP and a freely propagating one. When a broad WP is scattered by a potential, it acquires a phase shift (Φ), related to the delay of the transmitted WP by its energy derivative ($\partial_E \Phi$). This is the phase time, also called Eisenbud-Wigner-Smith (EWS) time, and applies to completed scattering processes.

It was observed already in the 1930's that *there is no appreciable delay in the transmission of the packet through the barrier* [11]. If one applies the EWS method to tunnelling, it appears that the tunnelling is instantaneous. For a one-dimensional scattering on a barrier of width d and height $V_0 > E$, where E is the energy of the incident particle, the tunnelled WP is advanced by, roughly, a distance d relative to a freely propagating one. The velocity of the WP in the potential is apparently superluminal, as it seems to exceed the speed of light. This suggests a contradiction with Einstein's special relativity.

This superluminal transmission is not just an artefact of using a non-relativistic equation, such as the Schrödinger equation, but the effect persists using a fully relativistic treatment [12–14]. The spatial delay that leads to this result can be obtained experimentally [2, 3, 15]. The explanation to this seemingly paradoxical result lies elsewhere.

A key aspect of the standard quantum theory is that there are no well-defined trajectories associated with tunnelling, as there are in a classically allowed scattering process. There have been attempts to include trajectories into the quantum

theory, most notably in the case of the de Broglie-Bohm theory, which has been applied to the case of tunnelling times [16]. Alternatively, one can also use Feynman's path formulation [17], where trajectories of alternative paths interfere to produce the transition amplitude [18, 19].

In order to avoid perturbing the transition, it has been proposed to use weak measurements to reconstruct the trajectory of a quantum particle, and calculate its traversal time [15, 20, 21], although the true meaning of these weak measurements is debated [22, 23]. The "weakness" of the measurement does not destroy the interference, as a usual (strong) measurement does. However, as stated by Bohm [24], any measurement in which the interference is not destroyed leads to inconsistent results.

In the case of tunnelling, the spatial delay experienced by the tunnelled particle is a result of the interference between alternatives which remain intact. The Uncertainty Principle forbids us from knowing which path the particle has taken [25], so the delay cannot be related to a "time spent in the barrier". It is generally accepted that the tunnelled particle is reshaped in the barrier [26–28], although the exact nature of this reshaping mechanism is under debate. Our aim in this Thesis is to study how the amplitudes of the alternative trajectories interfere, and, in the case of tunnelling, lead to the apparent superluminal transmission.

This Thesis is divided into two main parts. The first one considers non-relativistic scattering, while the second one focuses on relativistic scattering.

In the first part of the Thesis, we concentrate mainly on EWS delays, and analyse the reshaping mechanism of tunnelled WPs, that explains the apparent superluminal phase time. The tunnelled WP is not an advanced copy of the incident one, but the result of the interference of its delayed copies. We study the interference between the alternative spatial delays that the non-relativistic WP can acquire as it passes through the potential region. The classical traversal time, associated with a single trajectory, can be obtained as a semiclassical limit, only in the classically allowed case.

The problem of timing a quantum transition is closely related to the problem of quantum measurements. The different existing definitions of the tunnelling time, or of the duration of a quantum transition, are actually descriptions of *how* to perform the measurement. It is the difference between experiments that leads to different measured quantities. As stated in [6], *the fact that the particle is transmitted, not reflected, amounts to a measurement.*

We will see how quantum measurement theory helps us to interpret the results obtained for the tunnelling time. The measured times studied in this Thesis are naturally expressed as a convolution between complex amplitudes and an "apparatus" function coupled to the particle. This convolution takes different forms for the EWS or Larmor clock approaches, considered in the first part of the Thesis. It is a general feature of quantum mechanics that a measurement affects the interference. How accurately we measure a time or delay changes the outcome of the measurement [29].

Quantum tunnelling is an example of a scattering problem where a pure quantum approach is needed, because a straightforward extension of the classical analysis to a quantum situation gives contradictory results. There are other scattering situations where the classical analysis fails, such as low energy scattering on low barriers or shallow wells. We apply this quantum analysis to scattering by a smooth Eckart potential. We study the apparent superluminal tunnelling time discussed above and the effect that the poles of the transmission amplitude have on the spatial delays of the transmitted WPs. These poles are associated with bound or resonant states, and are related to the interference between alternative delays that the transmitted WP can acquire in the potential [30].

Although most of the Thesis is devoted to the EWS delays, we also analyse the difference between these and the tunnelling time obtained using a Larmor clock, already mentioned above. The latter uses the precession of the spin of the particle in the presence of a magnetic field to measure the time spent in a region of space [31]. We consider an ultra-quantum case of a zero-range potential, for which they are most different, and study how this difference appears.

In the case of a relativistic scattering, not only does the apparent superluminal effect not disappear, but one encounters more anomalous results. In the second part of the Thesis we consider the single-particle relativistic treatment of scattering, by studying the scattering of bosons and fermions through supercritical barriers, i. e. barriers high enough to bridge the gap between the negative and positive energy continua. WPs can propagate freely through the barrier region and there is no suppression of transmission, unlike in non-relativistic tunnelling. This is known as the Klein paradox [32, 33].

Our interest in these barriers lies again in the apparently paradoxical traversal times obtained by following the COMs of the WPs. Consider the transmission of a bosonic WP of energy E, which satisfies the Klein-Gordon equation, through a supercritical barrier of width d and height $V_0 = E/2$. In this scenario, we can find solutions where the transmitted part of the WP is advanced by $2d$, *twice* the width of the barrier. A time derived from this spatial delay in the same manner as in classical scattering leads to negative traversal times. This conclusion seems to contradict Einstein's causality, although, as we will show, the mechanism behind its appearance does not require superluminal velocities.

We also study how the supercritical scattering differs for Klein-Gordon bosons and Dirac fermions, and discuss the convergence and causality of their respective solutions. As we will see, bosons and fermions behave differently in the supercritical regime. We analyse these differences, and relate each solution to the Klein paradox.

This Thesis is organised as follows. **Part I** consists of three chapters. **Chapter 1** studies the transmission of non-relativistic Gaussian WPs in terms of interference of their delayed copies. This reshaping mechanism is studied in the classically allowed transmission and in the case of tunnelling. In the latter case, if the COM delay is used to deduce the time in the barrier, the apparent superluminal delays appear. In **Chapter 2**, the method presented in the previous chapter is applied to a smooth Eckart potential. The delay distribution is calculated in terms of the poles of the transmission amplitude. The effect of these poles on the transmitted

WP is studied for different Eckart barriers and wells. In **Chapter 3** the EWS and the Larmor clock results are compared in the case of a zero-range potential. Both can be understood as quantum measurements, although of different quantities. The difference is discussed in detail.

Part II of the Thesis studies relativistic scattering, and consists of a single chapter. **Chapter 4** considers transmission and reflection through supercritical barriers using a multiple-reflection series. The different scattering solutions for Klein-Gordon bosons and Dirac fermions are discussed and compared. Each solution is analysed in relation to pair creation and annihilation, and to the Klein paradox.

Finally, we present our Thesis **Conclusions**, also divided into two parts: relativistic and non-relativistic.

Part I

Non-relativistic scattering

Chapter 1

Superluminal scattering time

We study the transmission of non-relativistic Gaussian wave packets through a one-dimensional potential, barrier or well. It is well known that particles that tunnel through a potential seem to "take no time". We study the transmission as a result of the interference of delayed freely propagating wave packets, each with a different spatial delay, related to the potential. In the classical case, the particle experiences a speed-up or slow-down effect, where the interference is destroyed. This is not what happens in the quantum case, since the Uncertainty Principle does not allow us to relate the delay of the transmitted particle to a time spent in the potential region. The meaning of the apparent "superluminal" delay in tunnelling is discussed.

1.1 Introduction

A classical particle travelling through a one-dimensional short-range potential $V(x)$ speeds up over a well, $V(x) < 0$, and slows down over a barrier, $V(x) > 0$. This can be experimentally checked by measuring directly the difference between the position of the transmitted particle and a freely propagating counterpart, i. e. the spatial delay x', which can be positive or negative. Alternatively, one can compare the times at which the transmitted and the freely moving particles arrive at a fixed detector far enough from the potential, and obtain a time delay τ. For a classical particle, there is a direct relation between the results of the two approaches, since we have that $\tau = -x'/v_0$, where v_0 is the speed of the freely propagating particle.

This relation relies on the existence of a well-defined trajectory of the particle through the potential. This classical, single trajectory no longer exists in a pure quantum scattering problem. In the case of tunnelling, where the incident particle has an energy lower than the barrier's height, attempts to calculate the time it takes for the particle to cross the potential lead to anomalous results.

In the early 1930's it was observed that *there is no appreciable delay in the transmission of the packet through the barrier* [11]. The particle seems to cross the barrier region instantaneously. If we were to infer a velocity from this tunnelling time, as in the classical case, we would get an infinite velocity. This result directly contradicts Einstein's special relativity, since the velocity would be higher than the speed of light, hence the name "superluminal". The debate about the meaning of this apparent "superluminal" tunnelling time continues to date, encouraged by the recent progress in atto-second experimental techniques [1–3, 15].

The difficulty in trying to measure a quantum time is that quantum mechanics measure operators, and there is no self-adjoint operator for time [5]. Instead, time is a parameter of the systems, not an observable.

In this chapter and throughout the first part of the Thesis, we focus on non-relativistic particles, that satisfy the Schrödinger equation. These have no explicit

speed limit, so it could be argued that the superluminal delay does not violate Einstein's special relativity, because it is not considered. One can hope that this superluminal delay would disappear if one treats the particles in the relativistic approach. This is not the case, as anomalous values for the tunnelling delay persist in the transmission of relativistic particles [12–14].

The mechanism for the appearance of the delay in quantum tunnelling is very different from that for the speed-up or slow-down of the classical transmission. Considering the incident wave packet (WP) as a travelling smooth envelope, the transmission relies on the interference of delayed free envelopes. In the classical case, a single delayed envelope is selected, corresponding to the transmitted WP. This is not the case in quantum transmission [30, 34], as the particle undergoes a reshaping process in the barrier [35], in where all the envelopes contribute to the transmission. Therefore, no single delay is selected. The information about any selected single delay is hidden by the Uncertainty Principle [24, 25].

This chapter is organised as follows. Section 1.2 presents the Gaussian WP we will use throughout the chapter, and defines the delay as the difference between the centres of mass (COMs) of the transmitted and free particles. Section 1.3 discusses the semiclassical approximation, used in the following sections, and shows the mechanism behind the classical delay. Section 1.4 applies this semiclassical approximation to the tunnelling case, where the apparent superluminal nature of the tunnelling delay already appears. The transmitted WP, which is the result of interfering delayed envelopes, is studied in Section 1.5, where the amplitude distribution of the delays is presented. This distribution is studied further in Sections 1.6, where the delay appears as stationary points in the delay distribution, and 1.7, where the alternating nature of this distribution comes into play. Section 1.8 introduces the pole representation, which is further developed in Section 1.9, that gives analytical expressions for the transmitted WPs. Finally, Section 1.10 discusses the main results of the chapter, and gives the conclusions.

The main results in this chapter are general, for any shape of the potential. To

showcase some of these results, a square potential is used in some numerical calculations. Although helpful for illustrating the main ideas, the square potential has some analytical difficulties that need to be studied further with the pole representation method presented here. The following chapters are devoted to two examples of potentials, the Eckart and a zero-range potential, which are better suited for this treatment. For these potentials, the pole representation method will show to be more helpful in order to understand the appearance of the anomalous delays, and the nature of quantum scattering.

Throughout this chapter we will focus on transmission, although a similar study can be applied to reflection, which will also be studied in **Chapter 3**.

1.2 Centre of mass delay

We consider a one-dimensional scattering problem. The WP is incident from the left on a short-range potential $V(x)$, such that $V(x) \to 0$ for $x \to \pm\infty$ and has a maximum value V_0. The initial WP starts at a point to the left of the barrier, far enough to be unaffected by the potential, with energy $E(p) = p^2/2\mu$, where μ is the particle's mass ($\hbar = 1$),

$$\Psi^0(x,t) = \int A(p-p_0) \exp\left[ipx - iE(p)t\right] dp. \tag{1.1}$$

$A(p-p_0)$ is the momentum distribution around the mean momentum p_0. Throughout this Thesis we will consider Gaussian WPs, with a momentum distribution given by

$$A(p-p_0) = 2^{-1/4}\pi^{-3/4}\Delta p^{-1/2} \exp\left[-(p-p_0)^2/\Delta p^2 - i(p-p_0)x_0\right], \tag{1.2}$$

where Δp is the momentum width of the WP, with the spatial width given by $\Delta x = 2/\Delta p$, and $x_0 > 0$ is the initial point to the left of the barrier. Inserting Eq.(1.2) into Eq.(1.1), evaluating the Gaussian integral and using that $\int e^{-ax^2+bx+c}dx =$

$\sqrt{\pi/a}e^{b^2/4a+c}$, we have

$$\Psi^0(x,t) = \exp\left[ip_0x - iE(p_0)t\right] G_0(x,t), \tag{1.3}$$
$$G_0(x,t) = \left(\frac{2\Delta x^2}{\pi\Delta x_t^4}\right)^{1/4} \exp\left[-(x - \frac{p_0}{\mu}t - x_0)^2/\Delta x_t^2\right],$$

where $\Delta x_t = \Delta x\sqrt{1 + 2it/\mu\Delta x^2}$ is the complex width that takes into account the spreading of the WP over time. $G_0(x,t)$ is the smooth envelope that travels at a velocity proportional to the mean momentum, $v_0 \equiv p_0/\mu$.

As time evolves, the WP reaches the barrier and is transmitted and reflected. The transmitted WP is

$$\Psi^T(x,t) = \int T(p,V)A(p-p_0)\exp\left[ipx - iE(p)t\right] dp, \tag{1.4}$$

where $T(p,V)$ is the transmission amplitude for the potential $V(x)$. A diagram of scattering, showing classical transmission and quantum tunnelling, is shown in Fig.1.1.

At a time t, long enough for the scattering to have taken place, we compare the position of the COM of a freely propagating particle, in the absence of potential, with the COM of the transmitted WP. We obtain a delay

$$\delta x_{COM}(t) = x^T_{COM}(t) - x^0_{COM}(t), \tag{1.5}$$

where the centres of mass are at the positions

$$x^{T,0}_{COM}(t) = \frac{\int x|\Psi^{T,0}(x,t)|^2dx}{\int |\Psi^{T,0}(x,t)|^2dx}. \tag{1.6}$$

In Eq.(1.5) a positive delay means that the particle is advanced relative to free propagation, while a negative value means it is delayed.

This chapters shows some illustrative results using a square potential of width d, Appendix A. For the figures, dimensionless variables are used, taking the barrier's

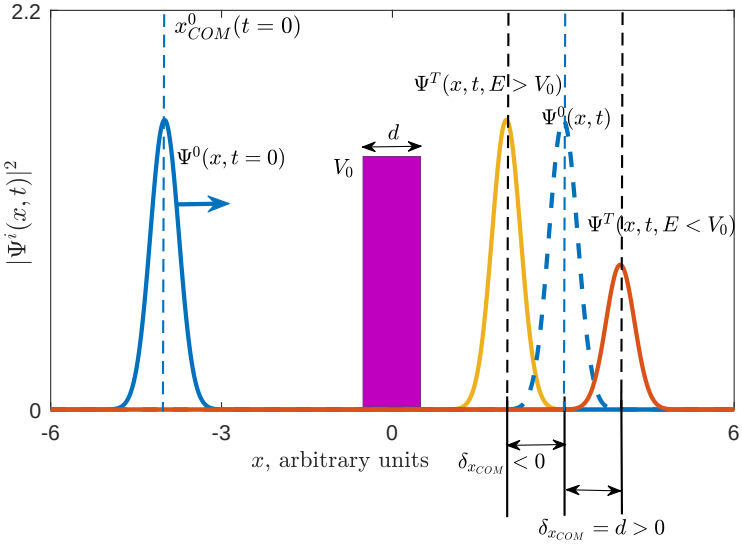

FIGURE 1.1: An incident WP, $\psi^0(x,t=0)$ (blue solid line) transmitted across a square potential with height V_0 and width d. The transmitted WP, $\psi^T(x,t)$, is shown for the case of $E > V_0$ (yellow solid line) and the case of tunnelling, $E < V_0$ (red solid line). The freely propagating WP at time t is also shown (blue dashed line). The COMs of all the WPs, Eq.(1.6), are marked by dashed vertical lines.

width as the reference. These variables, with $\hbar = 1$, are

$$X = x/d, \quad P = pd, \quad T = t/d, \quad W = V_0 d, \quad M = \mu d. \tag{1.7}$$

1.3 The classical limit and spatial delays

For a classically allowed transmission we have that $E(p) > V(x)$, and the local momentum of the WP inside the potential is $q(x,p) = \sqrt{p^2 - 2\mu V(x)}$. We consider here the case of a momentum distribution $A(p - p_0)$ such that all non-negligible momenta involved in the scattering process are positive, and in the same way $q(x,p)$ is positive for all these momenta.

In the case of a smooth potential, the semiclassical condition requires that the potential varies slowly compared to a local de Broglie wavelength, h/p. Assuming this condition is met, and neglecting over-barrier reflection, we can write the

transmission amplitude as a phase integral [36]

$$T(p,V) \approx \exp\left\{ i \int_{-\infty}^{\infty} \left[q(x,p) - p \right] dp \right\} \equiv \exp\left[i\Phi(p,V) \right]. \tag{1.8}$$

We can expand the phase of the transmission amplitude in Taylor series around the mean momentum p_0, using that $\partial_p \left[q(x,p) - p \right] |_{p=p_0} = p_0/q(x,p_0) - 1$,

$$\begin{aligned} \Phi(p,V) =& \Phi(p_0,V) - \int_{-\infty}^{\infty} \left[1 - \frac{p_0}{q(x,p_0)} \right] (p-p_0) dx \\ &+ \int_{-\infty}^{\infty} dx \sum_{n=2}^{\infty} \partial_p^n \Phi(p_0,V)(p-p_0)^n/n!. \end{aligned} \tag{1.9}$$

For the Gaussian WPs considered, the main momentum contributions lie in a range inversely proportional to the width of the WP in coordinate space, $\Delta p = 2/\Delta x$. Therefore, we have that $(p-p_0)^n \sim 2^n/\Delta x^n$. In order for the higher order terms in Eq.(1.9) to be negligible, the spatial distribution of the WP, Δx, has to be broad enough compared to the width of the potential so that $\sum_{n=2}^{\infty} \partial_p^n \Phi(p_0,V)(p-p_0)^n/n! \ll 1$. For the square potential used in the figures in this chapter, this condition is satisfied everywhere except at its edges. We will return to this point in the following chapters in order to check whether the semiclassical condition is satisfied by the potentials taken considered there. For now, we assume we can do so and leave the series up to the first order for the rest of the current chapter.

The first term of Eq.(1.9) only affects the transmitted WP, Eq.(1.4), as an overall phase. Renaming the term in brackets in the second term of Eq.(1.9) as $\tilde{x}'$ and inserting Eq.(1.9) into Eq.(1.4) we have

$$\Psi^T(x,t) \approx \int A(p-p_0) \exp\left[i\Phi(p_0,V) - i\tilde{x}'(p-p_0) \right] \exp\left[ipx - iE(p)t \right] dp = \tag{1.10}$$

$$= \exp\left[i\Phi(p_0,V) + i\tilde{x}'p_0 \right] \int A(p-p_0) \exp\left[ip(x-\tilde{x}') - iE(p)t \right] dp =$$

$$= \exp\left[i\Phi(p_0,V) + i\tilde{x}'p_0 \right] \Psi^0(x-\tilde{x}',t).$$

Apart from an overall phase, which does not affect the position of the centre of mass, the transmitted WP is just a free WP, shifted in space by $\tilde{x}'$. We can see the classical origin of this shift or delay, $\tilde{x}'$, more easily by rewriting it in terms of the velocity of the particle outside and inside the potential. Outside, the initial velocity of the particle is $v_0 \equiv p_0/\mu$ and, equivalently, inside the potential the particle has a velocity $v(x, p_0) \equiv q(x, p_0)/\mu$. We have that the delay is

$$\tilde{x}' = v_0 \int_{-\infty}^{\infty} \left[\frac{1}{v_0} - \frac{1}{v(x, p_0)} \right] dx. \tag{1.11}$$

It is clear that the positive or negative delays of the transmitted particle crossing a potential, barrier or well, is a result of it speeding up or slowing down. When the particle goes over a barrier, $V(x) > 0$, the momentum inside the potential $q(x, p)$ decreases, and with it the velocity $v(x, p_0) < v_0$. Looking at Eq.(1.11), this implies that $\tilde{x}' < 0$, and the transmitted particle appears behind the freely propagating one. Equivalently, in the case of a well, $V(x) < 0$, the particle speeds up, $v(x, p_0) > v_0$, so that the spatial delay becomes positive, $\tilde{x}' > 0$ and the transmitted WP appears ahead of a freely propagating one.

As an illustrative result, the case of WPs crossing over a square potential barrier or well, Appendix A, is shown in Fig.1.2. The WPs are calculated by numerical integration of Eqs.(1.1) and (1.4), using dimensionless variables, Eq.(1.7). For the square barrier, Fig.1.2 *a*), the difference between the numerical COMs of the WPs gives $\delta X_{COM} = -0.3001$, while applying Eq.(1.11) gives $\tilde{X}' = -0.3338$. For the square well, *b*), the numerical delay is $\delta X_{COM} = 0.1899$, while the analytical semiclassical approximation gives $\tilde{X}' = 0.1997$. The results are not in perfect agreement with Eq.(1.11) because, as mentioned above, the square potential does not satisfy the semiclassical condition at its sharp edges, where its value has a discontinuity. The potential used in the following chapter, the Eckart potential, does satisfy the semiclassical condition everywhere.

In a classical passage of a WP over a barrier, the trajectory of the COM of the WP is continuous and could be tracked everywhere, from the initial point, through the potential region to the final time. This is the case for a scattering as the one

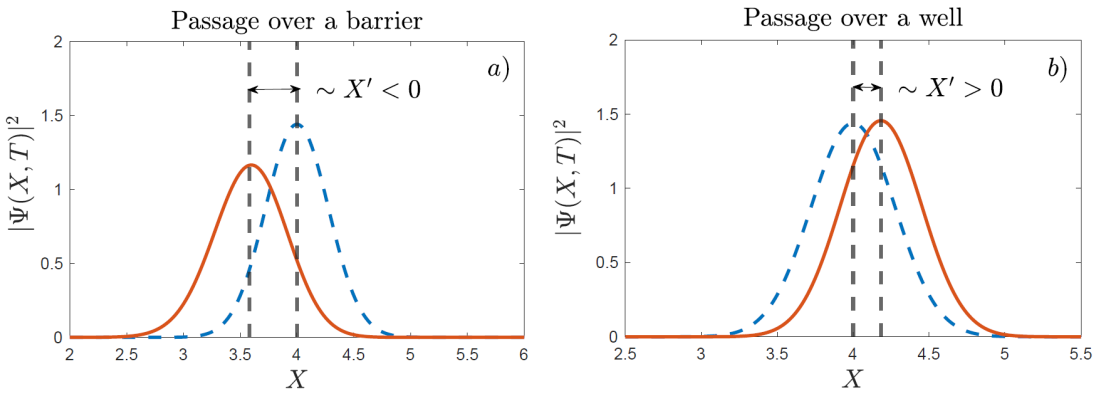

FIGURE 1.2: Freely propagating particle (blue dashed line) and transmitted particle (red line) for an incident Gaussian WP with $\Delta X = 0.15$, $P = 200$, $X_0 = -4$, $M = 1$ and $T = 0.04$, going over *a*) a square barrier potential with $W = 10^4$ and *b*) a square well potential with $W = -10^4$. The semiclassical delays X' are obtained from Eq.(1.11).

from Fig.1.2. We could measure the position of the particle at any given time t, and, for a large enough number of measurements at different times, have a definite and continuous trajectory of the COMs of both the freely propagating WP and of the transmitted one everywhere in space. This includes defining a trajectory of the COM of the transmitted particle inside the potential. There is a direct relation between the single delay after transmission and the trajectory of the particle as it passes over the potential.

One can equivalently define the time the particle spends inside the potential, and a velocity inside this region. The difference between the time taken by the transmitted and the free particle to cross the potential is related to the spatial delay x'. The condition for this relation is the existence of a continuous trajectory inside the potential. This condition is only met in the classical case. As we will see, in the pure quantum case of tunnelling there is no equivalence between the spatial delays after transmission and a real time spent in the potential.

1.4 "Instantaneous" semiclassical tunnelling and complex spatial delays

Now we consider the case of a barrier, $V(x) > 0$, and an incident WP with all energies $E(p) < V_0$, i. e. where the maximum momentum taken into account in the momentum distribution $A(p - p_0)$ corresponds to an energy lying below the maximum value of the potential. This defines the classical turning points $x_<$ and $x_>$, such that $q(x_{<,>}, p_0) = 0$, and the classically forbidden region, $x_< < x < x_>$. Inside this region, a classical WP cannot propagate, since its mean energy is below the potential, and will be completely reflected. This is not true in the quantum case, where a part of it still tunnels through this region and is partially transmitted, even though the WP is mostly reflected. The transmission is suppressed, but not forbidden in the quantum case.

Following the semiclassical analysis of Eqs.(1.8) and (1.11), we have now inside this classically forbidden region a pure imaginary local momentum, $q(x_< < x < x_>, p) = i|q(x,p)| = i\sqrt{2\mu V(x) - p^2}$. The expansion in Eq.(1.9) is now complex, and we have that $|T(p_0, V)|^2 \approx \exp\left[-2\int_{x_<}^{x_>} \sqrt{2\mu V(x) - p_0^2} dx\right] \ll 1$, which means that most of the particles are actually reflected, and only a small fraction of them, proportional to $|T(p_0, V)|^2$, tunnel through the barrier.

As before, the transmitted WP is shifted by the delay given in Eq.(1.11), which is now a complex spatial shift, $\tilde{x}' = \tilde{x}'_1 + i\tilde{x}'_2$. Its real and imaginary parts are

$$\begin{aligned} \tilde{x}'_1 &\equiv v_0 \int_{-\infty}^{\infty} \left\{ \frac{1}{v_0} - \mathrm{Re}\left[\frac{1}{v(x,p_0)}\right] \right\} dx, \\ \tilde{x}'_2 &\equiv -v_0 \int_{-\infty}^{\infty} \mathrm{Im}\left[\frac{dx}{v(x,p_0)}\right] = -v_0 \int_{x_<}^{x_>} \frac{dx}{|v(x,p_0)|}. \end{aligned} \tag{1.12}$$

Inserting these in Eq.(1.4), rearranging and taking into account the Gaussian envelope in Eq.(1.2), we have that

$$\exp\left[\tilde{x}'_2(p - p_0) - (p - p_0)/\Delta p^2\right] = \exp\left[\frac{p - (p_0 + \delta p_0)^2}{\Delta p^2} + \frac{\Delta p^2 \tilde{x}'^2_2}{4}\right], \tag{1.13}$$

where $\delta p_0 = \Delta p^2 \tilde{x}_2'/2$. Finally, the transmitted WP is

$$\Psi^T(x,t) \approx \exp\left[i\Phi(p_0,V) + ip_0\tilde{x}_1' + \frac{\Delta p^2 \tilde{x}_2'^2}{4}\right]\Psi^0(x-\tilde{x}_1', t, p_0+\delta p_0). \tag{1.14}$$

We can see now the effect that each part of the complex delay in Eq.(1.12) has on the transmitted WP. The real part, $\tilde{x}_1'$, acts as a spatial delay, in the same way as in the classical case. The imaginary part, $\tilde{x}_2'$, apart from an overall phase, increases the particle's mean momentum by δp_0. This is known as the momentum filtering effect (see, for example, [30, 35]), and it is due to the fact that higher momenta tend to tunnel through the barrier more easily. For low momenta the transmission amplitude increases rapidly as the momentum itself increases, and we have that $T(p_0+\delta p_0, V) \gg T(p_0, V)$, shifting the transmitted mean momentum. The wider the WP is in momentum space, the more pronounced this effect is, as it "includes" values further away from its initial mean momentum p_0. This last point can also be seen in the dependence of δp_0 on the width of the WP in momentum space, Δp.

Thus, the delay between the transmitted and the free particles, Eq.(1.5), is

$$\delta x_{COM}(t) = \tilde{x}_1' + \delta v_0 t, \tag{1.15}$$

where $\delta v_0 = \delta p_0/\mu = (p-p_0)/\mu$ is the shift in the transmitted velocity due to the momentum filtering. Note that the time t in Eq.(1.15) is the total time, from the initial point, when the WP is far from the barrier, and not the moment when the transmitted WP emerges from the right edge of the barrier.

From Eq.(1.12) we see that the classically forbidden region does not contribute to the spatial delay $\tilde{x}_1'$. This is the origin of the apparent "instantaneous" tunnelling, as the particle seems to take no time to pass through the classically forbidden region. For a general smooth barrier, such as the Eckart barrier studied in the following section, the WP slows down as the barrier grows before the left turning point $x_<$, and as it decreases after the right-turning point $x_>$. In these

cases, the delay is not exactly the width of the forbidden region, but a smaller one.

As before, we numerically compute the free and transmitted WPs through a square barrier, Appendix A, to see the delays appearing in a tunnelling scattering, Fig.1.3. In the case of the square barrier, the positions of the two edges are themselves the turning points and the whole region of the potential is the classically forbidden region. Thus, the delay is the width of the barrier, $\tilde{x}'_1 = d$. The numerical delay from the figure is, in the dimensionless variables, given in Eq.(1.7), $\delta X_{COM}(t) = 1.0304$, while the complete semiclassical approximation result for the delay, from Eq.(1.15), is $\delta X^{sc}_{COM}(t) = 1.0300$. The value for the real part of the complex shift in Eq.(1.12) is $\tilde{X}'_1 = 0.9800$, which is close to the width of the barrier, $D = 1$ in dimensionless variables. This is the spatial delay of the particle without taking into account the momentum filtering effect. For larger times, the second term in Eq.(1.15) dominates.

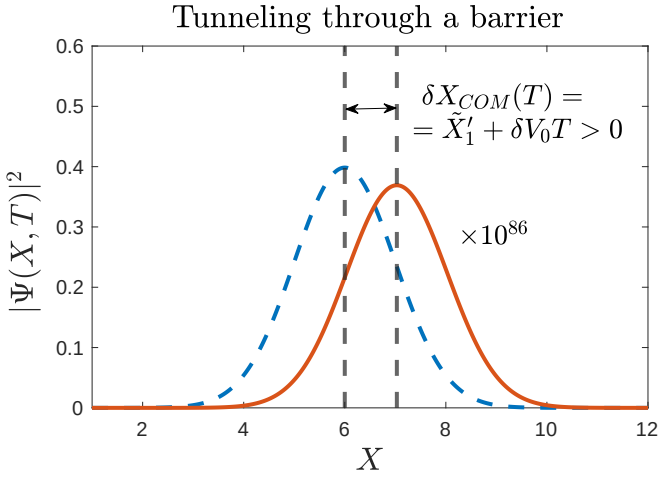

FIGURE 1.3: Freely propagating particle (blue dashed line) and transmitted particle (red line), enhanced for better viewing, for an incident Gaussian WP with $\Delta X = 2$, $P = 100$, $X_0 = -4$ and $M = 1$, going over a square barrier potential with $W = 10^4$ after a time $T = 0.1$.

Due to the low transmittance, the tunnelled WP is enhanced for better viewing in the figure. The total transmitted probability is reduced by, approximately, $|T(P_0, W)|^2 = 5.5356 \times 10^{-87}$. Numerically, we find the total transmitted probability to be $\int dX |\Psi^T(X,T)|^2 = 9.2181 \times 10^{-87}$, higher than the previous result, due to the contribution of momenta larger than P_0. Even though these values of

the transmitted probability are too small to be considered in practice, we are interested in the principle, which still holds. The effects studied are more noticeable for the parameters taken throughout this Thesis, for which the transmitted WP is orders of magnitude smaller than the incident one.

We could try, as we did for a particle over a barrier or well, to infere a time spent in the barrier by the transmitted WP, and a velocity from it. A naive way of evaluating the time spent is just by measuring the spatial delay between the COMs of the two WPs. By comparing it with the width of the forbidden region, we can evaluate the time spent there. For the apparently "instantaneous" tunnelling in Eq.(1.12), the time spent is close to zero, and therefore the particle seems to have an extremely high velocity while crossing this region.

This approach has several problems. Contrary to the classical case, it is not clear how to define a trajectory inside the forbidden region of the potential. The WP has no peak that could be traced, as it disappears at the left-turning point and it is formed again after the right one. Inside the potential, it is an evanescence wave, an exponentially decaying wave. In addition, the transmitted WP undergoes a reshaping in the barrier [35]. It is not just a shifted copy of the incident one. As we will see, this reshaping involves the interference between several delayed envelopes. Although we can measure the COM of the particle after the tunnelling, this gives no information about the existence of any well-defined trajectory inside the potential.

Treating the COM of the tunnelled particle as a classical result is misleading, as it is a quantum result, which does not contain the same information about the past of the particle as a classical result does.

1.5 Transmitted WPs result from the interference of delayed envelopes

Since we are interested in the spatial delays of the transmitted WP, we can transform the integral in Eq.(1.4), which is evaluated over the momentum p, into

an integral over the spatial coordinate x via a Fourier Transform (FT). Doing so, we get a convolution, as [34]

$$\Psi^T(x,t) = \exp\left[ip_0 x - iE(p_0)t\right] \int G_0(x-x',t)\eta(p_0,x')dx', \tag{1.16}$$

where $G_0(x-x',t)$ is the freely propagating envelope in Eq.(1.3), delayed by x', and $\eta(p_0,x')$ is the distribution of these delays. The distribution is computed as the FT of the transmission amplitude,

$$\eta(p_0,x') = \frac{\exp\left(-ip_0x'\right)}{2\pi} \int T(k)\exp\left(ikx'\right)dk. \tag{1.17}$$

Since the transmission amplitude satisfies $T(-k^*,V) = T^*(k,V)$, the integral in Eq.(1.17) can be calculated as $2 \times \mathrm{Re}\left[\int_0^\infty T(k)\exp\left(ikx'\right)dx'\right]$. Thus, $\exp(ip_0x')\eta(p_0,x')$ is a real function, although an alternating one between positive and negative values. This alternating nature, as we will see later, plays a central role in the superluminal nature of the spatial delays. The distribution itself, $\eta(p_0,x')$, is alternating and complex.

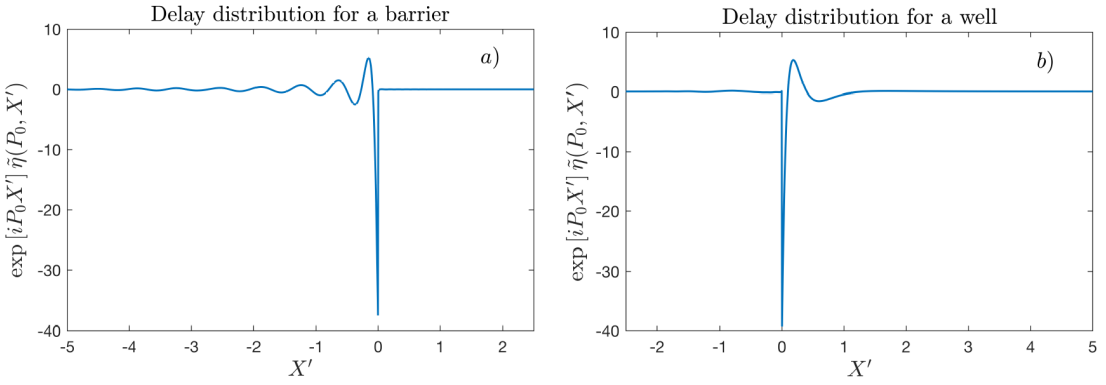

FIGURE 1.4: Smooth part of the delay distribution, computed as the numerical integration of Eq.(1.19), for $P_0 = 2$ and a square potential with *a*) $U_0 = 20$, corresponding to a barrier and *b*), $U_0 = -20$, corresponding to a well. As mentioned in the text, the depicted distribution, $\exp\left[iP_0X'\right]\tilde{\eta}(P_0,X')$ is a real function, and an alternating one.

For a freely propagating WP we would have $\eta(p_0,x') = \delta(x')$, since the particle is unaffected by any potential, $T(k,V) = 1$, and we recover the expression in Eq.(1.3). In transmission through a potential, all WPs with energies far above

the barrier, corresponding to high momenta, pass above the barrier unaffected, and thus we have that $T(k \to \infty) \to 1$. There is perfect transmission for these energies. Evaluating the FT of $\eta(p_0, x')$ we can separate the contribution of these high momenta, which consists of a Dirac delta, and a smooth distribution,

$$\eta(p_0, x') = \delta(x') + \tilde{\eta}(p_0, x'), \tag{1.18}$$

where

$$\tilde{\eta}(p_0, x') = \frac{\exp\left(-ip_0 x'\right)}{2\pi} \int \left[T(k) - 1\right] \exp\left(ikx'\right) dk, \tag{1.19}$$

since the function $T(k) - 1$ tends to 0 for $k \to \infty$. We can see examples of the smooth part of the distribution of delays, Eq.(1.19), for both a square barrier and a square potential in Fig.1.4.

We can now rewrite Eq.(1.16) as

$$\Psi^T(x,t) = \exp\left[ip_0 x - iE(p_0)t\right] \left[\int_{-\infty}^{\infty} G_0(x - x', t)\tilde{\eta}(p_0, x')dx' + G_0(x,t)\right]. \tag{1.20}$$

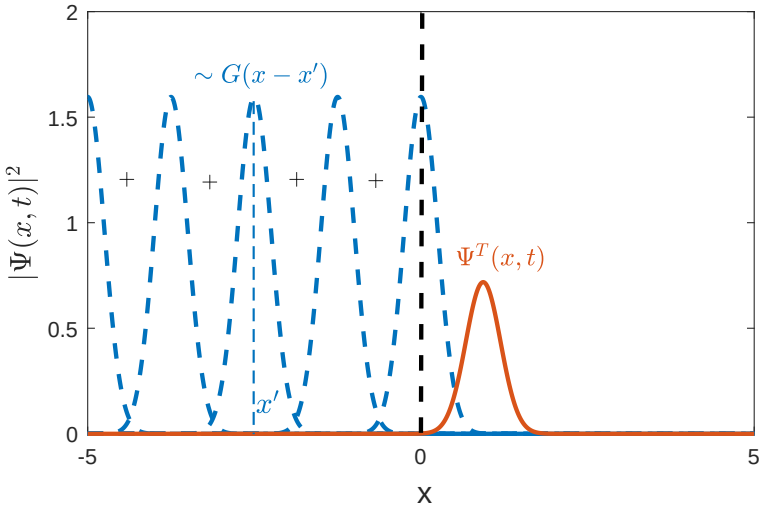

FIGURE 1.5: Interfering envelopes, negatively delayed by x' with respect to free propagation (the delay at $x' = 0$ corresponds to the freely propagating envelope) resulting in an advanced transmitted WP.

From Eq.(1.16) we see that the transmitted WP is actually formed by a recombination of a continuum of different freely propagating envelopes $G_0(x,t)$, each shifted by x' in space, with a complex weight $\eta(p_0,x')$, as illustrated in Fig.1.5. The interfering envelopes are weighted by $\eta(p_0,x')$, thus depending on the potential and the incident WP's mean momentum.

The potential can be understood as an "interferometer", in which there is a continuum of "paths" that the particle takes to reach the final state. Along each route the freely propagating envelope $G_0(x,t)$ is enhanced or suppressed by a factor $|\eta(p_0,x')|$, obtains an additional phase $\arg(\eta(p_0,x'))$ and is delayed in space by x'. All these envelopes recombine at the end to produce the transmitted, reshaped WP. In the case of a potential barrier, since $V(x)$ does not support bound states, we have that

$$\eta(p_0, x' > 0) = 0, \tag{1.21}$$

which can be seen in Fig.1.4 *a*). For a well it is not true, in general, that $\eta(p_0, x' < 0) = 0$. The delay distribution is non-zero everywhere, but the positive delays dominate. Zooming into Fig.1.4*b*) for negative X', it can be seen that $\tilde{\eta}(P_0, X')$ is indeed non-zero, although small compared to its value for positive X'. Why this is so will be studied in Section 1.8 and will be extended to the Eckart potential in the following chapter.

From Eq.(1.21), in the case of a barrier, only the scenarios where the envelopes are negatively delayed participate in the transmission. In the classical case of a particle going over a barrier, one of these negative delays is selected, making the transmitted WP to be behind a freely propagating one. In the case of tunnelling, the interference of these routes does not "select" a single delay. Besides, the recombined transmitted WP appears *ahead* of the freely propagating one, as if the "selected" delay was positive. This positive delay is outside the range of the available ones, at a point x' where the amplitude distribution of the delays is

zero.We also have that

$$T(p_0, V) = \int \eta(p_0, x')dx', \tag{1.22}$$

so that $\eta(p_0, x')$ acts as the probability amplitude for a WP with momentum p_0 to have a spatial shift x'. In the case of tunnelling, the delay of the transmitted WP has a probability amplitude of zero.

Although both the classical and the quantum cases appear from the same expressions, they behave very differently. In the classical case, the recombination selects a unique shift and substitutes the freely propagating envelope by one with that selected shift. In the quantum case, all delays interfere in such a way that the delay of the recombined WP falls outside the possible delays.

1.6 Delays as stationary regions in $\eta(p_0, x')$

To see the mechanism behind the transmission as an interference of envelopes we insert the semiclassical approximation of the transmission amplitude, given by Eq.(1.8), into Eq.(1.3) and evaluate it with the steepest descent method. The derivation of the results of this section is explained in more detail in Appendix B. Here we focus on the main results. For $\eta(p_0, x')$ we obtain

$$\eta(p_0, x') \sim \exp\left[-ip_0x' + i\Phi(\tilde{k}(x'), V) + i\tilde{k}(x')x'\right], \tag{1.23}$$

where $\tilde{k}(x')$ is the critical point, which satisfies that

$$\left.\frac{\partial\Phi(k, V)}{\partial k}\right|_{k=\tilde{k}(x')} + x' = 0. \tag{1.24}$$

We can use Eq.(1.23) and evaluate the integral for the transmitted WP, Eq.(1.16),

applying again the steepest descent method. For the WP, we recover the expression given by Eq.(1.14), where now $\tilde{x}'$ is a critical point of $\eta(p_0, x')$ which satisfies

$$\tilde{k}(\tilde{x}') - p_0 = 0. \tag{1.25}$$

Combining Eqs.(1.24) and (1.25) we obtain a saddle point at

$$\tilde{k}' = p_0, \qquad \tilde{x}' = -\,\partial_k \Phi(k, V)\big|_{k=p_0} = \int_{-\infty}^{\infty} dx \left[1 - \frac{p_0}{q(x, p_0)}\right]. \tag{1.26}$$

For the delay $\tilde{x}'$ we have recovered the expressions from the previous sections, Eqs.(1.11) and (1.12), but now with a new interpretation as a stationary point of $\eta(p_0, x')$.

The amplitude $\eta(p_0, x')$ has two important features. One is the finite dip near $x' = 0$, seen in Fig.1.4, whose contribution is to cancel the freely propagating envelope $G_0(x, t)$ (for a similar "Zeno peak" see [37]). The other one is the stationary point we have just studied, shown in Fig.1.6 for the same parameters as those in Figs.1.2 and 1.3. Note that, apart from the stationary point, the delay distribution has some superimposed oscillations, due to the fact that the FT of the transmission amplitude is a real function (see Appendix C).

The appearance, or "selection", of a delay as a result of $\eta(p_0, x')$ is different in the classical and quantum cases. In the classical case of the particle passing over a well, or above a barrier, this stationary point $\tilde{x}'$ is real. It indicates the region on the real x' axis where the rapid oscillations of the amplitude distribution of the delays, $\eta(p_0, x')$, are slowed down. Far from this point, the rapid oscillations cancel all interfering envelopes in Eq.(1.16). This is a result of the period of the oscillations appearing in the delay distribution being much shorter than the width of the envelopes. As a result, all the envelopes are cancelled except $G_0(x - \tilde{x}', t)$, the one with a delay corresponding to the stationary point. This is what we see in Fig.1.6 *a*) and *b*). The classical trajectory appears as a limit of the general quantum case, where the contribution of a single path dominates [17].

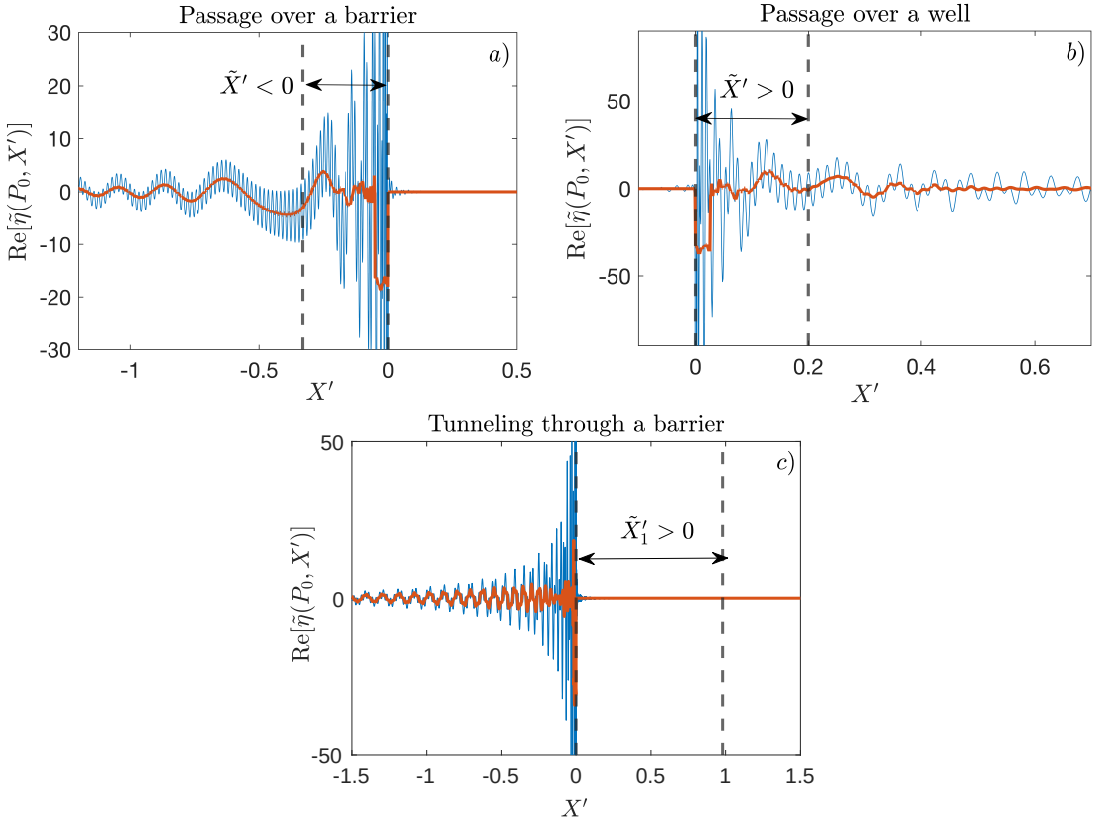

FIGURE 1.6: Real part of the delay distribution, Eq.(1.17) (blue solid line) and the average of the delay distribution, $\mathrm{Re}\left[y^{-1}\int_{X'}^{X'+y}\tilde{\eta}(P_0, X'')dX''\right]$, are shown (red solid line). The position of the real delay from Eqs.(1.11) and (1.12) is marked for each case. The parameters correspond to *a*) a passage over a barrier with $W = 10^4$ of a WP with mean momentum $P_0 = 200$ and $M = 1$, *b*) a passage over a well with $W = -10^4$ of a particle with mean momentum $P_0 = 200$ and $M = 1$, and *c*) tunnelling through a barrier with $W = 10^4$ of a WP with mean momentum $P_0 = 100$ and $M = 1$.

Going back to the "interferometer" picture, in quantum tunnelling, the stationary point becomes complex, Eq.(1.12). There is no stationary point along the real axis, and the amplitude distribution oscillates rapidly, since it corresponds to the classically forbidden region. We can see in Fig.1.6 *c*) that now there are only fast oscillations everywhere in $x' < 0$. These rapid oscillations interfere destructively, as they did in the classical case far from the stationary point. This makes the tunnelling WP exponentially small, although the amplitude $\eta(p_0, x')$ itself is not small. In this case there is no single delay selected and all negatively delayed envelopes $G_0(x - x', t)$ interfere and contribute to the transmitted WP. This interference occurs in such a way that, even though all interfering envelopes

are negatively delayed, i. e. have a COM behind the one of the freely propagating envelope, the result of their interference is an envelope with a COM ahead of the free one.

This advanced WP is the result of a delicate cancellation of all delayed envelopes, in which only the front tails interfere constructively in a reshaping process [35]. Thus, as we saw in Section 1.4, the resulting transmitted WP has an amplitude much smaller than the incident one. It is worth noting that the only difference between classically allowed and classically forbidden transmission is the mean momentum. That is, their delay distributions, $\eta(p_0, x')$, differ only by a phase.

We can use the stationary point to compute the momentum filtering. The increase in the mean velocity, $\delta v_0 = (p - p_0)/\mu$,can be expressed as

$$\delta v_0 = \delta p_0/\mu = \frac{\int (p-p_0)|T(p,V)|^2|A(p-p_0)|^2 dp}{\mu \int |T(p,V)|^2|A(p-p_0)|^2 dp}. \tag{1.27}$$

Taking the limit for a wide spatial WP or, equivalently, $\Delta p \to 0$, we can evaluate Eq.(1.27) using Eq.(1.26) and expanding the transmission amplitude in Taylor series around p_0,

$$\delta v_0 \approx 2\partial_p \ln|T(p,V)| \frac{\int (p-p_0)^2|A(p-p_0)|^2 dp}{\mu \int |A(p-p_0)|^2 dp} = \tilde{x}_2' \Delta p^2/2\mu, \tag{1.28}$$

and we recover the expression for the increase in the mean momentum that appeared in Eq.(1.14).

1.7 Delays as first moment of η

In order to see how these interferences behave, we can write the delay $\delta x_{COM}(t)$ differently, as a function of the amplitude distribution of the delays, $\eta(p_0, x')$. To do so, we assume that the envelope $G_0(x,t)$ in Eq.(1.16) is very broad and expand

it as $G_0(x-x',t) \approx G_0(x,t) - \partial_x G_0(x,t)x'$. After some calculations (see Appendix D), we have

$$\delta x_{COM}(t) = \mathrm{Re}\left[\overline{x}'\right] + 2\mathrm{Im}\left[\overline{x}'\right] \mathrm{Im}\left[\int x G_0^*(x,t)\partial_x G_0(x,t)dx\right], \tag{1.29}$$

where $\overline{x}'$ is the complex first moment of the distribution $\eta(p_0,x')$,

$$\overline{x}' = \frac{\int x'\eta(p_0,x')dx'}{\int \eta(p_0,x')dx'}. \tag{1.30}$$

From Eqs.(1.17) and (1.22) we have that $\int x'\eta(p_0,x')dx' = \int -\partial_k\, \eta(k,x')\big|_{k=p_0}\, dx' =$

$i\partial_k T(k,V)\big|_{k=p_0}$, and therefore, for the first moment in Eq.(1.30) we have

$$\overline{x}' = \left.\frac{i\partial_k T(k,V)}{T(k,V)}\right|_{k=p_0} = i\,\partial_k \ln\left[T(k,V)\right]\Big|_{k=p_0} = -\,\partial_k \Phi(k,V)\big|_{k=p_0}\,, \tag{1.31}$$

where $\Phi(k,V)$ is the phase of the transmission amplitude in the semiclassical approximation, Eq.(1.8). With this, we have recovered the complex delay of Eq.(1.26), and we can identify $\mathrm{Re}[\overline{x}'] = \tilde{x}_1$ and $\mathrm{Im}[\overline{x}'] = \tilde{x}_2$. The second term in Eq.(1.29) is the spatial distance advanced due to the momentum filtering (see Appendix E), while the first term is the delay acquired in the barrier.

Equation (1.30) helps us to understand the reason for the appearance of the anomalous delay in a classically forbidden transmission. It is an "average" obtained with the delay distribution $\eta(p_0,x')$. There are two characteristics of the delay distribution for a barrier, as the one shown in Fig.1.4*a*), that come into play here. First, since $\eta(p_0,x')$ is zero for all positive x', the real part of the integral in the numerator, $\int x'\eta(p_0,x')dx'$, is negative. Second, it is an alternating distribution. The key is that the integral in the numerator, $\int \eta(p_0,x')dx'$, has a negative real part, because the delay distribution is an alternating function. It is in the division between the negative numerator and the also negative denominator that

the positive value for Re$[\overline{x}']$ appears. This positive value $\overline{x}'$ corresponds to a delay distribution equal to 0, $\eta(p_0, \overline{x}') = 0$.

The mechanism behind this delay, which is outside the range of the available ones, is better understood compared to a usual quantum measurement, where the selected value of the delay is within on the range of the available ones. This involves an average done with probabilities, which are positive and real. A measurement of a value f has the form

$$\tilde{f}' = \frac{\int f'|A(f')|^2 df'}{\int |A(f')|^2 df'}, \tag{1.32}$$

where $A(f)$ is the probability amplitude associated with the eigenvalue f, and the square of its absolute value, $|A(f)|^2$, is the probability. In this case, the value of the measured quantity $\tilde{f}'$ lies in the range of the available eigenvalues f', weighted by their probabilities. There is no interference between the amplitudes of different eigenvalues, since the square of their absolute value is being evaluated and not the amplitudes themselves.

The first moment of $\eta(p_0, x')$ in Eq.(1.30) has a similar form to the quantum measurement in Eq.(1.32). The main difference is that in the case of the first moment of $\eta(p_0, x')$ the probability amplitudes are being evaluated, instead of the probabilities. These probability amplitudes are, as mentioned before, alternating functions. Thus, $\int \eta(p_0, x')dx'$, in the denominator of Eq.(1.30), is not necessarily positive, as is $\int |A(f')|^2 df'$ in Eq.(1.32). For some given delay distribution, $\int \eta(p_0, x')dx'$ can take negative values. This is what happens in the classically forbidden transmission. The real part of the numerator, $\int x'\eta(p_0, x')dx'$, is negative, in the range of available delays, and is divided by a small negative quantity. This makes the apparently "selected" delay to have a positive real part, outside the range of available delays.

This delay has no upper limit, as $\int \eta(p_0, x')dx'$ itself can take arbitrarily small values. Increasing the width of the forbidden region in the barrier increases the delay, but the probability amplitude of the transmitted particle decreases drastically.

The mechanism for the selected $\overline{x}'$ in Eq.(1.30) is similar to that of the "weak measurements" [22, 30, 38]. These are highly inaccurate measurements which do not destroy the interference of the probability amplitudes, in contrast to a strong measurement which results in a measured value, as in Eq.(1.32). Due to the Uncertainty Principle, this measurement cannot tell which of the eigenvalues the system has taken. The result of this weak measurement is not a single eigenvalue, but an interfering combination of all eigenvalues [23].

1.8 Pole representation

We have used a square potential in the numerical calculations of this chapter, as an illustrative example of the characteristics of superluminal tunnelling. The following chapters are devoted to examples of two different potentials, the Eckart potential and a zero-range potential, better suited for an analytical treatment. We now present the method of the pole representation, which gives an analytical expression for the amplitude distribution of the delays in Eq.(1.17), that allows us to study how the bound and resonant states of the potential affect the quantum scattering.

In order to evaluate the integral in Eq.(1.17), we can close the contour of the equation in the upper and lower half-planes of the complex k-plane, corresponding to $x' > 0$ and $x' < 0$ respectively, as shown in Fig.1.7. $\eta(p_0, x')$ is obtained by summing over all the contributions of the pole singularities of the transmission amplitude. For a barrier, all poles appear in the lower half-plane, corresponding to scattering resonances, since a potential barrier does not support bound states [39]. Closing the integral contour in the upper half-plane, corresponding to $x' > 0$, the integral is zero, since there are no singularities there. This is the reason why $\eta(p_0, x' > 0) = 0$ for barriers. In the case of a one-dimensional well always at least one bound state is supported [40], corresponding to poles in the upper half of the complex k-plane, and $\eta(p_0, x')$ is non-zero for all available delays x'.

$\eta(p_0, x')$ can be then computed from the poles using the Cauchy integral formula. We close anti-clockwise around the upper half-plane for bound states and

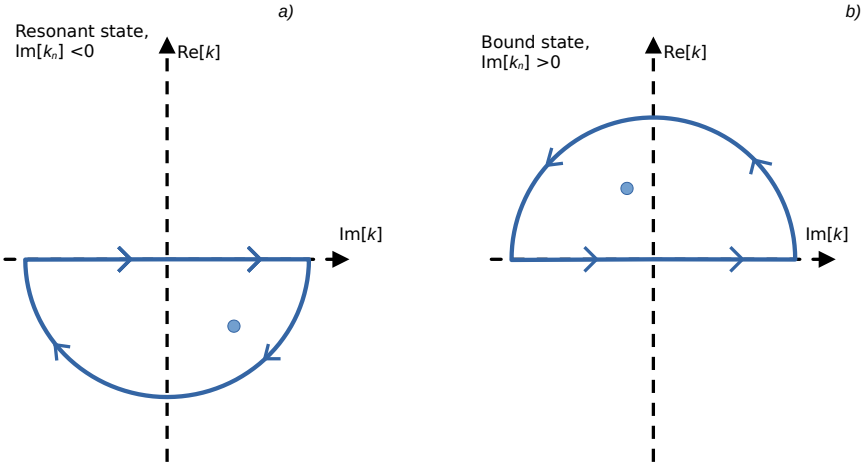

FIGURE 1.7: Contour integration around the poles in the complex k-plane a) for a resonant state, which is done clockwise, and b) for a bound state, which is done anti-clockwise.

clockwise in the lower half-plane, Fig.1.7. In the latter case a factor of (-1) has to be taken into account. This gives

$$\eta(p_0, x') = \delta(x') + i\exp(-ip_0x') \times \begin{cases} \sum_{n_B} \text{Res}(k_{n_B})\exp[ik_{n_B}x'], & x' > 0 \\ \sum_{n_R} -\text{Res}(k_{n_R})\exp[ik_{n_R}x'], & x' < 0, \end{cases} \tag{1.33}$$

where k_{n_B} and k_{n_R} are the poles corresponding to the bound and resonant states, respectively, n_R and n_B their total number and $\text{Res}(k_{B,R})$ the residue of the pole $k_{B,R}$. It is worth noting that the functions $T(p, V)$ and $T(p, V) - 1$ have the same poles, so we can separate the smooth part of the delay distribution and solve the integral for $\tilde{\eta}(p_0, x')$ with its corresponding residues, as in Eq.(1.33).

The result in Eq.(1.33) is a general and analytical expression, that gives an exact result as long as we are able to calculate the value of all the poles and their corresponding residues. In the case of barriers, there are no bound states. Thus, only the sum corresponding to the resonant states, for $x' < 0$, needs to be considered.

The contribution of each pole is a decaying exponential from $x' = 0$ to positive x', in the case of bound states, or to negative x', in the case of resonant states. The pole controls the decay, and each of these exponentials has a weight given by

its residue. We can integrate Eq.(1.33) to recover the transmission amplitude,now expressed as a function of the sum over the poles,

$$T(p,V) = 1 - \sum_{n_B} \frac{Res(k_{n_B})}{k_{n_B} - p} - \sum_{n_R} \frac{Res(k_{n_R})}{k_R - p}. \tag{1.34}$$

We can also explicitly write the transmitted WP from Eq.(1.20) using Eq.(1.33),

$$\begin{aligned} \Psi^T(x,t) = &\exp\left[ip_0 x - iE(p)t\right] \{G_0(x,t) \\ &+ i\sum_{n_B} \mathrm{Res}(k_{n_B}) \int_0^\infty G_0(x-x',t)\exp[i(k_{n_B}-p_0)x']dx' \\ &- i\sum_{n_R} \mathrm{Res}(k_{n_R}) \int_{-\infty}^0 G_0(x-x',t)\exp[i(k_{n_R}-p_0)x']dx'\}. \end{aligned} \tag{1.35}$$

The effect of each kind of pole on the delay of the transmitted WP is now clear. Bound states contribute to positively delayed envelopes, while resonant states contribute to negatively delayed ones. In the case of a well, both kinds of poles are present and, as we will see in the following chapter, positive delays dominate the behaviour. This is due to the fact that their corresponding residues have a higher value than those corresponding to the resonances. In the case of a barrier there are no bound states present, and therefore only envelopes delayed with respect to free propagation contribute to the transmitted WP.

This reshaping mechanism is consistent with the semiclassical case. We have seen from Eq.(1.3) that wells advance the transmitted WP. This can be understood as an effect of the bound states of the well. Equivalently, potential barriers delay the transmitted WP, where this negative delay appears as a result of the resonant states of the potential. In tunnelling, the advanced transmitted WP appears as a recombination of negatively delayed envelopes.

1.9 Error functions

Eq.(1.35) can be further developed analytically, evaluating the Gaussian integrals in terms of error functions [41]. From Eqs.(1.20) and (1.33) the transmitted

envelope for the case of a barrier, not containing any resonant states, is

$$G^T(x,t) = \exp\left[ip_0 x - iE(p)t\right]\left(\frac{2\Delta x^2}{\pi\Delta x_t^4}\right)^{(1/4)}\Big\{\exp[-(x-v_0t-x_0)^2/\Delta x_t^2] \quad (1.36)$$
$$-\,i\sum_{n_R}\mathrm{Res}(k_{n_R})\int_{-\infty}^{0}\exp[-(x-x'-v_0t-x_0)^2/\Delta x_t^2]\exp[i(k_{n_R}-p_0)x']dx'\Big\}.$$

The integral can be rearranged as

$$\begin{aligned}&\int_{-\infty}^{0}\exp[-(1/\Delta x_t^2)x'^2 + (ik_{n_R} + 2(x-v_0t-x_0)/\Delta x_t^2)x' \qquad (1.37)\\ &-(x-v_0t-x_0)^2/\Delta x_t^2]dx'\\ \equiv&\frac{\exp[b^2/4a+c]\sqrt{\pi}(1-\mathrm{erf}[b/2\sqrt{a}])}{2\sqrt{a}},\end{aligned}$$

where $a = (1/\Delta x_t^2)$, $b = (ik_{n_R} + 2(x-v_0t-x_0)/\Delta x_t^2)$, $c = -(x-v_0t-x_0)^2/\Delta x_t^2]$ and erf is the error function, $\mathrm{erf}(z) = 2/\sqrt{\pi}\int_0^z e^{-t^2}dt$.

For a well, Eq.(1.36) also includes terms with an integral from 0 to ∞, which can be evaluated in a similar manner,

$$\int_0^{\infty}\exp[-ax'^2 + bx' - c]dx' = \frac{\exp[b^2/4a+c]\sqrt{\pi}(1+\mathrm{erf}[b/2\sqrt{a}])}{2\sqrt{a}}. \qquad (1.38)$$

The final expression, for both barriers and wells, is

$$\begin{aligned}G^T(x,t) =& \exp[-ip_0x]\left(\frac{2\Delta x^2}{\pi\Delta x_t^4}\right)^{(1/4)}\times \qquad (1.39)\\ &\times\left(\sum_n C_n\frac{\exp\left[\frac{b^2}{4a}+c\right]\sqrt{\pi}(1-\mathrm{sign}(\mathrm{Im}(k_n))\mathrm{erf}\left[\frac{b}{2\sqrt{a}}\right])}{2\sqrt{a}}\right.\\ &\left.+\exp\left[\frac{-(x-v_0t-a)^2}{\Delta x_t^2}\right]\right),\end{aligned}$$

where C_n is the residue of the pole k_n, whether it corresponds to a bound or a resonant state. From this expression we can write, as before, the transmitted WP

as

$$\Psi^T(x,t) = \exp[ip_0x - iE(p_0)t]G^T(x,t). \tag{1.40}$$

1.10 Conclusions and discussion

1.10.1 Phase time and weak measurements

We have seen that a scattering process is related to the recombination of envelopes evolving through several different paths. Each of these scenarios has a different spatial delay associated with it. Thus, the incident WP is "separated" into differently delayed envelopes which interfere to form the transmitted particle. In the classical case, the interference is destructive for most of the interfering envelopes, and only a single envelope, with a delay given by Eq.(1.11), is selected as a result of the recombination. This does not happen in the tunnelling case, as the interference between delays remains intact.

If we want to measure experimentally a duration of the WP in the barrier we can take one of two approaches. We can measure the spatial delay δx_{COM}, Eq.(1.5), measuring the position of several transmitted WPs with and without the potential, at a time t large enough so that the scattering has already taken place. With enough of these measurements, we can obtain the delay $\tilde{x}'$ directly as the difference of the COMs of the transmitted and free WPs. Alternatively, we can place a fixed detector to the right of the barrier and obtain the detection time.

In a classically allowed transmission we have for this detection time

$$\delta\tau^{classical}(p_0) = \tau^T(p_0) - \tau^0(p_0) = -\tilde{x}'/v_0, \tag{1.41}$$

where the spatial delay is that obtained in Eq.(1.11).

We can do the same to measure the tunnelling delay. We know, from Eq.(1.14), that the transmitted WP has increased its mean velocity. In order to obtain a delay related to the time spent in the barrier, and not due to the acceleration

after transmission, we compare the transmitted particle with a freely propagating one with a mean momentum $p_0 + \delta p_0$. The detection time is therefore

$$\delta\tau^{tunnel}(p_0) = \tau^T(p_0) - \tau^0(p_0 + \delta p_0) = -\mathrm{Re}\left[\tilde{x}'\right]/v_0. \tag{1.42}$$

Although the analytical semiclassical delay is complex, Eq.(1.12), experimentally its real part of can be measured as a spatial delay.

The interpretation of the classical duration of Eq.(1.41) is straightforward, as the particle speeds up or slows down in the potential, resulting in a spatial shift. This interpretation cannot be applied to the measured duration in Eq.(1.42). As we have seen, this duration, like the measured spatial delay of a tunnelled particle, is not related to a single trajectory inside the potential, a single transmitted envelope that speeds up or slows down crossing the potential. Instead, it is an interference of all the available delays, of all the weighted delayed envelopes. Even though we can experimentally measure the instantaneous position [15] and, from it, following Eq.(1.42), relate the particle's position to a detection time, this can only be done *after* the scattering has already taken place. We cannot deduce the time taken by the particle to pass through the potential, as this information remains "hidden" by the Uncertainty Principle [25], just as we cannot know which slit the particle has passed through in the double-slit experiment.

We can rewrite Eq.(1.42) as

$$\delta\tau^{tunnel} = -\frac{1}{v_0}\,\partial_k\Phi(k,V)\big|_{k=p_0} = \partial_E\Phi(k,V). \tag{1.43}$$

This is a phase time, the Eisenbud-Wigner-Smith (EWS) time delay [8–10], which is one of several attempts to define a tunnelling time [6, 7]. We will return to the attempts to define a tunnelling time in **Chapter 3**, and compare the EWS approach with a Larmor clock approach [31].

The Eisenbud-Wigner-Smith phase time in Eq.(1.43) involves a quantum weak measurement of a time shift [30], and one has to be careful to treat it as a physical duration in the barrier, as it leads to a contradiction. The anomalous superluminal

value of the phase time for tunnelling only indicates that the interference between the delays has not been destroyed, as it would in a usual, strong, measurement, but says nothing about what happened inside the potential [22]. Any measurement in which the interference is not destroyed leads to inconsistent results [24]. Therefore, the result from Eq.(1.42) should not be interpreted as the actual time spent in the barrier.

1.10.2 Superluminal delays and causality

The transmitted WP gives information about the spatial delay, but does not say much about the nature of this delay. Alternatively, one can study the reshaping mechanism behind the transmitted WP. This is formed by the sum of freely propagating interfering envelopes, each with a given delay and complex weight. In Section 1.5 we presented a distribution for the delays of the interfering envelopes, and studied its relation with the apparent superluminal tunnelling delay studied in the following Sections.

With this approach, we obtain that the anomalous value of the delay of the classically forbidden transmission appears as the real part of the first moment of this delay distribution, Eq.(1.29), which is an alternating one. The oscillatory nature of this distribution may give values outside the range of available delays, as happens for tunnelling through a barrier. In this case, all the interfering envelopes are negatively delayed, but the reshaping mechanism makes the transmitted WP to appear ahead of the free one. The apparent delay is not bounded, and thus can take extremely large values.

At first glance, the superluminal nature of the delays seems to contradict Einstein's special relativity, since its velocity is not bounded. For wide enough barriers, the velocity inside the potential region can take values larger than the speed of light, or even an infinite value, as in the case of the apparent "instantaneous" transmission in Section 1.4. This would be true if the transmitted WP was an advanced copy of the incident one, shifted to the right a certain distance and with

the same probability amplitude. But the actual transmitted WP undergoes a reshaping process in the barrier, it is formed as the constructive interference of the front tails of the negatively delayed envelopes. This reshaping mechanism forbids the transfer of information ahead of the freely propagating particle.

As an example of the causal transfer of "information", one could cut the rear tail of the incident WP and place a detector to the right of the barrier, to see when the information about the cut arrives. From Eq.(1.16), we see that the front tails would interfere constructively and produce a whole transmitted WP, with front and rear tails [34]. The information about the cut will only arrives when the COM of the first envelope, the freely propagating one, arrives at the detector, and thus there is no causality violation.

Although we are considering here non-relativistic Schrödinger particles, which do not take special relativity into account, the superluminal effect persists when a proper relativistic transmission is considered (see for example [12]).

1.10.3 Bound and resonant states

Finally, we have obtained the delay distribution and the transmitted WP in terms of the bound and resonant states of the potential, Eqs.(1.33) and (1.35) respectively. As we have seen, the superluminal shift of the transmitted WP appears as a result of a very delicate interference of the delay distribution. This is formed by decaying exponentials, related to these bound and resonant states through their residues. The bound states are related to advanced envelopes, while resonant states are related to delayed envelopes.

In the following chapters we will consider two potentials that can be treated analytically, the Eckart potential and a zero-range potential. We will study there, in more detail, the mechanism behind the delay distribution, the role played by the different kind of poles and the effect they have on the transmission and the appearance of the anomalous spatial delays discussed in this chapter. We will see this that method is specially useful in low-energy scattering through shallow wells or low barriers, where few poles dominate the transmission.

Chapter 2

Eckart potential

The transmission of Gaussian wave packets through a one-dimensional smooth Eckart potential is discussed in detail. The effect of the poles of the transmission amplitude on the position of the transmitted particle is analysed. The advance or delay experienced by the transmitted particle relative to a freely propagating one is related to the support of bound, resonant or virtual states in the scattering potential. The pole representation of the delay distribution and its limits are studied for the cases of barriers and wells. This representation is found to be more useful in the cases of low-energy scattering on low barriers and shallow wells.

2.1 Introduction

In the previous chapter we have studied the apparent "superluminal" tunnelling time, a quantum scattering effect. This situation is an example where the classical analysis fails, and one has to rely on a pure quantum approach. Although the anomalous delays that occur are one of the most interesting quantum features, there are other situations where the classical analysis fails, such as, low-energy scattering by a shallow well or a low potential. In these cases, only a few bound or resonant states determine the scattering.

In Section 1.8 we introduced the pole representation. This helped us to describe the delay distribution and the evolution of the WPs in terms of the singularities of the transmission amplitude. This approach was applied to the tunnelling-time problem, previously discussed in [34].

This method is not suitable for the square potential. Therefore, in this chapter we present the Eckart potential [40], a one-dimensional smooth potential, which can be further developed using the pole representation, and analysed in some different scenarios, to see how the different poles affect the transmission of a WP.

The chapter is organised as follows. In Section 2.2 we briefly introduce the Eckart potential. The tunnelling delays obtained in Sections 1.3 and 1.4 are derived in Section 2.3 for the Eckart potential. We compare the results with those seen in Section 1.6. In Section 2.4 we obtain the pole representation of the Eckart potential, writing the WP in terms of bound and resonant states. We also introduce the residues of the poles, which play an important role in the delay distribution, and show the behaviour of these residues for high barriers or deep wells. In Section 2.5 we focus on an Eckart well, and show how the bound states determine the transmission, with special attention to shallow wells. In Section 2.6 we analyse the Eckart barrier, and show that not all the poles are needed to calculate the transmitted WP. Low barriers are studied in detail. The conclusions for the chapter appear in Section 2.7.

2.2 Transmission through an Eckart potential

We consider an Eckart potential [40], a one-dimensional smooth potential,

$$V(x) = \frac{V_0}{\cosh^2(\alpha x)}, \tag{2.1}$$

where V_0 determines the strength of the potential, and α^{-1} is its width, Fig.2.1. This potential is a barrier or a well depending on the sign of V_0.

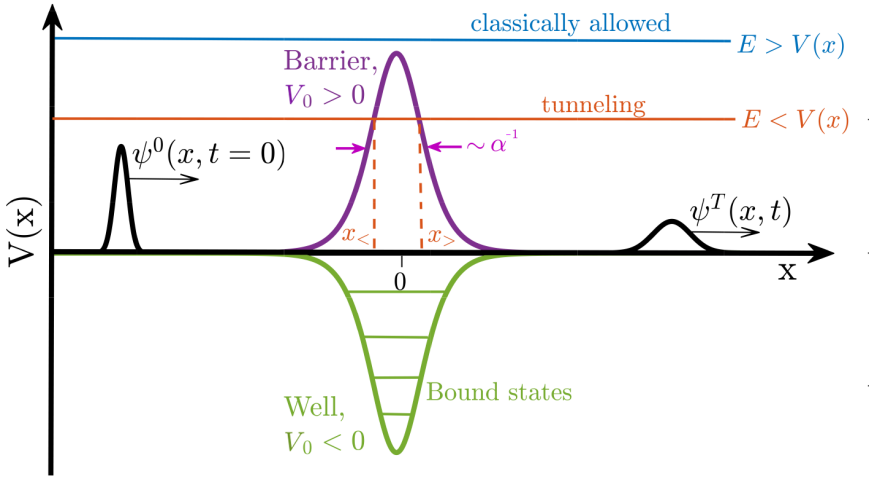

FIGURE 2.1: An incident WP, $\psi^0(x, t = 0)$, over an Eckart potential, barrier or well, with height V_0, and the transmitted WP, $\psi^T(x, t)$. The width of the barrier is controlled by the parameter α^{-1}. The energies for classically allowed and tunnelling transmissions are also shown, and in the latter case the turning points, $x_<$ and $x_>$, are marked.

The transmission amplitude of the Eckart potential is known to be [40],

$$T(p, V) = \frac{\Gamma(-ip\alpha^{-1} - s)\Gamma(-ip\alpha^{-1} + s + 1)}{\Gamma(-ip\alpha^{-1})\Gamma(1 - ip\alpha^{-1})}, \tag{2.2}$$

where $\Gamma(z)$ is the Gamma function [41], s is given by

$$s = \frac{1}{2}\left(-1 + \sqrt{1 - \frac{8\mu V_0}{\alpha^2}}\right), \tag{2.3}$$

μ is the particle's mass and we have used $\hbar = 1$. The parameter s is real for $V_0 \leq \alpha^2/8\mu$, which corresponds to wells and low barriers, and complex for high barriers, $V_0 > \alpha^2/8\mu$. It is worth noting that this change from a real to a complex

s does not occur between wells and barriers, since low barriers have a real s. The transmission amplitude in Eq.(2.2) satisfies $T(-p^*, V) = T^*(p, V)$.

For the numerical results shown in this chapter dimensionless variables are used, taking as a reference the barrier's width α^{-1} and $\hbar = 1$,

$$X = x\alpha, \quad P = p\alpha^{-1}, \quad T = t\alpha, \quad W = V_0\alpha^{-1}, \quad M = m\alpha^{-1}. \tag{2.4}$$

2.3 Delays

First, we extend the semiclassical results for the delays obtained in Sections 1.3 and 1.4 to the Eckart potential, using the Gaussian WP given by Eqs.(1.1) and (1.4). The delay, positive or negative, of the transmitted WP relative to free propagation is calculated as the spatial distance between their COMs, Eq.(1.5). We consider very wide WPs, so that the results from Chapter 1 are valid here.

The semiclassical condition gives

$$1/\min[q(x,p)] \ll 1/\alpha, \tag{2.5}$$

where $q(x,p) = \sqrt{p^2 - 2\mu V(x)}$ is the WP's momentum inside the potential region.

For the semiclassical expansion in Eq.(1.9) to be valid up to first order, we need that the sum $\sum_{n=2}^{\infty} \partial_p^n \Phi(p_0, V)(p-p_0)^n/n! \ll 1$. The derivatives of the phase scale as α^{-n}. Thus, we need that $(p-p_0)^n \ll \alpha^{-n}$ for the sum to be negligible. Since $(p-p_0) \sim \Delta p \sim 1/\Delta x$, this is satisfied for wide WPs in coordinate space, which is equivalent to narrow WPs in momentum space. This condition and Eq.(2.5) will be satisfied for the parameters taken here since we consider wide WPs.

Fig.2.2 shows two cases, *a*) a WP transmitted across a well and *b*) over a barrier. The WP over a well is advanced relative to a freely propagating one, because, since it goes faster over the potential, while in the case of the barrier this delay is negative, since the positive potential slows the particle down.

These delays, in this semiclassical case, can be computed directly from the difference between the velocity of free motion and the velocity of the WP inside the potential, as in Eq.(1.11). For a particle going over the well (Fig.2.2 *a*)) we obtain, in dimensionless units, $\tilde{X}' = 0.6931$, which is consistent with the delay $\delta X_{COM} = 0.6931$, by numerically integrating the WPs from Eqs.(1.1) and (1.4). In the case of the particle going over the barrier (Fig.2.2 *b*), $\tilde{X}' = -0.6931$, while the numerical delay is $\delta X_{COM} = -0.6932$.

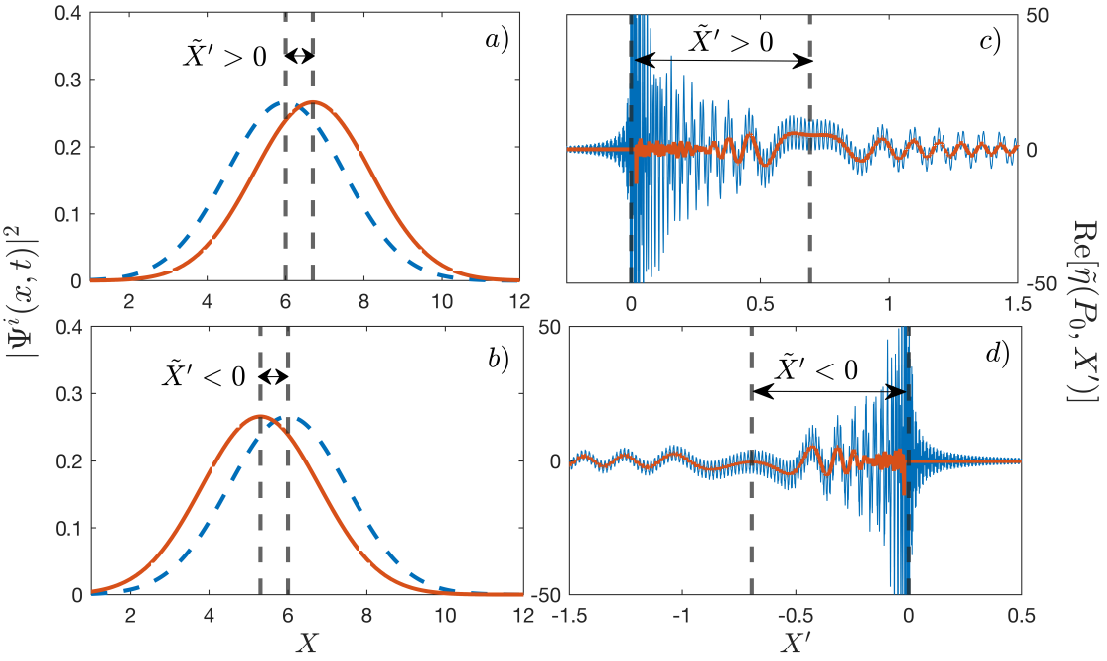

FIGURE 2.2: *a*) Transmitted WP over an Eckart well, (red solid line) for $W = -2 \times 10^4$, $P_0 = 200$, $\Delta P = 0.67$, $X_0 = -4$ and $T = 0.05$. Also shown, the freely propagating counterpart (blue dashed line). *b*) Same as *a*) but for an Eckart barrier with $W = 10^4$. In this case, as expected, the particle is delayed. *c*) and *d*) show $\mathrm{Re}\left[\tilde{\eta}(P_0, X')\right]$ (blue solid line) and its average, $\mathrm{Re}\left[y^{-1}\int_{X'}^{X'+y}\tilde{\eta}(P_0, X'')dX''\right]$ (red solid line) for the cases *a*) and *b*), respectively. The stationary region, which corresponds to the real delay, is marked.

The real part of $\tilde{\eta}(p_0, x')$, Eq.(1.17), is shown in Fig.2.2 *c*) for a well and in *d*) for a barrier. These are computed numerically, integrating Eq.(1.17). Although we should have $\tilde{\eta}(P_0, X' < 0) \sim 0$ for wells and $\tilde{\eta}(P_0, X' > 0) = 0$ for barriers, this is not exactly the case in the figures due to numerical inaccuracies. Nevertheless, the part of the peak at $X' \sim 0$ not shown in the figures has a value of $\tilde{\eta}(p_0, x') \sim 800$, making the errors to be negligible in comparison.

As we saw in Section 1.6, the delay of the semiclassical transmitted particles appears as a stationary region in the real axis $\tilde{X}'$, Fig.2.2 *c*) and *d*). As with the square potential, some fast oscillations appear superimposed on the stationary region.

The case of tunnelling is shown in Fig.2.3. Since most of the incident particles are reflected, the transmitted WP is enhanced in the figure for better viewing. The WP is reduced by, approximately, $|T(P_0)|^2 = 3.44 \times 10^{-250}$. Numerically, we find its total probability to be $\int |\Psi^T(x,t)|^2 = 7.57 \times 10^{-250}$. Again, these extremely small values for transmittance are impractical, but we are interested in the principle here.

Fig.2.3*a*) shows the advanced transmitted WP. The positive delay is due to the real spatial delay $\tilde{X}_1'$ and the momentum filtering, Eq.(1.12). In Fig.2.3*b*) the real part of $\tilde{\eta}(p_0, x')$ is shown. There is no stationary region on the real axis X'. The delay distribution oscillates rapidly for $\tilde{X}' < 0$. Nevertheless, if we evaluate the real part of this complex delay, $\tilde{X}_1'$ from Eq.(1.12), corresponding to the real spatial delay, we obtain $\tilde{X}_1' = 1.9455$. Taking into account the momentum filtering we obtain a total delay of $\tilde{X}_1' + \delta V_0 T = 3.1937$, close to the numerically computed delay, $\delta X_{COM}(T) = 3.1910$.

The turning points for the parameters of Fig.2.3 are $X_{<,>} = \mp 1.7$. Thus, the classically forbidden region is $X_> - X_< = 3.4 > \tilde{X}_1'$. As the potential is smooth, the WP slows down before and after the turning points. Due to this effect, the delay $\tilde{X}_1'$ is smaller than the width of the classically forbidden region.

2.4 Pole representation of the Eckart potential

The poles of the transmission amplitude are obtained directly from Eq.(2.2), since the Gamma function $\Gamma(z)$ has simple poles located at $z = -n, \quad n = 0, 1, 2, ...$ These poles fall into two categories,

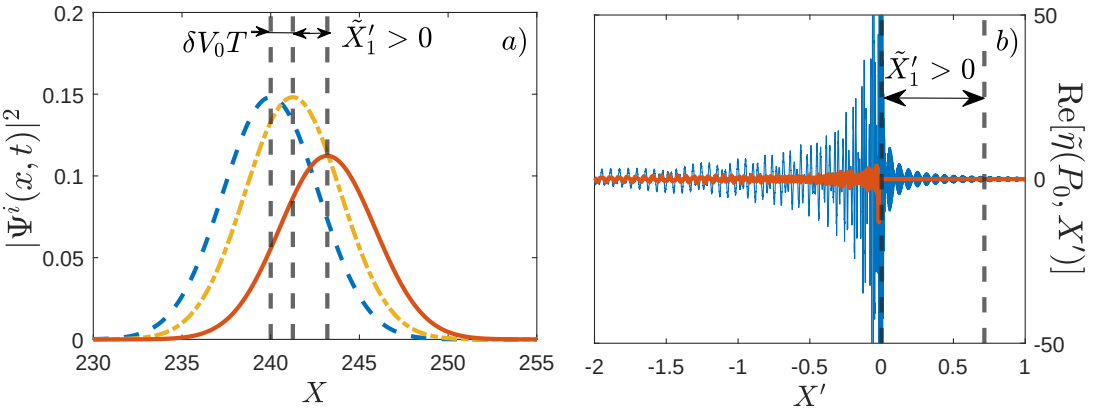

FIGURE 2.3: *a*) tunnelled WP (red solid line) (multiplied by $z = 10^{249}$ for better viewing) across an Eckart barrier, with $W = 10^4$, $P_0 = 50$, $\Delta P = 0.4$, $X_0 = -10$ and $T = 5$. Freely propagating WPs with mean momenta P_0 (blue dashed line) and $P_0 + \delta P_0$ (yellow dot dashed line) are shown. Figure *b*) shows $\mathrm{Re}\left[\tilde{\eta}(P_0, X')\right]$ (blue solid line) and its average, $\mathrm{Re}\left[y^{-1}\int_{X'}^{X'+y}\tilde{\eta}(P_0, X'')dX''\right]$ (red solid line). The value for the real delay $\tilde{X}_1'$ is also shown. This value falls outside the range of available delays.

$$\left.\begin{aligned} k_n^I &= -i\alpha(n-s) \\ k_n^{II} &= -i\alpha(n+s+1) \end{aligned}\right\} n = 0, 1, 2, ... \tag{2.6}$$

The behaviour of the poles differs between barriers and wells. s is real for wells and very low barriers, with $V_0 < \alpha^2/8\mu$, and complex for barriers with $V_0 > \alpha^2/8\mu$. For any barrier, both kinds of poles will appear in the lower half-plane, symmetrically located around the negative imaginary axis, Fig.2.4*a*). They correspond to scattering resonances (R).

Although still a barrier, for $\alpha^2/8\mu < V_0 < 0$, corresponding to a real s, $-1/2 < s < 0$, the poles have no imaginary part, Fig. 2.4*b*). As $V_0 \to 0$, the pole $k_0^I \to 0$, corresponding to a virtual state. These are long-lived states, [39], and we will discuss their effect on transmission further in the following section. The first bound state will emerge for $V_0 = 0$, corresponding to $s = 0$.

In the case of a well, all the poles lie on the imaginary axis, with a finite number of the poles of the first kind, k_n^I, appearing on the positive half-axis, corresponding

to bound states (B), Fig.2.4*c*). The number of bound states is controlled by s. For $M < s < M+1$, with M integer, there will be $M+1$ bound states. The rest of the poles of both kinds will again correspond to resonant states. For any depth of the potential well at least one bound state is supported [40].

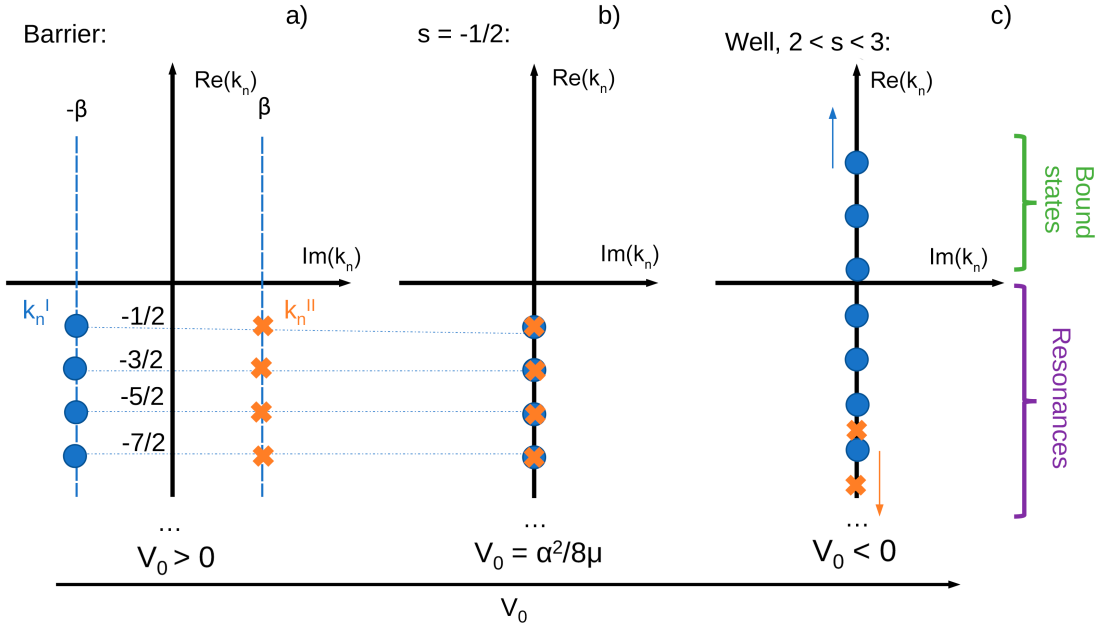

FIGURE 2.4: Poles of the transmission amplitude, of the first kind (blue circles) and second kind (red crosses) for three different scenarios; a) in the case of a barrier, b) for $s = -1/2$, in which the poles are purely imaginary but there are not bound states yet, and c) in the case of a well with three bound states. $\pm\beta$ is the real part of the complex poles of a barrier.

In general, the poles are of order 1.When s is an integer or half integer, the poles of the well coalesce into the same value, making them double poles. This situation will be treated in more detail in Section 2.5.3. For now, we focus on the general case of the simple poles. Their residues can be computed using the Cauchy differentiation formula for a simple pole of a Gamma function, using that $\Gamma(z+1) = z\Gamma(z)$,

$$\begin{aligned} \mathrm{Res}(\Gamma(z), z=-n) &= \lim_{z\to -n}(z+n)\Gamma(z) \\ &= \lim_{z\to -n}(z+n)\frac{\Gamma(z+n+1)}{z(z+1)\times ...\times (z+n)} = \frac{(-1)^n\Gamma(1)}{n!} = \frac{(-1)^n}{n!}. \end{aligned} \tag{2.7}$$

In the Gamma functions of Eq.(2.2) we have $-ip/\alpha$ instead of p so, to compute the total residue, we can make a change of variables, from which we get a factor

$\alpha/-i$. The residues for both kinds of poles are

$$\begin{aligned} \text{Res}(k_n^I) &= \frac{\alpha}{-i}\frac{(-1)^n}{n!}\frac{\Gamma(-ik_n^I/\alpha+s+1)}{\Gamma(-ik_n^I/\alpha)\Gamma(-ik_n^I/\alpha+1)}, \\ \text{Res}(k_n^{II}) &= \frac{\alpha}{-i}\frac{(-1)^n}{n!}\frac{\Gamma(-ik_n^{II}/\alpha-s)}{\Gamma(-ik_n^{II}/\alpha)\Gamma(-ik_n^{II}/\alpha+1)}. \end{aligned} \tag{2.8}$$

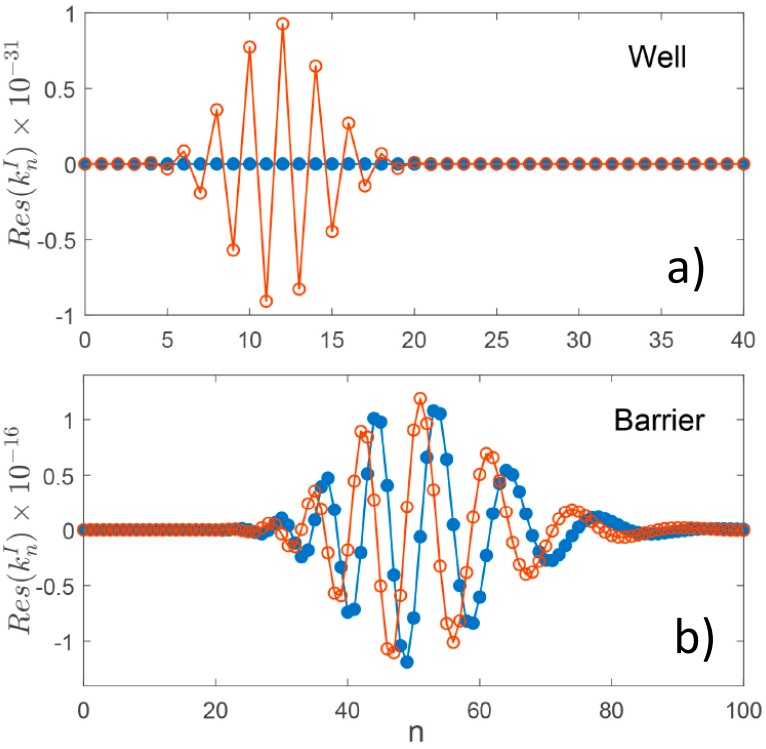

FIGURE 2.5: Real (blue closed circles) and imaginary (red open circles) parts of the residues of *a*) an Eckart well with $W = -861$, $s = 41$, supporting 42 bound states and *b*) an Eckart barrier with $W = 2485$, $s \approx -0.5 + 70,5i$.

From here, we can calculate the amplitude distribution of the delays using Eq.(1.33) and the transmitted WP with Eq.(1.35). In the following sections we will study the effect of the poles on the scattering. To do so, we numerically compute the residues from Eq.(2.8). Note that these numerical calculations are done with Matlab, and due to the high values of the Gamma functions involved in the residues for large n, some approximations need to be made. This is explained in Appendix F.

The pole representation becomes impractical for these semiclassical cases. Fig.2.5 shows the residues for two examples, a deep well in *a*) and a high barrier in *b*). These are classical or semiclassical cases. We will see, in Figs.2.6 and 2.9, that the

value of some of these residues is much higher than the delay distribution itself. This happens for some of the first values, as for higher n than those shown, the value of the residues decrease. The value of these high residues is also seen to oscillate. These oscillations make the consecutive contributions of each pole to cancel each other and reduce the value of the sum. The same effect can be seen in [34]. The amount of very accurate cancellation needed in order to recover the correct distribution of delays becomes prohibitive for the approximations used. The pole representation will prove to be much more useful for smaller $|V_0|$. In these cases, only a few poles are needed in order to describe the transmission.

2.5 Eckart well

For $V_0 < 0$, the poles are purely imaginary and align along the imaginary axis, moving in opposite directions as the well deepens. k_n^I moves upwards to positive imaginary values, while k_n^{II} moves downwards (see Fig.2.4*c*)). For wells there is always at least one pole k_n^I with a positive value, corresponding to a bound state. The number of bound states is determined by s, which is real. For $M < s < M+1$, $M = 0, 1, 2, ...$, there are $M + 1$ bound states.

Since s is real, the Γ functions in the residues, Eq.(2.8), are real and thus the residues are pure imaginary.

2.5.1 Cancellation of residues for deep wells

For very deep wells, the residues become huge, many orders of magnitude larger than $\tilde{\eta}(p_0, x')$, and show an oscillatory behaviour. These oscillations ensure that when all the decaying exponentials are summed, most of their contribution to $\tilde{\eta}(p_0, x')$ will cancel out (Fig.2.6). Note the different scale between each individual contribution, which may reach 10^{14} near $x' = 0$ in the case shown, and the final $\tilde{\eta}(p_0, x')$, which is of order $\sim 10^2$.

From this figure we also notice that most of the contributions to $\tilde{\eta}(p_0, x')$ come from the bound state poles, that will dominate the scattering. The delay distribution, taking into account these poles, is exactly 0 for $X' < 0$, since all the contributions from the bound states are for positive delays (Fig.2.6*c*) and *d*)). If we also consider the resonant states, we obtain a region of non-zero $\tilde{\eta}(p_0, x')$ for $X' < 0$ (Fig.2.6*d*)). However, the resonant states contribute with a peak orders of magnitude smaller that the part of the delay distribution that lies on positive X'.

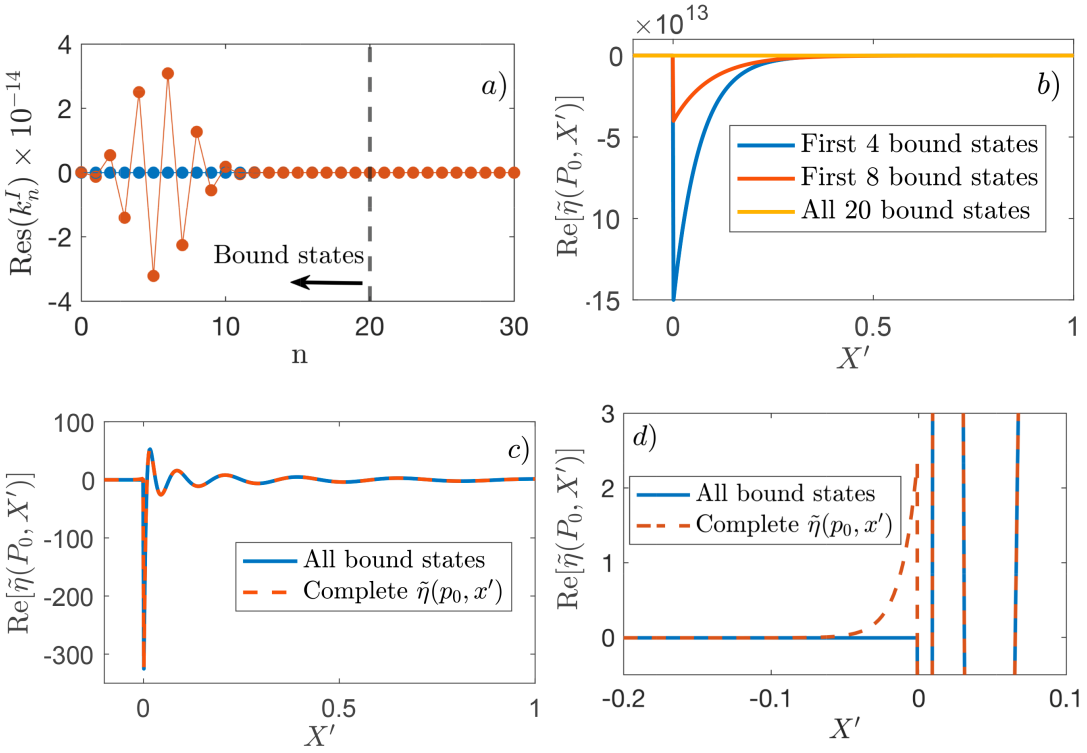

FIGURE 2.6: For $W = -200$, $s = 19.5062$ there are 20 bound states, figure *a*). Figure *b*) shows $\mathrm{Re}[\tilde{\eta}(P_0, X')]$ calculated with the first 4 bound states (blue solid line), the first 8 bound states (red solid line) and all the 20 bound states (yellow solid line). Figure *c*) shows the real part of $\tilde{\eta}(p_0, x')$ computed only with the bound states (blue solid line) and with the complete poles (red dashed line). Figure *d*) is a zoom of *c*). It shows the difference between only taking into account only bound states to compute $\tilde{\eta}(P_0, X')$ and considering also resonant states.

2.5.2 Integer s

As the well deepens, the poles k_n^I move upwards along the imaginary negative k-axis and k_n^{II} downwards. From Eq.(2.6) we have that $(-i/\alpha)(k_n^{II} - k_n^I) = 2s + 1$.

Thus, if s is an integer or half integer both kind of poles will coalesce. We start with the case of an integer s, $s = M$.

For this value of s, the potential is $V_0 = -\alpha^2 M(M+1)/2\mu$ and the pole k_M^I lies just at 0. It is about to become a bound state, but it is not one yet. This pole does not contribute, because its residue is

$$\mathrm{Res}(k_M^I) \sim \lim_{-n+s\to 0} \frac{\Gamma(-n+2s+1)}{\Gamma(-n+s)\Gamma(-n+s+1)} \to \frac{s!}{\infty \times 1} = 0. \tag{2.9}$$

The rest of the resonant states residues are zero, since both Γ functions in their denominator become infinite. Therefore, for integer s $\eta(p_0, x' < 0) = 0$. The transmission is exactly determined only by the bound states. The delay amplitude is now a finite sum over the bound states,

$$\eta(p_0, x') = \delta(x') + i\exp(-ip_0 x') \times \begin{cases} \sum_{n_B} \mathrm{Res}(k_{n_B}) \exp[ik_{n_B} x'], & x' > 0 \\ 0, & x' < 0, \end{cases} \tag{2.10}$$

with $k_{n_B}^I = i\alpha(M-n)$ and

$$\mathrm{Res}(k_{n_B}^I) = (-1)^n i\alpha \frac{(2M-n)!}{n!(M-n)!(M-n-1)!}. \tag{2.11}$$

In this case, we also have that $|T(p,V)| = 1$ (see Appendix G). This implies that, when a new bound states enters the well, there is perfect transmission. The transmitted WP is advanced and has the same amplitude as the incident one. A case with integer s is shown in Fig.2.7.

2.5.3 Semi-integer s

In the case where s is a semi-integer, $s = M + 1/2$, $M = 0, 1, 2, ...$, we need to consider the resonant states. There are $2M+2$ simple poles of k_n^I, $M+1$ in the positive half-plane of $\mathrm{Im}(k)$, corresponding to bound states, and $M+1$ in the negative one, corresponding to resonant states. All poles in the negative half-plane

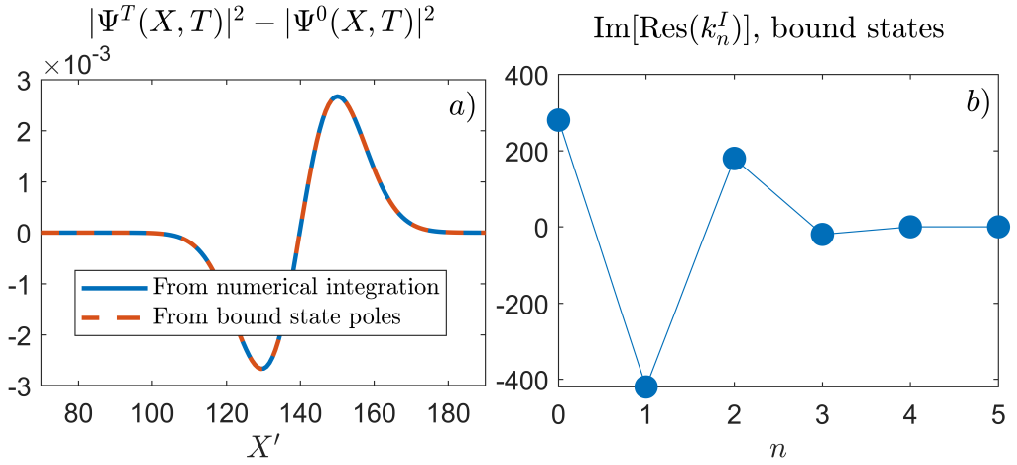

FIGURE 2.7: For a well with $W = -10$, $s = 4$ and thus 5 bound states, *a*) difference between transmitted and freely propagating WP, with the WPs computed as a numerical integration over the momentum (blue solid line) and from the 5 bound states, using Eq.(2.10) (red dashed line). *b*) shows the residues for these bound states, which are pure imaginary values.

$\mathrm{Im}(k)$, for $n > 2M+2$, are double poles, since k^I_{n+2M+2} and k^{II}_n have the same value for all $n > 2M+2$.

For the simple poles, Eq.(2.8) is still valid. For the double poles we use Cauchy's differentiation formula and obtain (see Appendix H)

$$\begin{aligned} &\mathrm{Res}_2(k^I_{n+2M+2}) = \mathrm{Res}_2(k^{II}_n) = \\ =&\frac{-2\alpha^2}{n!(n+2M+2)!}\left(\sum_{k=1}^{k=n}\frac{1}{k} + \sum_{k=n+1}^{k=n+2M+2}\frac{1}{2k} - \gamma(1)\right)\times \\ &\times\frac{1}{\Gamma(-n-M-3/2)\Gamma(-n-M-1/2)}, \end{aligned} \tag{2.12}$$

where $\gamma(1) \approx 0.5772$ is the Euler-Mascheroni constant [41]. Therefore, we finally obtain

$$\eta(p_0,x') = \delta(x') + i\exp(-ip_0x')\times\begin{cases} \sum_{n=0}^{M} Res(k^I_n)\exp(ik^I_n x'), & x' \geq 0 \\ \left[\sum_{n=M+1}^{2M+1} Res(k^I_n)\exp(ik^I_n x') + \right. & \\ \left.\sum_{n=2M+2}^{\infty} Res_2(k^I_n)\exp(ik^I_n x')\right], & x' < 0. \end{cases}$$

The coalescence of the poles does not change the general mechanism of transmission. As in the general case, the residues corresponding to bound states dominate, and make the main contribution to the final transmitted particle.

2.5.4 Shallow well

The pole expansion is more useful for shallow wells, since the residues are small, and only the few bound states present, which can be easily computed, determine the whole transmission.

We consider a well with a value of s close to an integer M, this is, $|s-M| \ll 1$. This corresponds to the case of a bound state about to emerge or having just emerged. We can write $\eta(p_0, x')$ considering only this state and the rest of the few bound states. Using $1/\Gamma(s-M \to 0) = s-M$,

$$\eta(p,x') \approx \delta(x') + \sum_{n=0}^{M-1} i\, \frac{\alpha(-1)^n(2M-n)!}{n!(M-n-1)!(M-n)!} \times \exp\{-\left[\alpha(M-n)+ip\right]x'\}\theta(x') \tag{2.13}$$

$$+ i\frac{\alpha(-1)^M(2M-1)!}{M!(M-1)!}(s-M)\exp\{-\left[\alpha(s-M)+ip\right]x'\}\times$$

$$\times\,[\theta(x')\theta(s-M)+\theta(-x')\theta(M-s)].$$

We assume now that the momentum of the incident WP is very small, $p/\alpha \ll 1$. Integrating Eq.(2.13) to obtain the transmission amplitude, we have

$$T(p,V) \approx \exp[i\Theta(p)] - \frac{(-1)^M(2M-1)!}{M!(M-1)!}\frac{(s-M)}{(s-M)+ip/\alpha}, \tag{2.14}$$

where

$$\Theta(p) = -i\ln\left\{1 - \sum_{n=0}^{M-1}\frac{(-1)^n(2M-n)!}{n!(M-n-1)!(M-n)!}\frac{1}{(M-n)+ip/\alpha}\right\}. \tag{2.15}$$

The last term in Eq.(2.14) is a Breit-Wigner term, that causes $|T(p,V)|$ to be peaked around $s = M$ with a width $2p/\alpha$. This term becomes larger as p/α becomes smaller, and it is the main contribution around $s \sim M$. The centre-of-mass delay, taking into account the momentum filtering, is given by

$$\delta x^T_{COM}(t) - \delta v_0 t \approx \frac{\alpha(s-M)}{\alpha^2(s-M)^2 + p_0^2} - \partial_p \Theta(p_0). \tag{2.16}$$

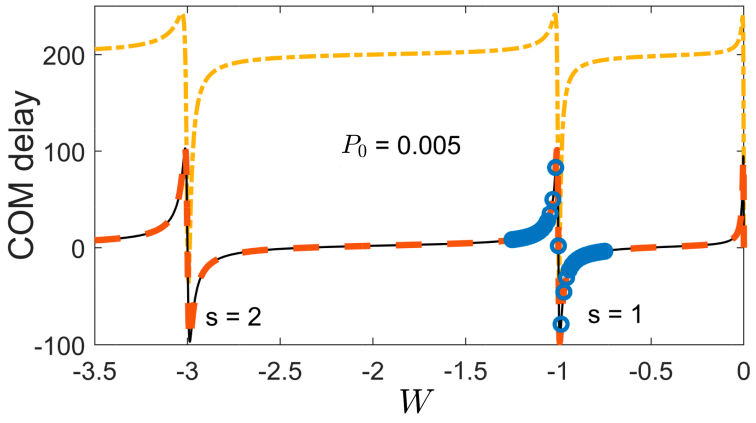

FIGURE 2.8: COM delay for an incident particle with $P_0 = 0.005$, $\Delta P = 0.001$, $X_0 = -3\times10^3$ and $T = 2\times10^6$, for a potential W from -3.5 to 0. We show the delay computed with Eq.(1.29) (black solid line), numerical integration of the WP, with no momentum filtering (yellow dashed line) and taking into account it (red dashed line), and with Eq.(2.16) for $M = 1$ (blue dots).

As an example, we calculate the case of $M = 1$ in Eq.(2.16) and compare it with the delays obtained with Eq.(1.29), Fig.2.8. We see from the expressions above that the largest advance occurs for $s = 1 + p_0/\alpha$, with $\delta x^T_{COM}(t) - \delta v_0 = 1/2p_0$, Fig.2.8. This is due to the emerging bound state at $E \approx -p_0^2/2\mu$. For $s = M$, maximum advance occur for $s = M + p_0/\alpha$. The fact that the advance is related to the inverse of the momentum is the reason why this effect is more noticeable for low-energy scattering, $p_0/\alpha \ll 1$.

Similarly, the largest delay appears at $s = M - p_0/\alpha$, with $\delta x^T_{COM}(t) - \delta v_0 = -1/2p_0$, Fig.2.8. In this case, the scattering is dominated by a long-lived virtual state [39]. Consider the pole corresponding to a bound state, closest to the origin, which dominates the transmission. If we reduce the depth of the well, this pole, which was in the positive half-plane of $\mathrm{Im}(k)$, the pole will cross the origin. It

will then be in the negative half-plane, but still lying on the imaginary axis and being the closest pole to the origin. This pole now corresponds to the virtual state. Although this is not a bound state, it dominates the transmission and delays the transmitted WP.

2.6 Eckart barrier

For $V_0 > \alpha^2/8\mu$, s becomes complex and all the poles lie parallel to the imaginary axis in the negative half-plane. From Eq.(2.8), using $\Gamma(z^*) = \Gamma^*(z)$, we see that $\mathrm{Res}(k_n^I) = -\mathrm{Res}^*(k_n^{II})$. Both kinds of residues have the same imaginary part and opposite real part. We can write

$$\begin{aligned} \mathrm{Re}\left[k_n^{II}\right] &= \alpha\sqrt{8V_0\mu/\alpha^2 - 1}/2 = -\mathrm{Re}\left[k_n^I\right] \equiv \beta, \\ \mathrm{Im}\left[k_n^{II}\right] &= -\alpha(n+1/2) = \mathrm{Im}\left[k_n^I\right], \quad n = 0, 1, 2, ... \end{aligned} \tag{2.17}$$

2.6.1 Cancellation of residues

As in the case of very deep wells, for high barriers the residues take very high values, orders of magnitude higher than $\tilde{\eta}(p_0, x')$. Using Eq.(1.33), we find that each pole contributes with a decaying exponential, much larger than $\tilde{\eta}(p_0, x')$. These high values tend to cancel each other out (see Fig.2.9). As more contributions are added to the series, each one larger than $\tilde{\eta}(p_0, x')$, the sum decreases in absolute value. Note in the figure the difference in magnitude between the individual contributions of the poles, and the final delay distribution.

We obtain these large residues for low values of n. For larger n, the residues tend to a constant value, smaller than the previous ones. Even though in principle we should take all poles into account in order to compute the delay distribution, we will see now that for low barriers a finite number of poles can be enough to compute the transmitted WP without any noticeable error.

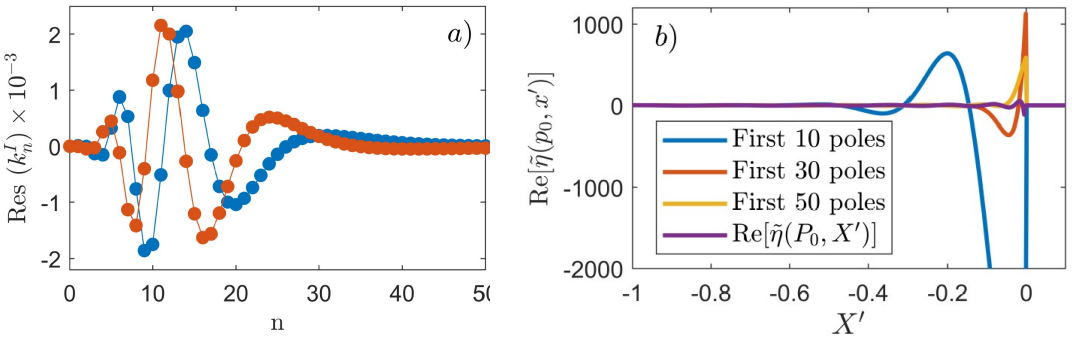

FIGURE 2.9: For a barrier with a potential $W = 200$ and $P_0 = 0.2$, the first 50 residues are shown, figure a), real (blue dots) and imaginary (red dots) parts. In b) $\mathrm{Re}[\eta(\tilde{p_0}, x')]$ is shown, calculated with the contributions of the first 10 poles, (blue solid line) the first 30 poles (red solid line) the first 50 poles (yellow solid line). The final delay distribution, using 5×10^3 poles (purple solid line), is also shown.

2.6.2 Asymptotic behaviour of the residues for an Eckart barrier and geometric progression

As n gets larger, the residues tend to a non-zero limit. This limit can be computed evaluating the limit of the Γ functions in Eq.(2.8) for $n \to \infty$. The approximation is only valid for $\left|\arg(z)\right| < \pi$, which is satisfied by barriers, but not by wells. For barriers, both kinds of residues have a real limit (see Appendix I)

$$\lim_{n\to\infty} \mathrm{Res}(k_n^I) = -\frac{\alpha}{2\pi}, \quad \lim_{n\to\infty} \mathrm{Res}(k_n^{II}) = \frac{\alpha}{2\pi}, \tag{2.18}$$

shown in Fig.2.10a). Even thought the sum of the residues does not converge, the complete series, with the exponentials, does so. We can write

$$\begin{aligned}\tilde{\eta}(p_0, x') &\sim \sum_n \mathrm{Res}(k_n) \exp[ik_n x'] \qquad (2.19)\\ &= \sum_n \left\{ \left[\mathrm{Res}(k_n^I) + \alpha/2\pi\right] \exp(ik_n^I x') + \left[\mathrm{Res}(k_n^{II}) - \alpha/2\pi\right] \exp(ik_n^{II} x') + \right.\\ &\left. + \alpha/2\pi \left[-\exp(ik_n^I x') + \exp(ik_n^{II} x')\right] \right\}.\end{aligned}$$

Using Eq.(2.18) we see that the first two terms converge directly to 0. The remaining terms converge as we will show now. We can write, using Eq.(2.17),

$$\begin{aligned} &\frac{\alpha}{2\pi}\sum_n \exp\left[\alpha(n+1/2)x'\right]\left[-\exp(-i\beta x')+\exp(i\beta x')\right] \\ =&-\frac{\alpha}{\pi}\exp(\alpha x'/2)\sin(\beta x')\sum_n \exp(\alpha n x'), \end{aligned} \tag{2.20}$$

where the sum in Eq.(2.20) is a geometric series,

$$\sum_n \exp(\alpha n x') = \frac{1}{1-\exp(\alpha x')} = -\exp(-\alpha x'/2)\left[2\sinh(\alpha x'/2)\right]^{-1}. \tag{2.21}$$

Thus, the complete sum in Eq.(2.19) converges. We are analysing the case of a barrier, so all poles correspond to resonant states, and $\eta(p_0, x'>0)=0$. We can insert Eqs.(2.20) and (2.21) into the main expression for $\tilde{\eta}(p_0,x')$, Eq.(1.33), and obtain an alternative expression

$$\tilde{\eta}(p_0, x'>0) = (2\pi)^{-1}\exp\left[-ip_0x'\right]\left[F(x') - \frac{\alpha\sin(\beta x')}{\sinh(\alpha x'/2)}\right]. \tag{2.22}$$

The last term in Eq.(2.22) is the contribution from the last term in Eq.(2.19), computed as a geometric series, and $F(x')$ is a converging function,

$$F(x') \equiv 4\pi\sum_{n=0}^{\infty}\exp\left[(n+1/2)\alpha x'\right]\mathrm{Im}\left\{\left[\mathrm{Res}(k_n^I)+\alpha/2\pi\right]\exp(-i\beta x')\right\}. \tag{2.23}$$

The role of the higher poles, far from the real axis, is to cancel the contribution of the δ in the delay distribution, and thus to cancel the freely propagating WP in the convolution Eq.(1.16) (see Figs.2.10*b*) and *c*)). This ensures the correct amplitude of the transmitted WP, Fig.2.10*d*).

As we see, for low barriers not a huge number of poles is needed in order to recover the same transmitted WP as that computed by numerical integration, Fig.2.10*d*), since the residues converge rapidly to their limit, Fig.2.10*a*). In the case shown, the probability of tranmission computed with numerical integration is 0.7518 and the position of its COM is $X^T_{COM}(t) = 784.7297$. Taking only the first

2 poles into account, it gives a probability of 0.6096, with $X^T_{COM}(t) = 748.9430$. Taking 10 poles into account gives a probability of 0.7375 , already close enough, with $X^T_{COM}(t) = 748.8302$. Taking 5×10^3 gives a probability of 0.7517, with $X^T_{COM}(t) = 748.7297$, almost the same result as the probability of the WP obtained numerically. The number of poles needed increases as the potential of the barrier increases.

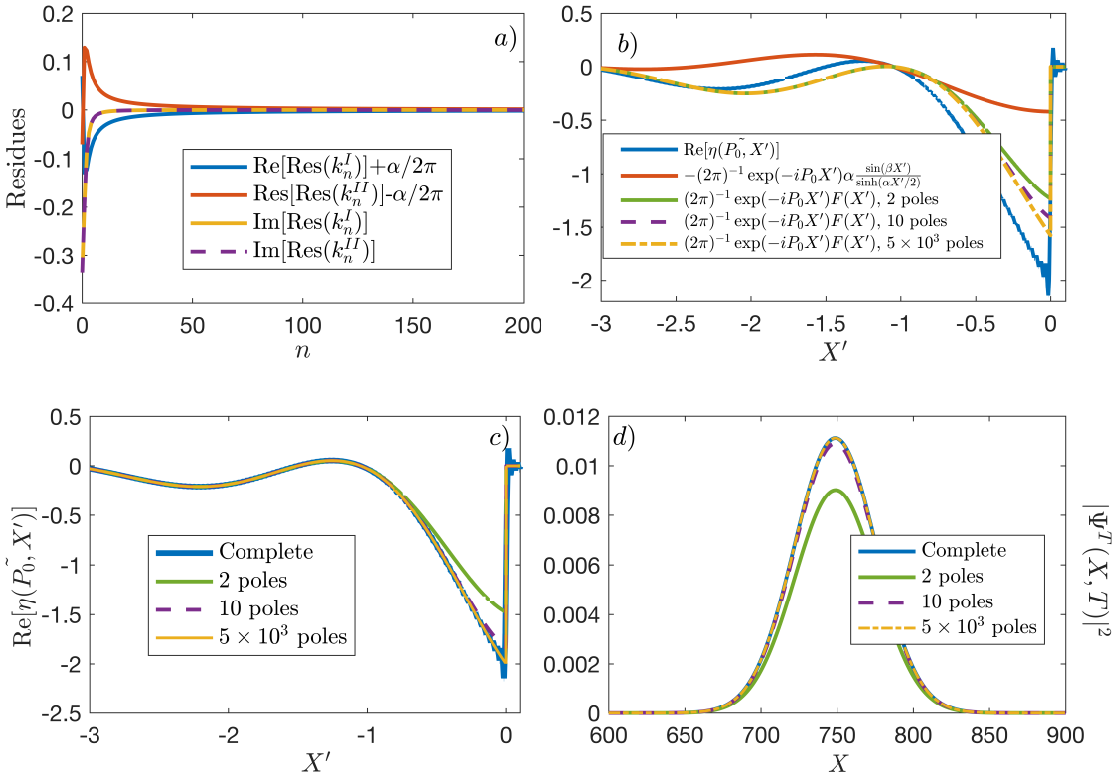

FIGURE 2.10: For a barrier with $W = 1$, $s = -0.5 + 1.3229i$, figure *a*) shows its residues and their limit. Figure *b*) shows the contribution from each term in Eq.(2.22) for an increasing number of poles. Figure *c*) shows the complete delay distribution and the effect that taking more poles into account in Eq.(2.22) has in the distribution. Finally, figure *d*) shows a transmitted WP through this potential, with $\Delta P = 0.004$, $P = 1.5$ and $T = 500$, computed with numerical integration and as a convolution with the delay distribution, taking an increasing number of poles.

2.6.3 Low barrier

The pole expansion is very useful for a low barrier. In this case, a few number of poles dominate the scattering. We consider here the case $-1/2 < s < 0$, and

assume $|s| \ll 1$ for the approximations used. For these values of s, the poles lie on the imaginary axis, with k_n^I approaching the origin as s decreases, and k_n^{II} moving in the opposite direction. The scattering is dominated by the single pole closest to the origin, k_0^I. As explained in Section 2.5.4, this pole, the closest to the origin and in the negative half-plane, corresponds to a virtual state, a long-lived state. Thus, it delays the transmitted WP.

We can write the delay distribution taking only this state into account. Using $1/\Gamma(s \to 0) \approx s$, we have

$$\eta(p_0, x') \approx \delta(x') - \alpha s \exp\left[-(\alpha s + ip_0)x'\right] \theta(-x'), \tag{2.24}$$

where $\theta(x' > 0) = 1$ and 0 otherwise is the Heaviside function. The delay distribution is now formed by the δ function of the freely propagating WP and a single decaying exponential, corresponding to the virtual state. We can calculate the transmission amplitude

$$T(p, V) \approx \frac{ip_0/\alpha}{s + ip_0/\alpha}, \tag{2.25}$$

and, using Eq.(1.29), the COM delay,

$$\delta x_{COM}(t) - \delta v_0 t \approx \frac{\alpha s}{\alpha^2 s^2 + p_0^2}. \tag{2.26}$$

From Eq.(2.26) we see that the delay experienced is larger for smaller incident momentum, $p_0/\alpha \ll 1$, and it has a maximum at $s = -p_0^2/\sqrt{\alpha(2-\alpha)}$, where the delay is $\sqrt{\alpha(2-\alpha)}/2p_0$, Fig.2.11. In dimensionless units, from Eq.(2.4), this maximum delay happens at $s = -P_0^2$, and has a value of $1/2P_0$.

This approximation can be used up to $s = -1/2$. For higher values of the potential, s becomes complex, and the poles become resonant states.

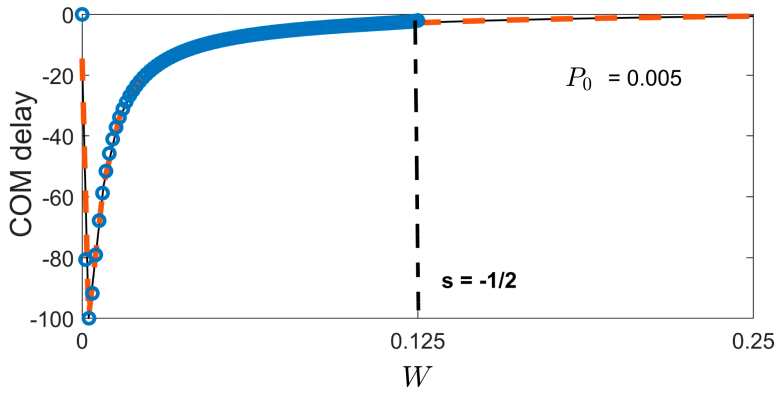

FIGURE 2.11: COM delay for an incident particle with $P_0 = 0.005$, $\Delta P = 0.001$, $X_0 = -3 \times 10^3$ and $T = 2 \times 10^6$, for a potential W from 0 to 0.25. The delay is computed with Eq.(1.29) (black solid line), integrating numerically the WP, taking into account the momentum filtering (red dashed line) and with Eq.(2.26) (blue dots).

2.7 Conclusions

We have seen some concrete examples of the pole representation presented in **Chapter 1**. The delay distribution, $\eta(p_0, x')$, and hence, the transmitted WP, $\Psi^T(x,t)$, can be written in terms of the poles of the transmission amplitude. These poles correspond to bound states or resonant states of the potential.

The pole representation depends on the residues of these poles, which become extremely large for high barriers or very deep wells (see Fig.2.5). Although these high values cancel each other out, they become prohibitively large for numerical calculations in semiclassical scenarios. The pole representation is better suited to describe low-energy scattering in low barriers and shallow wells, which are pure quantum scenarios. In those cases, a few number of poles determine the transmission.

In the case of wells, both bound and resonant states are present. The number of bound states depends on the depth of the well. Their residues are much larger than those of the infinite resonant states, and thus the bound states determine the transmission. For the case of integer s, from Eq.(2.3), only the bound states are needed to recover the transmitted WP exactly.

In the case of shallow wells, we can write the delay distribution using only the

poles corresponding to bound states and the pole closest to 0, be it a bound state or a resonant state. Classically, wells are related to an advance of the transmitted WP (see Section 1.3). For these shallow wells, the barrier can delay or advance the transmitted WP. There exist long-lived "virtual states" [39] that delay the particle maximally. These correspond to poles lying on the imaginary axis close to the origin, and determine the scattering. As the well deepens, this pole emerges to the positive imaginary axis, and its corresponding state becomes a bound state, related to a maximum advance.

In the case of barriers, all poles correspond to resonant states. Although the number of these is infinite and their residues tend no a non-zero limit, a finite number is enough to recover the transmitted WP with negligible error. In the case of low barriers, transmission is determined by a single pole, corresponding to a "virtual state", that delays the transmitted WP.

Chapter 3

Zero-Range Potential

The Eisenbad-Wigner-Smith delay and the Larmor time give different results for the time a tunnelled particle spends in a potential region. This is more pronounced in the ultra-quantum case of a zero-range potential, considered here. We discuss both approaches and analyse the apparent contradiction between them. For the Eisenbud-Wigner-Smith delay the effect of the accuracy of the meter is also studied, in the cases of transmission and reflection. The effect of the single pole of the transmission and reflection amplitudes on the position of the COM of the scattered particles is studied.

3.1 Introduction

So far in this Thesis, we have considered spatial delays of transmitted particles in order to discuss the time spent in the barrier. This approach is the Eisenbud-Wigner-Smith method, and relies on the propagation of WP states, calculating the distance between the COMs of a WP transmitted through a potential and a free WP. As we saw in **Chapter 1**, in the quantum case the transmitted WP is not the result of the incident one crossing the potential through a single well-defined trajectory. Instead, the transmitted WP undergoes a reshaping mechanism, in which WP with different delays interfere. Therefore, we cannot infer any "actual time" from the spatial delay. Only in the classical case can this interference be neglected and we can speak about a "time spent in the potential". This is the reason why the apparently "superluminal" tunnelling time is not in conflict with Einstein's special relativity.

An alternative method for measuring the tunnelling time was proposed by Baz' [42]. It measures the Larmor time, that uses the precession of the spin of the particle in a magnetic field introduced in the region of interest. As the spin acquires an angle during its passage through the magnetic field, by measuring this angle we can obtain the time spent in the region. This method has seen a renewed interest recently due to its experimental realisation [15].

If we consider the Larmor time as a candidate for the "actual time" in a quantum scenario, we face similar issues as with the phase time. Instead of measuring spatial delays, one measures time delays. But, as with the EWS time, the final measurement involves an interference of different delays available in the system. If we measure "weakly" so as not to perturb the system, the measurement does not destroy this interference. Thus, the resulting measured time is not a single delay among the available ones and it is, therefore, impossible to say that the particle has "selected" a single delay [31]. This measured time is in fact complex [19], like the phase time in Eq.(1.42).

One might expect both methods to give the same time delay, but this is not always the case for quantum transitions [1]. In this case the quantity measured

by each method is different. One cannot say that one is right and the other one is wrong. This question has been discussed in [6, 43], and, more recently, in [1].

In this chapter, we will study both methods for the simplest case of a zero-range potential centred at the origin, that can be expressed as

$$V(x) = \Omega\delta(x), \tag{3.1}$$

where $\delta(x)$ is a Dirac delta and Ω is the strength of the potential. A general scattering is shown in Fig.3.1.

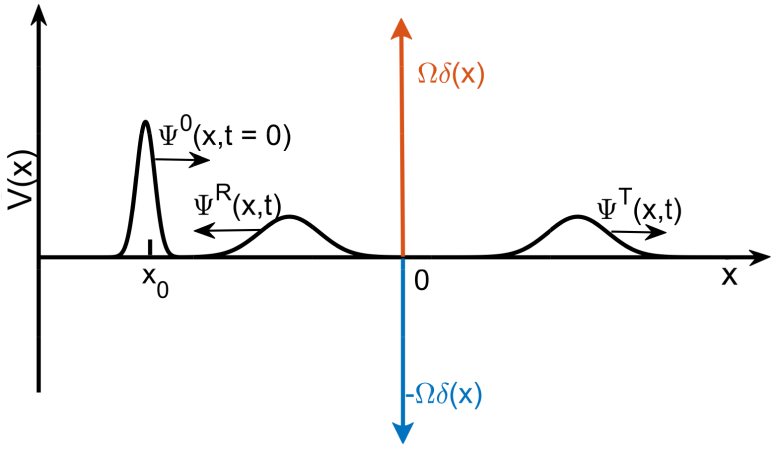

FIGURE 3.1: An incident WP, $\Psi^0(x, t = 0)$, through a zero-range potential, barrier or well, with strength Ω, the transmitted WP, $\Psi^T(x, t)$, and the reflected one, $\Psi^R(x, t)$, are shown.

This particular potential was chosen for two main reasons. The first one is that this is an ultra-quantum case [18], where the difference between the results obtained by the EWS method and the Larmor clock is most pronounced. Since the particle's de Broglie wavelength exceeds the width of the potential, no semiclassical analysis is useful. The second reason is that the amplitudes for reflection and transmission through the zero-range potential can be easily expressed in terms of their single pole. With it, we can easily study the properties of the scattering for the phase time, using the pole representation explained in Section 1.8.

The chapter is organised as follows. In Section 3.2 we describe the use of the Larmor time to measure a tunnelling time. This method is applied to the zero-range potential in Section 3.3, where the Larmor clock is introduced as a pointer

coupled to the particle. The measured time for a zero-range potential is discussed. In Section 3.4 we study the Eisenbud-Wigner-Smith for this potential, which gives a contradiction to the Larmor time. The pole representation of the transmission is studied in Section 3.5. We extend the EWS analysis to reflected WPs in Sections 3.6 and 3.7. Reflection has some particular characteristics not considered in the case of transmission. Finally, in Section 3.8 we study how the width of the incident WPs affects the phase delay. Our conclusions are given in Section 3.9.

3.2 Larmor time

The goal of the Larmor clock is to measure the time taken for a particle to cross some region of space $[a, b]$. To do so, we consider the transmission of a particle with a spin, and introduce a magnetic field in the region. After the passage, the spin acquires an angle ϕ, related to the duration of the transmission through the magnetic field. We can divide this angle by the Larmor frequency w_L and obtain the time spent in the region $[a, b]$.

Conceptually, the idea is to measure the time it takes for the particle to make a transition between an initial and a final state. This is shown in Fig.3.2, where the region $[a, b]$ contains the potential and the magnetic field, and the particle has a spin that precesses due to the magnetic field. In a general way, we can express the transition between any two states using Feynman's path integrals [17]. We consider the case of a particle making a transition from a state Ψ at $(x, 0)$ to a state Φ at (x', t). The amplitude for this transition is given by

$$A(\Phi, \Psi, t) = \sum_{paths} \Phi^*(x') \exp\left[iS(x, x', t)\right] \Psi(x), \tag{3.2}$$

where S is the classical action functional and $\sum_{paths} = \int dx' \int dx \int_{(x,0)}^{(x',t)} Dx(t)$ sums over all possible paths $x(t)$ connecting the initial and final points.

We are interested in transitions spending some time τ in the region $[a, b]$. We define the net time the particle spends in the region $[a, b]$ as a functional of the

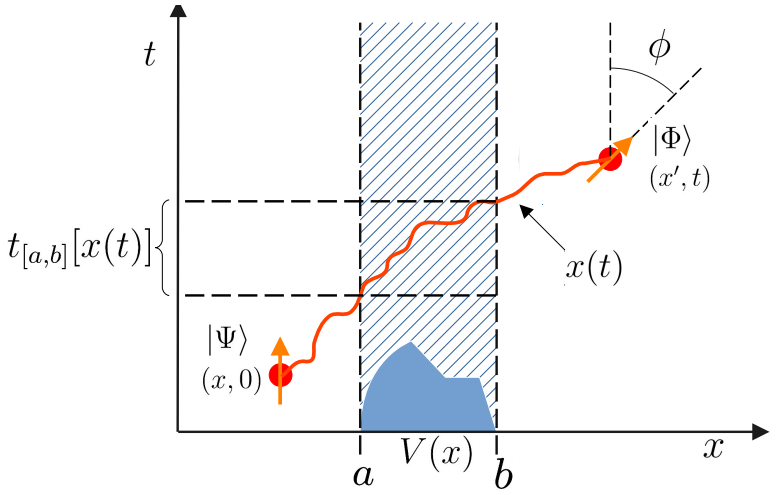

FIGURE 3.2: A particle, initially in state $|\Psi\rangle$ at $(x, 0)$ makes a transition to a state $|\Phi\rangle$ at (x', t) through a path $x(t)$, passing through a potential in $x = [a, b]$. The spin of the particle acquires an angle ϕ due to the presence of a magnetic field in the region $[a, b]$.

path $x(t)$,

$$t_{[a,b]}[x(t)] = \int_0^t \Theta_{[a,b]}\left[x(t')\right] dt', \tag{3.3}$$

where $\Theta_{[a,b]}\left[x(t)\right] = 1$ if $x(t)$ is inside the region $[a, b]$, and 0 otherwise. We use Eq.(3.3) to obtain the restricted transition amplitude for a particle that spends a time τ in the region $[a, b]$,

$$A(\Phi, \Psi, t|\tau) = \sum_{paths} \delta\left(t_{[a,b]}\left[x(t)\right] - \tau\right) \Phi^*(x') \exp\left[iS(x, x', t)\right] \Psi(x). \tag{3.4}$$

Writing the Dirac delta as an integral, $\delta(z) = (2\pi)^{-1} \int dW \exp(-iWz)$, we can rewrite Eq.(3.4) as

$$\begin{aligned} A(\Phi, \Psi, t|\tau) = \sum_{paths} (2\pi)^{-1} \int dW \exp\left[iW\tau\right] \Phi^*(x') \\ \times \exp\left\{i\left[S(x, x', t) - Wt_{[a,b]}\left[x(t')\right]\right]\right\} \Psi(x). \end{aligned} \tag{3.5}$$

We recall the definition of the classical action, $S = \int_0^t L dt'$, where the Lagrangian is $L = K - V$, with K and V being the kinetic and potential energy, respectively. Therefore, the exponential in Eq.(3.5) is $\int_0^t K - \left\{V + W\Theta_{[a,b]}\left[x(t')\right]\right\} dt'$ and we

can rewrite Eq.(3.5) as

$$A(\Phi,\Psi,t|\tau) = (2\pi)^{-1}\int dW\,\exp(iW\tau)A_{V(x)+W\Theta_{[a,b]}}(\Phi,\Psi,t), \tag{3.6}$$

where $A_{V(x)+W\Theta_{[a,b]}}(\Phi,\Psi,t)$ is the transition amplitude in the modified potential $V(x)+W\Theta_{[a,b]}\left[x(t')\right]$. Note that measuring the time τ implies an uncertainty in the potential, introduced by the term W in the region where the time is measured.

In the case of transmission through a barrier, the transition takes place between an incident particle with momentum p and a final particle with the same momentum p. Thus, $|\Psi\rangle = |\Phi\rangle = |p\rangle$, and the amplitude, $A_V(\Phi,\Psi,t)$, is the barrier's transmission amplitude, $T(p,V)$. Introducing the transmission amplitude into Eq.(3.6), renamed $A_T(p,\tau)$ for simplicity, we have

$$A_T(p,\tau) = (2\pi)^{-1}\int dW\,\exp(iW\tau)T(p,V+W\Theta_{[a,b]}). \tag{3.7}$$

The amplitude $A_T(p,\tau)$ in Eq.(3.7) is the Fourier Transform of the transmission amplitude $T(k,V+W)$ and it can be calculated from the poles of the transmission amplitude. In this case, these are poles in the W-complex plane. The transmission is characterised by a range of durations τ, each with an amplitude $A_T(p,\tau)$. In order to calculate the complete transmission amplitude, we integrate over the range of durations, $T(p,V) = \int A_T(p,\tau)d\tau$.

The amplitude in Eq.(3.7) has the potential W and the time τ as conjugate variables. We can compare it with the amplitude distribution of the spatial delay from the previous chapters (see Eq.(1.17)),

$$\eta_T(p_0,x') = (2\pi)^{-1}\exp(-ip_0x')\int dp\,\exp(ipx')T(p,V). \tag{3.8}$$

We can analyse the similarities between Eqs.(3.7) and Eq.(3.8). Both are Fourier Transforms of the transmission amplitude, which is a function of the momentum of the incident particle, p, and of the potential in the region of interest, V. To measure a delay, spatial or temporal, one has to vary one of these two variables, p or V. The measurement of the time delay τ introduces a variation, or uncertainty,

in its conjugate variable, the potential, as seen in Eq.(3.7). This leads to an amplitude distribution of the *temporal* delays, $A_T(p,\tau)$. The measurement of the spatial delay x' is related to a variation of the momentum of the incident particle, p (see Eq.(3.8)), that results in an amplitude distribution of the *spatial* delays, $\eta_T(p_0,x')$.

An important difference between $A_T(p,\tau)$ and the amplitude for the spatial delays in Eq.(1.17) is that the former is a smooth function. We can see this by taking the limit $\lim_{W\to\pm\infty} T(p,V+W\Theta_{[a,b]}) \to 0$. Thus, $A_T(p,\tau)$ does not contain any δ-term, whereas $\eta_T(p_0,x') = \delta(x') + \tilde{\eta}(p_0,x')$, where $\tilde{\eta}(p_0,x')$ is a smooth function.

In principle, we cannot tell apart the interfering durations in Eq.(3.7). To do so, we need to introduce a measuring device, the Larmor clock.

3.3 Larmor clock for a zero-range potential

A general quantum transition amplitude, as the one given in Eq.(3.2), satisfies the usual Schrödinger equation. To measure the time delay, we have constructed a restricted path integral in Eq.(3.4). This amplitude satisfies a "clocked" Schrödinger equation, [44], as

$$i\partial_t A_T(p,\tau) = \left[p^2/2\mu + V(x) - i\partial_\tau \Theta_{[a,b]}(x)\right] A_T(p,\tau), \tag{3.9}$$

where x and p are the transmitted particle's position and momentum, respectively. The expression in Eq.(3.9) is similar to that of a particle coupled to a von-Neumann meter in the region $[a,b]$[45]. We consider a pointer, or meter, with position f and momentum λ, that interacts with the particle while it passes through the region $[a,b]$. The interaction Hamiltonian is $H_{int} = -i\partial_f \Theta_{[a,b]} = \lambda\Theta_{[a,b]}$. The coupled Hamiltonian is

$$H = p^2/2\mu + V(x) + \lambda\Theta_{[a,b]}, \tag{3.10}$$

that has the same form as the Hamiltonian governing the particle in Eq.(3.9). Outside the region $[a, b]$, the Hamiltonian in Eq.(3.10) is that of a particle going through the unmodified potential $V(x)$. Thus, the meter introduces a potential in the region of interest, just as the restricted path integral in Eq.(3.4) led to a modified potential, $V + W$, in the region $[a, b]$.

For the final pointer's reading, we measure its position f at the initial time $t = 0$, before entering the region, and at a time t, after passing through the region. The pointer's momentum λ is set to 0 so that it does not perturb the particle. The final position of the pointer is proportional to the time spent in the region by the particle. Solving Hamilton's equations for the pointer's position f from Eq.(3.10), the reading after a time t is

$$f(t) - f(0) = \int_0^t \Theta_{[a,b]}(x^{cl}(t'))dt' = \int_a^b \mu^{1/2} dx / \sqrt{2\left[E - V(x)\right]} \equiv \tau(E), \quad (3.11)$$

where $E = p^2/2\mu + V(x)$ is the energy of the particle and $x^{cl}(t')$ is the classical trajectory of the particle.

To obtain the quantum version of Eq.(3.11), we prepare the pointer in an initial state $|G\rangle$. We consider an initial Gaussian clock around $f = 0$, as $\langle f|G\rangle = G(f) = C \exp\left(-f^2/\Delta f^2\right)$, where Δf is the uncertainty in the pointer's position. If the clock is coupled to the system, its final state is given by

$$\Phi(f) = \int G(f - \tau) A_T(p, \tau) d\tau, \quad (3.12)$$

where $A_T(p, \tau)$ is the amplitude distribution of the temporal delays from Eq.(3.7).

Thus, the pointer's final state is formed by the interference of envelopes, $G(f)$, shifted in space by some distance proportional to the time τ. Each envelope delayed by τ has a complex weight, given by $A_T(p, \tau)$. Eq.(3.12) has the same form as the final state of the WP obtained in the previous chapters, where the spatial delay was being measured (see Eq.(1.16)).

To obtain the reading given by the final state we calculate the expectation value of the pointer, as the COM of its final state,

$$\langle f\rangle = \frac{\int f|\Phi(f)|^2 df}{\int |\Phi(f)|^2 df}. \tag{3.13}$$

The accuracy of the meter is controlled by its width Δf. Sending $\Delta f \to 0$ for a very accurate measurement, we quench the transmission, and the particle is reflected. This is due to the fact that $\Delta f \to 0$ implies that $\Delta W \to \pm\infty$, making the transmission amplitude $T(p, V + \Delta W \to \pm\infty) \to 0$ for all incident momenta. The perturbation introduced by a meter with very high accuracy is larger than the effect of the potential $V(x)$, and destroys the transmission through the potential.

To have a pointer that does not perturb the dynamics of the particle, we take $\Delta f \to \infty$, which is equivalent to an inaccurate measurement. The position of the COM of the pointer is found to be [18]

$$\lim_{\Delta f\to\infty} \langle f\rangle = \mathrm{Re}[\overline{\tau}_{[a,b]}(p)], \tag{3.14}$$

where

$$\overline{\tau}_{[a,b]}(p) = \frac{\int_0^\infty \tau A_\tau(p,\tau)d\tau}{\int_0^\infty A_\tau(p,\tau)d\tau} = -i\partial_W \left[\ln T(p, V + W\Theta_{[a,b]})\right]|_{W=0}. \tag{3.15}$$

Eq.(3.15) gives a complex time [19, 31]. It has the same form as Eq.(1.29), since in both cases we evaluate the integral over a transition amplitude, and not over a probability. This is a consequence of the measurement being inaccurate or "weak".

Our interest in this chapter is the calculation of the dealy experienced by a particle through a zero-range potential, that can be defined as the limit of a square

barrier,

$$V(x) = \lim_{a-b\to 0} V_0 \Theta_{[a,b]}(x), \tag{3.16}$$
$$\text{with} \quad V_0 \to \infty \quad \text{and} \quad (a-b)V_0 = \Omega = const.$$

From Eq.(3.3) it can be seen that the net time tends to zero for any smooth path as $a - b \to 0$. Nevertheless, Feynman's paths are generally not smooth [17]. We can check the time delay measured in a zero-range potential more rigorously by evaluating the amplitude distribution in Eq.(3.7). As mentioned above, the transition amplitude $A_T(p,\tau)$ can be calculated from the poles in the W-complex plane of the transmission amplitude $T(p, V+W)$. In the limit $a-b \to 0$ only the contribution of one pole survives, and we obtain [46]

$$\lim_{a-b\to 0} A_\tau(p,\tau) \to \tau_0^{-1} \exp\left[-i\Omega\tau/(b-a)\right] \exp\left(-\tau/\tau_0\right), \tag{3.17}$$

where $\tau_0 \equiv \mu(b-a)/p = (b-a)/v$. The amplitude in Eq.(3.17) tends to $\delta(\tau)$, and thus the measured time in Eq.(3.15) tends to 0. In the limit, there is a single duration available, $\tau = 0$, and the Larmor clock always measures a zero duration in the region for the zero-range potential. We can now compare these results with the time obtained with the EWS method for the same potential.

3.4 Eisenbad-Wigner-Smith times

We can alternatively measure the time spent in the potential region from the spatial delays of WPs, as seen in **Chapter 1**. In order to do so, we consider the time at which the COMs of the transmitted and freely propagating WP arrive at a particular point to the right of the barrier. The time delay between their arrivals is proportional to the spatial delay between the two WPs. We consider this spatial delay as the distance between the positions of the COMs of the transmitted WP and the freely propagating one,

$$\delta x^T_{COM}(t) = x^T_{COM}(t) - x^0_{COM}(t). \tag{3.18}$$

The time delay is therefore

$$\delta\tau^{EWS} = -\delta x^T_{COM}(t)/v_0, \tag{3.19}$$

where $v_0 = p_0/\mu$ is the velocity of the incident particle. Again, we consider Gaussian WPs, given by Eqs.(1.1), (1.2) and (1.3).

The transmission amplitude for a zero-range potential, Eq.(3.1), is known,

$$T(k,\Omega) = 1 - \frac{i\Omega}{k + i\Omega}, \tag{3.20}$$

and can be written as $T(k,\Omega) = |T(k,\Omega)| \exp\left[i\Phi_T(k,\Omega)\right]$. Using Eq.(1.26) we obtain a complex delay

$$\tilde{x}'_T = -\partial_k \Phi_T(k,\Omega)|_{k=p_0} = \frac{-\Omega}{p_0^2 + \Omega^2} + i\frac{\Omega^2}{p_0(p_0^2+\Omega^2)} = \tilde{x}'_{T1} + i\tilde{x}'_{T2}, \tag{3.21}$$

where $\tilde{x}'_{T1}$ and $\tilde{x}'_{T2}$ are the real and imaginary parts of $\tilde{x}'_T$, respectively. The real part corresponds to the distance between the COM of the two WPs, while the imaginary part is related to the previously explained "momentum filtering" effect. Due to this effect, the resulting transmitted WP has a mean momentum higher than the incident one, $p_0 + \delta p_0$, where $\delta p = \Delta p^2 \tilde{x}'_{T2}/2$. The spatial delay is therefore

$$\delta x^T_{COM}(t) = x^T_{COM}(t,p_0) - x^0_{COM}(t,p_0) = \tilde{x}'_{T1} + \delta p_0 t/\mu. \tag{3.22}$$

We are interested in comparing the EWS time delay, Eq.(3.19), with that obtained with the Larmor clock. Thus, we want to avoid measuring any delay caused by the momentum filtering effect. To do this, we can calculate the COM distance between the transmitted WP and a freely propagating one with mean momentum $p_0 + \delta p_0$. As we will see later, we can equally acomplish this using dispersionless WPs, with $E(k) = ck$, where c is a constant. These "dispersionless" spatial delays

are

$$\delta x^T_{COM}(t) = x^T_{COM}(t, p_0) - x^0_{COM}(t, p_0 + \delta p_0) = \tilde{x}'_{T1}. \tag{3.23}$$

For any $\Omega \neq 0$, the time delay calculated with Eq.(3.23) has clearly a non-zero value. This seems to contradict the result of the Larmor clock seen in Section 3.2. In Section 3.5 we will show that for the spatial delay distribution non-zero delays are still available.

There is another unusual aspect of the delays for a zero-range potential. For the square and Eckart potentials seen in **Chapters** 1 and 2, the tunnelled WP was advanced relative to a freely propagating one. In the case of a zero-range potential, we see from Eq.(3.21) that for a barrier, with $\Omega > 0$, the transmitted WP is always delayed with respect to a freely propagating one, $\mathrm{Re}[\tilde{x}'_T] < 0$. Although the WP does tunnel there is no advance for any $\Omega > 0$. The transmitted WP is only advanced in the case of a well, $\Omega < 0$.

Thus, the EWS delays have a different behaviour for zero-range barriers. The key to understand this difference is the role played by the poles of the transmission amplitude in the momentum plane play, that we will analyse next.

For the numerical results presented in Sections 3.5 and 3.7 dimensionless units will be used, taking as a reference the mean momentum of the incident WP, p_0, (with $\hbar = 1$ and $c = 1$)

$$\underline{p} = p/p_0, \quad \underline{x} = xp_0, \quad \underline{\mu} = \mu/p_0, \quad \underline{\Omega} = \mu\Omega/p_0^2, \quad \underline{t} = tp_0^2/\mu. \tag{3.24}$$

3.5 A pole representation of transmission

It is useful to recall the expression for the transmitted WP as a convolution of envelopes,

$$\Psi^T(x,t) = \exp\left[ip_0x - iE(p_0)t\right] \int G_0(x - x', t)\eta_T(p_0, x')dx', \tag{3.25}$$

where $G_0(x,t)$ is the envelope of the incident WP and $\eta_T(p_0,x)$ the delay distribution given in Eq.(1.17), calculated as the Fourier Transform of the transmission amplitude.

The transmission amplitude in Eq.(3.20) has a single pole. Hence, in this case it is easy to write the delay distribution using the pole representation. By calculating the residue for this single pole, placed at $k_p = -i\Omega$, we can obtain an exact expression for $\eta_T(p_0,x')$. For a barrier, $\Omega > 0$, the pole appears on the negative Im(k)-axis, corresponding to an anti-bound state, while for a well with $\Omega < 0$, it corresponds to a bound state, and appears on the positive Im(k) axis. We can compute the residue using Cauchy's formula, as

$$\mathrm{Res}(k_p) = \lim_{k\to k_p}(k-k_p)T(k_p)\exp\left(ik_px'\right) = -i\Omega\exp(\Omega x'). \tag{3.26}$$

Closing the contour of integration in the upper or lower half, for poles corresponding to bound or anti-bound states, respectively, we obtain the delay distribution

$$\eta_T(p_0,x') = \delta(x') - \exp(-ip_0x') \times \begin{cases} \Theta(-x')|\Omega|\exp(+|\Omega|x'), \text{for} \quad \Omega > 0 \\ \Theta(x')|\Omega|\exp(-|\Omega|x'), \text{for} \quad \Omega < 0. \end{cases} \tag{3.27}$$

It can be split into a δ contribution and a smooth function, $\tilde{\eta}_T(p_0,x')$. Since we have a single pole, $\eta_T(p_0,x'>0) = 0$ for barriers, and $\eta_T(p_0,x'<0) = 0$ for wells. To obtain the transmission amplitude we insert the delay distribution, Eq.(3.27), into the integral for the WP in Eq.(3.25) and solve it using error functions to get an analytic expression for the WP (see Appendix J).

For an incident wave on a barrier with $\Omega > 0$ we have a transmitted WP

$$\exp(ipx) \to T(p,\Omega)\exp(ipx) = \exp(ipx) - \Omega\int_{-\infty}^{0}\exp(\Omega x')\exp[ip(x-x')]dx', \tag{3.28}$$

i. e. it is the sum of a free WP, which is the incident one, and a negatively delayed wave. Again, we can think of the barrier as an "interferometer". It splits the incident wave into components, each with a phase shift that corresponds to a

spatial delay. In the case of barriers, the phase shifts correspond to delays, with $x' < 0$, while for wells, the delays are positive, $x' > 0$.

Contrary to the cases of the square and Eckart potentials from **Chapters 1** and **2**, the delay distribution is formed by a single exponential, corresponding to the single pole. In the case of a barrier, the single pole, corresponding to an anti-bound state, *delays* the transmitted WP. For a well, the single pole corresponds to a bound state, and thus *advances* the transmitted WP. This is a classical feature that survives in this quantum case. There is no "anomalous" value for the delay, as in the case of tunnelling through a potential of a non-zero width.

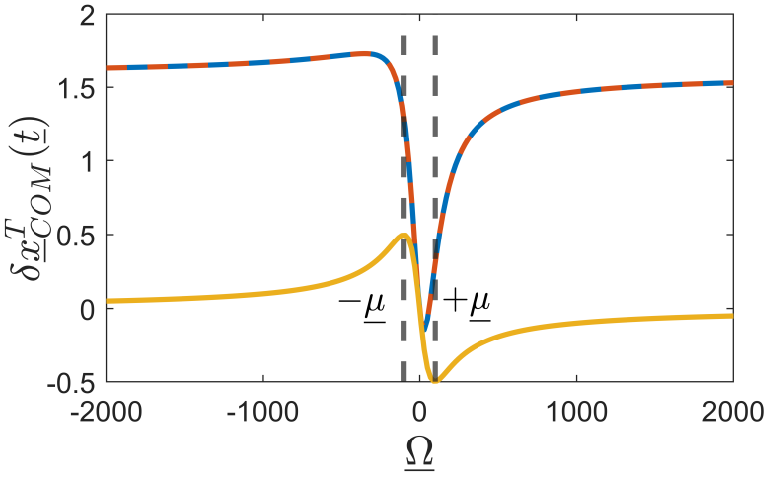

FIGURE 3.3: COM delay for transmission of a WP with $\Delta \underline{p} = 0.2$, $\underline{\mu} = 100$, $\underline{x}_0 = -20$ and $\underline{t} = 80$, incident on a barrier with $\underline{\Omega} = -2 \times 10^3$ to $\underline{\Omega} = 2 \times 10^3$. Shown are the delays between transmitted and freely propagating WPs with the same mean momentum (see Eq.(3.22)), computed with the numerical integration of the WPs (blue solid line) and from the analytical results (red dashed line). The same COM delays are shown for the dispersionless case (see Eq.(3.23)) of $E(k) = ck$, with $c = 1$ (yellow solid line). The points for the maximum advance, at $\underline{\Omega} = -\underline{\mu}$, and maximum delay, at $\underline{\Omega} = \underline{\mu}$, are also shown.

So far, we have only used particles with energy $E(k) = k^2/2\mu$. For large times, these WPs spread. Now we will also consider dispersionless WPs, with an energy $E(k) = ck$, where c is a constant. For these WP, although there is momentum filtering, there is no speed-up of the transmitted WP associated to it, since all momenta have the same velocity. All free and scattered WPs travel at a constant velocity c and the delay corresponds exactly to $\tilde{x}'_{T1}$ in Eq.(3.21). Fig.3.3 shows the

effect of the poles on the COM delay for both cases, dispersive, with $E(k) = k^2/2\mu$, and dispersionless, with $E(k) = ck$.

Using Eq.(3.21), we obtain the maximum delay of $-1/2p_0$ ($-1/2$ in the dimensionless units in the figure) for $\Omega = p_0$ ($\underline{\Omega} = \underline{\mu}$). It corresponds to the long-lived anti-bound state. The maximum advance appears for $\Omega = -p_0$ ($\underline{\Omega} = -\underline{\mu}$), corresponding to the bound state, and has a value of $1/2p_0$ ($1/2$).

3.6 Reflection

A similar analysis can be applied to the reflected WP,

$$\Psi^R(x,t) = \int R(p,\Omega)A(p-p_0)\exp\left[-ipx - iE(p)t\right]dp, \tag{3.29}$$

moving from right to left, and where

$$R(k,\Omega) = \frac{-i\Omega}{k+i\Omega} \tag{3.30}$$

is the reflection amplitude for the potential in Eq.(3.1). It can be checked, using Eq.(3.20), that $|T(k,\Omega)|^2 + |R(k,\Omega)|^2 = 1$. We can write the reflected WP as a convolution of freely propagating envelopes,

$$\Psi^R(x,t) = \int G_0(-x-x',t)\eta_R(p_0,x')dx' \tag{3.31}$$

where $\eta_R(p_0,x')$ is the delay distribution for reflection. Note that the envelope G_0 in Eq.(3.31) has the opposite sign in x to that of the transmitted WP. This is equivalent to a perfect reflection from an infinite potential at $x = 0$. The reflected WP appears as soon as the incident one reaches the potential, and travels from the potential to the left, in the direction opposite to the transmitted one. Both WPs move away from the barrier as t increases (see Fig.3.1).

In the case of transmission, we have calculated the COM delay as the distance between the COMs of the transmitted WP and a freely propagating one. In order to calculate the delay for reflection, we compare the reflected WP with the

reflection from an infinite potential placed at the origin. This is the mirror image of the freely propagating WP used in the case of transmission. Its COM is that of the free WP with a minus sign, $-x^0_{COM}(t)$. Thus, the delay for reflection is

$$\delta x^R_{COM}(t) = x^R_{COM}(t) + x^0_{COM}(t). \tag{3.32}$$

The reflected WP is delayed if $\delta x^R_{COM}(t) > 0$. That is, when, travelling from the potential to negative x, the reflected WP appears behind the perfectly reflected one. Equivalently, the reflected WP is advanced if $\delta x^R_{COM}(t) < 0$. In this case, the reflected WP appears ahead of the perfectly reflected one. This convention is illustrated in Fig.3.4. We can think of placing a detector of the COM of the WP to the left of the potential, far enough from it, and turning it on once the incident WP has reached the potential. We can repeat the experiment with an infinite potential barrier (or, for practical purposes, very large compared to the initial one). Using the convention defined above, "delayed" reflected WPs reach the detector *after* the perfectly reflected one. On the other hand, "advanced" reflected WPs reach the detector *before* the perfectly reflected one.

The delay distribution is computed as the Fourier Transform of the reflection amplitude, $\eta_R(p_0, x') = (2\pi)^{-1} \exp(-ip_0x') \int R(k, \Omega) \exp(ikx')\, dk$. It is worth noting that in this case the delay distribution, $\eta_R(p_0, x')$ is already a smooth function. This is due to the large momentum contributions going through the potential unaffected, and thus not being reflected. We can see from Eq.(3.30) that $R(k \to \infty, \Omega) \to 0$.

The case of reflection has one more detail that it is not present in the case of transmission. The position of the potential does not affect the transmitted WP for large enough times. The transmission amplitude for $V(x-s)$, shifted by a distance s, is the same as that obtained for $V(x)$. The contribution to the delay by the momentum filtering is proportional to the total time, Eq.(3.22), and therefore is unaffected by a spatial shift in the potential.

This is not the case with reflection, since the reflected WP emerges from the potential once the incident WP has reached it. For a potential $V(x - s)$, the

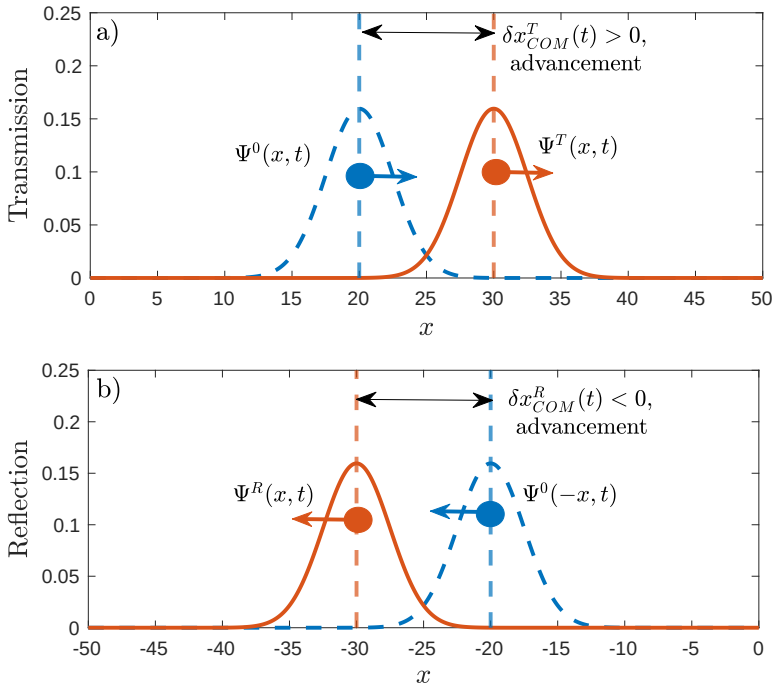

FIGURE 3.4: Schematic of the delays in the cases of a) transmission and b) reflection over a well. When $\delta x^T_{COM}(t) > 0$ and $\delta x^R_{COM}(t) < 0$, the transmitted and reflected WPs are advanced with respect to a free WP and its mirror image, respectively.

incident WP has to travel some extra distance, if $s > 0$, or travel less distance, if $s < 0$. In the same way, the reflected WP travels this extra distance back again, or travels less distance. Thus, the reflection amplitude obtains an extra phase, $R(k,V) \to \exp(2iks)R(k,V)$ (see Fig.3.5). We can see this by making the change $x \to x - s$ in the following expression,

$$\begin{aligned} &\exp(ikx) + R(k,V)\exp(-ikx) \to T(k,V)\exp(ikx) \qquad (3.33)\\ &\qquad\qquad \downarrow \quad x \to x - s \\ &\big[\exp[ik(x-s)] + R(k,V)\exp[-ik(x-s)] \to T(k,V)\exp[ik(x-s)]\big] \times \exp(iks) \\ &= \exp(ikx) + R(k,V)\exp(2iks)\exp(-ikx) \to T(k,V)\exp(ikx). \end{aligned}$$

So, for reflection, the mirror image of the freely propagating WP will be affected by the choice of the position of the potential. For the rest of the analysis, we put the potential at the origin.

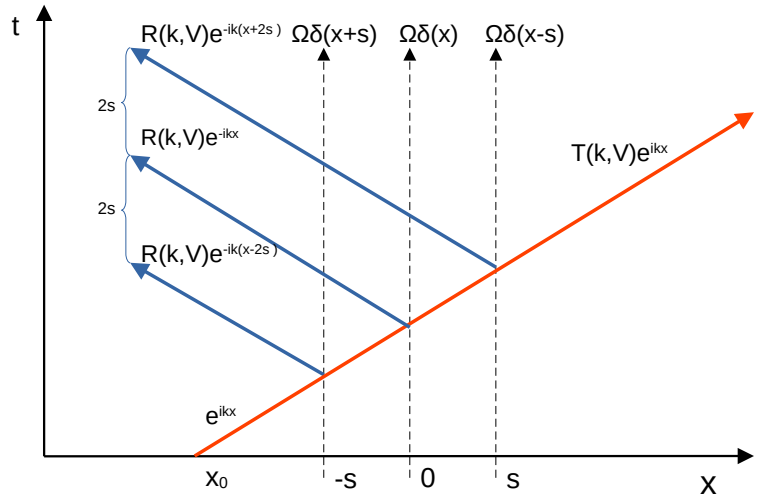

FIGURE 3.5: Plane wave scattering for a potential in three different positions. An incident plane wave e^{ikx} over a zero-range potential, centred at $x = 0$ or displaced $\pm s$. The phase obtained by the reflection amplitude (see Eq.(3.33)) as the potential is shifted is a consequence of the extra distance it has to travel. The transmission is unaffected by the displacement.

With this choice we can obtain the delays for reflection, calculating a "phase delay". Writing $R(k,\Omega) = |R(k,\Omega)| \exp\left[i\Phi_R(k,\Omega)\right]$, we have that

$$\tilde{x}'_R = -\partial_k \Phi_R(k,\Omega)|_{k=p_0} = -\frac{\Omega}{\Omega^2 + p_0^2} - i\frac{p_0}{\Omega^2 + p_0^2} \equiv -\tilde{x}'_{R1} - i\tilde{x}'_{R2}. \tag{3.34}$$

The first term, $\tilde{x}'_{R1}$, corresponds to a spatial delay, while the second one $\tilde{x}'_{R2}$ is related to the momentum filtering, $\delta p_0^R = \Delta p^2 \tilde{x}'_{R2}/2$. Therefore, the delay for reflection is given by

$$\delta x_{COM}^R(t) = \tilde{x}'_{R1} + \delta p_0^R t/\mu. \tag{3.35}$$

We have added a minus sign in Eq.(3.34) to account for the reflected WP travelling in opposite direction to the incident one. Comparing with the delays for transmission, Eq.(3.21), we see that $\tilde{x}'_{R1} = -\tilde{x}'_{T1}$. With our convention for the reflection delays, both account for an advance in the case of wells, and for a delay in the case of barriers. For any incident WP with $p_0 > 0$, $\tilde{x}'_{R2}$ is always positive, and thus δp_0^R is always positive. Therefore, the reflected WP is always slowed down. The effect of the momentum filtering in the reflected WP is opposite to the effect it has on the transmitted one, as it slows down the reflected WP and speeds up

the transmitted one.

We can write the reflected WP in terms of a freely propagating WP, as we did for transmission in **Chapter 1**, Eq.(1.14). Taking into account that it moves from right to left, by changing $x \to -x$ we have

$$\Psi^R(x,t) = R(p_0,\Omega)\exp\left[\Delta p^2 \tilde{x}'^2_{R2}/2 + ip_0\tilde{x}'_{R1}\right] \times \Psi^0(-x+\tilde{x}'_{R1}, t, p_0 - \delta p_0^R). \tag{3.36}$$

We see from the last term in Eq.(3.36) that the mean momentum of the reflected WP has decreased, and that a positive value of $\tilde{x}'_{R1}$ moves the reflected WP to the right, delaying the reflected WP.

3.7 A pole representation for reflection

We can use the pole representation to calculate both the delay distribution and the complete reflected WP. The reflection amplitude has the same pole as the transmission amplitude, $k_p = -i\Omega$. The pole representation of the delay distribution is given by

$$\eta_R(p_0,x') = -\exp(ip_0x') \times \begin{cases} \Theta(-x')\exp(|\Omega|x'), \text{for} \quad \Omega > 0 \\ \Theta(x')|\Omega|\exp(-|\Omega|x'), \text{for} \quad \Omega < 0, \end{cases} \tag{3.37}$$

which is equal to the smooth part of the delay distribution for transmission, $\eta_R(p_0,x') = \tilde{\eta}_T(p_0,x')$, Eq.(3.27). We can solve the integral in Eq.(3.31) using the delay distribution in Eq.(3.37) and error functions (see Appendix J).

As for the transmission case, we have that $\eta_R(p_0,x'>0) = 0$ for barriers, $\Omega > 0$, and $\eta_R(p_0,x'<0) = 0$ for wells, $\Omega < 0$. Since the envelope in the convolution formula in Eq.(3.31) has $-x$, a barrier shifts the left going envelopes *to the right*, delaying them. In the case of a well, the envelopes are shifted *to the left*, advancing them. This is the same as for transmission, as barriers delay the reflected WP and wells advance it, but travelling in opposite directions.

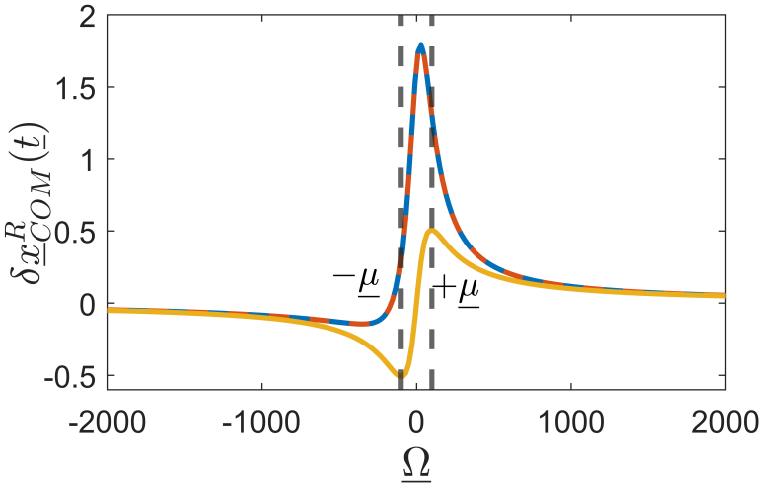

FIGURE 3.6: COM delay for reflection of a WP with $\Delta\underline{p} = 0.2$, $\underline{\mu} = 100$, $\underline{x}_0 = -20$ and $\underline{t} = 80$, incident on a barrier with $\underline{\Omega} = -2 \times 10^3$ to $\underline{\Omega} = 2 \times 10^3$. Shown is the delay computed with the numerical integration of the WPs (blue solid line), and using the results from Eq.(3.34) (red dashed line), taking momentum filtering into account, in Eq.(3.34), and in the dispersionless case of $E(k) = ck$, with $c = 1$ (yellow solid line). The points for the maximum delay, at $\underline{\Omega} = -\underline{\mu}$, and maximum advance, at $\underline{\Omega} = +\underline{\mu}$, are also shown.

The COM delays are shown in Fig.3.6 for different values of Ω. The spatial delay, with no momentum filtering (yellow solid line), is the same as the transmission one in Fig.3.3, but of opposite sign. The maximum advance occurs for $\Omega = -p_0$ ($\underline{\Omega} = -\underline{\mu}$ in the figure) with a value of $-1/2p_0$ ($-1/2$) and corresponds to the bound state. The maximum delay occurs for $\Omega = p_0$ ($\underline{\Omega} = +\underline{\mu}$) with a value of $1/2p_0$ ($1/2$), and is due to the virtual state.

3.8 COM delays for WP of an arbitrary width

We have focused on the cases of inaccurate measurements, $\Delta x \to \infty$, and calculated the delays, in Eqs.(3.21) and (3.34), in this limit. We can calculate a more general expression for the COM delay, and see the effect of the width of the particle on it. Since the particle itself acts as the measuring device, the width of the envelope will give the accuracy of the measurement. The COMs can be

obatined from the averages over the amplitudes (see Appendix K for more details)

$$\langle x\rangle_0 = x_0 + \langle v(k)\rangle_0\, t, \tag{3.38}$$
$$\langle x\rangle_{T,R} = \pm x_0 \pm \langle v(k)\rangle_{T,R}\, t \mp \langle \partial_k \Phi_{T,R}(k,V)\rangle_{T,R}\,.$$

In the limit $\Delta x \to \infty$, we have that $\lim_{\Delta x\to\infty}\langle f(k)\rangle = f(k)$ for any function f, and we recover the delays of Eqs.(3.21) and (3.34).

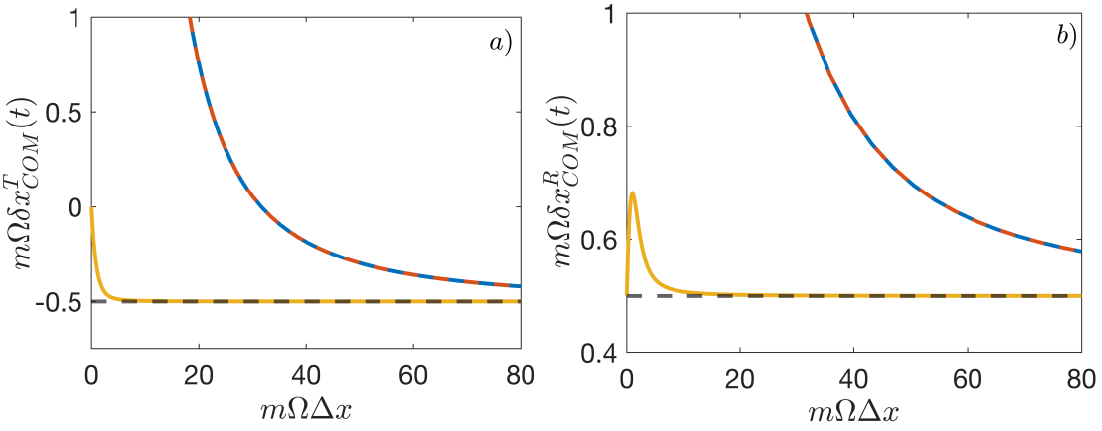

FIGURE 3.7: COM delay for a) transmission and b) reflection, for a varying width of the incident WP. The parameters are $x_0 = -200$, $m\Omega^2 t = 500$ and $m\Omega\Delta x$ changes from 0 to 80. Shown are the delays for the dispersive case $E(k) = k^2/2\mu$, obtained integrating numerically the WPs (blue solid line) and using the results from Eqs.(3.38) (red dashed line), and for the dispersionless case, $E(k) = ck$, with $c = 1$, from Eqs.(3.38) (yellow solid line). The limit of the delay for $\Delta x \to \infty$ is also shown in both cases (black dashed line).

Figure 3.7 shows the delays for transmission and reflection as a function of the width of the incident WP. In the limit $\Delta x \to \infty$, the delays tend to the values obtained in Eqs.(3.21) and (3.34), the dispersive and dispersionless cases, respectively.

We consider first the accurate limit, $\Delta x \to 0$. The width of the WP in momentum space increases, since $\Delta p \sim \Delta x^{-1}$. For transmission, since $T(k \to \infty) \to 1$ we have that $|T(k)A(k)|^2 \approx |A(k)|^2$. Most of the WP gets transmitted without any distortion or delay. We can see this in Fig.3.7a), where, in the dispersionless case, the delay for transmission of a very narrow WP tends to 0. For reflection, we insert Eq.(3.37) into Eq.(3.31) and find $|\Psi^R(x,t)|^2 \sim \Theta(\pm x \mp ct \mp x_0)\Delta x \exp\left[-2|\Omega|(\pm x \mp ct \mp)\right]$, where the upper sign corresponds to a barrier and

the lower one to a well. Calculating the COM delay in the limit for the dispersionless case we have that

$$\lim_{\Delta x \to 0} \delta x^R_{COM}(t) = 1/2\Omega. \tag{3.39}$$

This limit is shown in Fig.3.7*b*).

For $E(k) = k^2/2\mu$, the dispersion increases as $\Delta x \to 0$. We can see it by analysing the spreading of the envelopes. Using Eq.(3.25) for transmission, or Eq.(3.31) for reflection, we obtain the envelope of the WP and the square of its absolute value

$$\begin{aligned} G_0(x,t) =& [2\Delta x^2/\sigma_t^4]^{1/4} \exp\left[-(x - vt - x_I)^2/\sigma_t^2\right], \\ \sigma_t \equiv& (\Delta x^2 + 2it/m)^{1/2}, \\ |G_0(x,t)|^2 =& \left[2\pi\Delta x_t^2\right]^2 \exp\left[-2(x - vt - x_I)^2/\Delta x_t^2\right], \\ \Delta x_t \equiv& (\Delta x^2 + 4t^2/\Delta x^2 m^2)^{1/2}. \end{aligned} \tag{3.40}$$

where $\sigma_t(x,t)$ is the time-dependent spatial width of the WP and Δx_t is the real time-dependent width. For $\Delta x \to 0$, the time-dependent width increases as $\Delta x_t \sim 2t/\Delta x\mu \to \infty$. The narrower the WP, the more dispersion it experiences.

3.9 Conclusions

3.9.1 The Larmor clock and the EWS method measure different quantities

In a classical case, one can think of different ways of measuring the time a particle takes to cross some region of space. For example, one can measure it directly coupling a clock to the particle. Alternatively, once can measure a spatial shift between the particle and a freely travelling one, and then calculate the time from the spatial delay. The result is independent of the method used for the measurement, and both lead to the same result. This is due to the quantity being measured, the time spent in the region, being unique in the classical case. This is

not the case for a quantum transition, as different methods, or different definitions of this time, lead to different results [1, 6].

In the previous chapters we have focused on the EWS time. To compute it, the position of the COM of the transmitted WP is compared with the position of the COM of a freely propagating WP. The difference between the position of their COMs is divided by the mean velocity in order to obtain the phase time in Eq.(1.43). The WPs considered are very broad compared to the de Broglie wavelength. Thus, all possible *spatial* delays interfere, and the phase time cannot be associated with any single one of them (see Section 1.10).

An alternative method consists in using the precession of the spin of the transmitted particle inside the potential to measure the time spent in the region. This is the Larmor clock [39, 42]. Similar to the phase shift, the Larmor clock involves the interference between available *temporal* delays. As the potential becomes narrower, the range of available durations decreases, and in the limit of a zero-range potential there is a single duration available, $\tau = 0$. Thus, there is no interference. The Larmor clock measures $\tau = 0$ for any accuracy of the measuring device.

The case of the EWS for the zero-range potential gives a different result to that of the Larmor clock. Even in the limit of the zero-range potential there is still a range of different spatial shifts available. So, there is still interference, and a weakly perturbing measurement preserves this interference. The resulting spatial delay is non-zero even for the zero-range potential. There is no contradiction between this result and that obtained with the Larmor clock, since in each case we measure different quantities.

The Larmor clock method measures the duration in the potential region. This measurement is related to the time the particle spends *inside* the potential. The EWS method does not measure a time, but a spatial shift. The time one can infer from the measured spatial delay (see Eq.(3.19)) is not being measured directly in the same way as the Larmor clock [46, 47]. Only in the classical limit both quantities coincide.

In the quantum case, each method results in a different measured duration. There is no unique definition of the time a quantum particle spends in a region, and thus no method is "right" or "wrong". In both cases, the accuracy of the measurement affects the result, and for a weakly perturbing measurement may lead to complex times [1, 19, 31]. Thus, neither method measures the "actual time", which exists only in the classical limit, but a quantity specified by the method. This is the reading of a coupled meter in the Larmor clock case, and the spatial shift between transmitted and free particles in the case of the EWS method. There is no contradiction since both are different quantities.

3.9.2 The accuracy of the measurement in a zero-range potential

As mentioned above, when measuring the duration of transmission of a WP through a zero-range potential there is a single available duration, $\tau = 0$. Thus, the accuracy of the meter does not affect the result, as there is no interference related to it. The Larmor clock measures a duration $\tau = 0$ through a zero-range potential both for $\Delta f \to 0$ and $\Delta f \to \infty$.

This is not the case for a measurement of the EWS time, as even in the limit of a zero-range potential, there are several available spatial delays. The accuracy of the measurement, related to the width of the WP, affects the result. In the case of a very broad incident WP, the available delays interfere, and the resulting measured delay is not zero. Only in the limit $\Delta x \to 0$ the measured delay tends to zero (see Fig.3.7).

Part II

Relativistic scattering

Chapter 4

Relativistic scattering across supercritical barriers

We analyse different aspects of relativistic scattering across supercritical barriers for Klein-Gordon and Dirac particles. We study transmission and reflection through multiple-reflection series, for which both convergent and divergent expansions can be found. Some of these expansions allow for acausal transmission, which is related to apparent "negative durations" in the barrier. For supercritical scattering, the divergent solution of the Klein-Gordon equation is related to pair creation. For Dirac particles, the causal solution converges, and there is no fermionic pair creation. We study the Klein paradox for both bosons and fermions.

4.1 Introduction

In the previous chapters we have discussed the tunnelling times in the case of non-relativistic scattering. One of our main focuses, and an initial motivation behind this study, is the apparent "superluminal" tunnelling time.

It has been known since the 1930's [11] that the centre of mass (COM) of a quantum wave packet (WP) tunnelled through a rectangular barrier is advanced by the width of the barrier with respect to a freely propagating one. Thus, if the spatial delay is related to the time spent in the barrier, as in the classical case, the WP appears to have crossed the barrier region infinitely fast. This would contradict Einstein's special relativity, since this speed exceeds that of light. One may think that this apparent superluminal speed is an artefact of non-relativistic scattering. But if one considers a one-particle relativistic treatment of tunnelling, replacing the Schrödinger particles by relativistic ones, such as Klein-Gordon bosons or Dirac fermions, the apparent superluminal tunnelling time persists [12–14, 28, 48]. Thus, the contradiction is not resolved with a relativistic treatment. The reason behind the apparent superluminal tunnelling is in the reshaping of the tunnelled WP in the barrier (see **Chapter 1**), that remains in the relativistic case.

We are interested in supercritical barriers, with a potential $V_0 > E + \mu c^2$, where E is the energy of the incident particle and μ, its mass. For these barriers, the height of the barrier exceeds the gap between the negative and positive energy continua (see Fig. 4.1*c*)), and there is no suppression of transmission.

4.1.1 Supercritical barrier

For a particle with energy $E^2 = (p_0 c)^2 + (\mu c^2)^2$, where p_0 is its mean momentum, incident on a potential barrier with V_0, we can distinguish three regimes, depending on the height of the barrier. The momentum inside the potential is $q = \sqrt{(E - V_0)^2 - \mu^2 c^4}/c$. These regimes are:

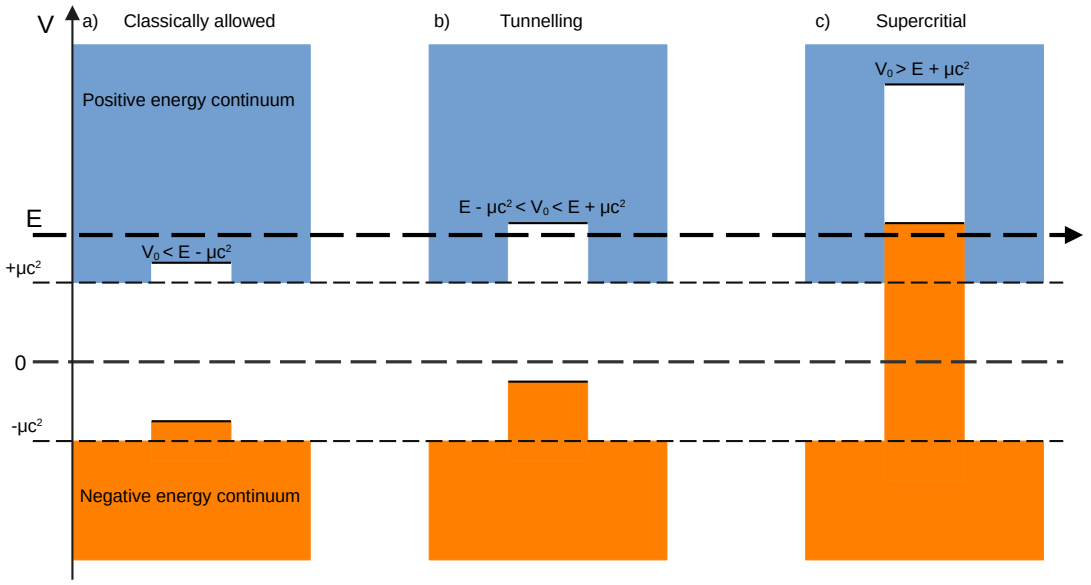

FIGURE 4.1: The energy states for *a*) classically allowed, *b*) tunnelling and *c*) the supercritical regimes for a fixed energy E of the incident particle. In *a*) the positive energy states, in blue, and the negative energy ones, in orange, are shown for a non-supercritical potential. There is a separation of $2\mu c^2$ between the highest negative energy state and the lowest positive energy state. In the case of a supercritical barrier, *c*), the potential is high enough so it allows the incident particle to propagate through the second energy continuum.

- For $V_0 < E - \mu c^2$, Fig. 4.1 *a*), the transmitted WP goes over the barrier, since q is real and finite. This is a classically allowed transmission, explained in Section 1.3.

- For $E - \mu c^2 < V_0 < E + \mu c^2$, Fig. 4.1 *b*), the momentum inside the barrier becomes imaginary and the solution corresponds to evanescent waves. This is the tunnelling regime, as explained in Section 1.4. In this regime, as the potential increases, the transmitted amplitude becomes exponentially smaller. There are no states inside the barrier through which the WP can propagate.

- For $V_0 > E + \mu c^2$, Fig. 4.1 *c*), corresponding to a supercritical barrier, the momentum inside the barrier becomes real again, which implies that there is an energy continuum through which the particles can propagate [32, 33, 49, 50]. We recover solutions with travelling WPs inside the barrier with a single and well-defined trajectory. This is the Klein regime [51].

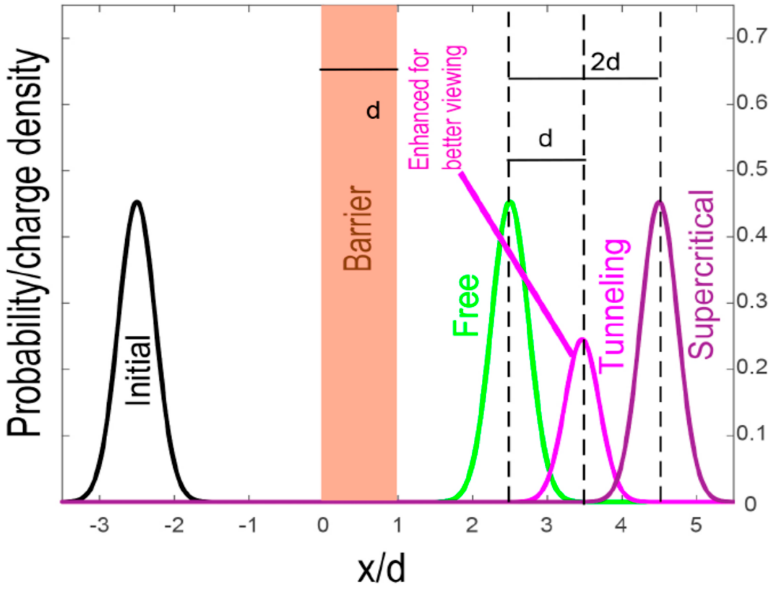

FIGURE 4.2: Shown are the incident WP over a barrier of width d, a freely propagating WP after a time t and for the same time, a tunnelled WP and a bosonic WP transmitted through a supercritical barrier for $E = V_0/2$, all in arbitrary units. The tunnelled WP is advanced the width of the barrier relative to the freely propagating one, while the advancement for the supercritical one, with this choice of incident energy, is twice the width of the barrier.

In the supercritical regime, both fermions and bosons behave in a similar way, since there is no suppression of transmission for either type of particle. Nevertheless, the scattering in the relativistic regime is very different for each kind of particle, as we will study through this chapter.

We will consider the particular case of Klein-Gordon particles incident on a supercritical barrier with an energy $E = V_0/2$. For a broad WP, there is no reflection, and we find that the transmitted particle is advanced by *twice* the width of the barrier, $2d$. Thus, the apparent time the WP spends inside the barrier becomes *negative*, $\tau \approx -\mu d/p_0$. This solution, along with free propagation and a tunnelled WP, is depicted in Fig.4.2. The total transmission of quantum particles through a potential barrier, with the condition $E = V_0/2$, is known as the super-Klein tunnelling (see [52] and [53]).

This solution is acausal, since there is a WP propagating inside the barrier even before the arrival of the incident one. As we will see, the Klein-Gordon equation allows for this kind of solutions. One can alternatively solve the scattering via a

finite difference method. This forces the solution to be causal, since no particle can propagate in the barrier before the arrival of the incident one. We will analyse both the causal and acausal solutions with the Multiple Reflection Expansion (MRE) method, expanding the transmission amplitude in a series. This method allows us to describe the scattering in terms of transmitted and reflected parts of the WP at the edges of the barrier, and can describe pair creation and annihilation [54, 55].

This apparently negative traversal time is not obtained for fermions. We will apply the MRE method to Dirac fermionic particles, and study the differences that arise between the two types of particles in the supercritical regime.

4.1.2 Organisation of the chapter

The chapter is divided into two main sections, discussing bosonic and fermionic scattering. The solutions of the Klein-Gordon equation are presented in Section 4.2. Section 4.2.1 introduces the transmission amplitude of Klein-Gordon particles for a square potential. The MRE is presented in Section 4.2.2, where the convergent solution for the non-relativistic scattering is discussed. The divergent solution of the MRE is analysed in Section 4.2.3, again for non-relativistic scattering. The relativistic scattering for a supercritical barrier is treated in Section 4.2.4 for both the convergent and divergent solutions. The super-Klein regime, where $E = V_0/2$, is also studied using the MRE method.

The solutions of the Dirac equation are analysed in Section 4.3. Section 4.3.1 introduces the transmission amplitude and the solutions for a Gaussian incident fermionic WP. The MRE for the convergent and divergent solutions are presented in Section 4.3.2. Relativistic scattering for a critical barrier is studied in Section 4.3.3.

Section 4.4 discusses the different results obtained for fermions and bosons, and the relation of those with pair creation. The general conclusions of the chapter are summarised, and the limitations and validity of the single-particle approach are discussed.

4.2 Bosons

The Klein-Gordon equation is the relativistic equation for spin-0 particles. It can be obtained substituting the energy E and the momentum p by their operators in the relativistic relation, $E^2 = p^2c^2 + \mu^2c^4$, where μ is the mass and c the speed of light. In the one-dimensional case considered here, $\hat{E} = i\hbar\partial_t$ and $\hat{p} = -i\hbar\partial_x$. The free Klein-Gordon equation is then,

$$\left[\frac{1}{c^2}\frac{\partial^2}{\partial t^2} - \frac{\partial^2}{\partial x^2} + \frac{\mu^2c^2}{\hbar^2}\right]\Psi(x,t) = 0. \tag{4.1}$$

The conserved quantity for the Klein-Gordon equation is the total charge [32]. Throughout this chapter we will use the charge density to describe bosonic scattering. In the presence of a potential $V = eA$, this is

$$\rho = \frac{i\hbar e}{2\mu}(\Psi^*\frac{\partial}{\partial t}\Psi - \Psi\frac{\partial}{\partial t}\Psi^*) - \frac{e^2}{\mu c^2}A\Psi\Psi^*. \tag{4.2}$$

The free Klein-Gordon equation in Eq.(4.1) allows for both positive and negative energy solutions. Positive energy solutions are labeled as "particles", and negative energy solutions as "antiparticles". As we will see in Section 4.2.4, in the presence of a supercritical potential the charge density in Eq.(4.2) becomes negative.

For the numerical calculations we use dimensionless variables, taking the barrier's width d as a reference,

$$X = x/d, \quad T = tc/d, \quad W = dV/\hbar c, \quad M = \mu dc/\hbar \quad \text{and} \quad P = pd, \tag{4.3}$$
$$\text{with} \quad c = 1, \quad e = 1 \quad \text{and} \quad \hbar = 1.$$

4.2.1 Transmission amplitude and scattering solution

We consider an incident WP from the left on a square potential with $V(x) = V_0$ for $0 < x < d$ and 0 otherwise. The transmission amplitude can be obtained

starting from a plane wave with momentum p travelling to the right after crossing the barrier,

$$x > d: \quad e^{ipx}. \tag{4.4}$$

Inside the potential region there are waves moving to the left and to the right, each with a coefficient,

$$0 < x < d: \quad a_+ e^{iqx} + a_- e^{-iqx} \leftarrow e^{ipx}, \tag{4.5}$$

where q is the particle's momentum inside the barrier, $qc = \sqrt{(E - V_0)^2 - \mu^2 c^4}$ and $E = \sqrt{p^2c^2 + \mu^2 c^4}$ is the energy of the incoming wave. Matching the ingoing and outgoing waves at the left of the barrier,

$$\begin{aligned} x < 0: \quad & b_{++} e^{ipx} + b_{-+} e^{-ipx} \leftarrow e^{iqx} \\ x < 0: \quad & b_{+-} e^{ipx} + b_{--} e^{-ipx} \leftarrow e^{-iqx}, \end{aligned} \tag{4.6}$$

and imposing continuity of the wave functions and their derivatives at $x = d$ and $x = 0$, we get the coefficients,

$$\begin{aligned} a_+ &= \frac{1}{2}\left(1 + \frac{p}{q}\right) e^{i(p-q)d}, & a_- &= \frac{1}{2}\left(1 - \frac{p}{q}\right) e^{i(p+q)d} \\ b_{++} &= b_{--} = \frac{1}{2}\left(1 + \frac{q}{p}\right), & b_{-+} &= b_{+-} = \frac{1}{2}\left(1 - \frac{q}{p}\right). \end{aligned} \tag{4.7}$$

The transmission amplitude can be obtained from $e^{ipx}(x < 0) = T(p, q) e^{ipx}(x > d)$,

$$T(p, q) = \frac{1}{b_{++} a_+ + b_{+-} a_-} = \frac{4pq \exp[-ipd]}{(p + q)^2 \exp[-iqd] - (p - q)^2 \exp[iqd]}. \tag{4.8}$$

Naming the three regions of space, $x \leq 0$, $0 \leq x \leq d$ and $x > d$ as 1, 2 and 3 respectively, the complete solution for the scattering states is

$$\begin{aligned} \phi^1(x,p) &= R(p,q)e^{-ipx} + e^{ipx}, & x \leq 0 \\ \phi^2(x,p) &= B_+(p,q)e^{iqx} + B_-(p,q)e^{-iqx}, & 0 \leq x \leq d \\ \phi^3(x,p) &= T(p,q)e^{ipx}, & x > d, \end{aligned} \tag{4.9}$$

with

$$B_\pm(p,q) = a_\pm T(p,q), \qquad R(p,q) = (b_{-+}a_+ + b_{--}a_-)T(p,q). \tag{4.10}$$

We can use the scattering states given in Eq.(4.9) to write the WPs that we will use throughout this chapter. We consider an initial Gaussian WP. The WPs for each region of space are

$$\begin{aligned} \Psi_i(x,t) &= \int dp A(p,p_0)\exp[-iE(p)t]\phi^i(p,x), \\ A(p,p_0) &= 2^{-1/4}\pi^{-3/4}\Delta p^{-1/2}\exp\left[-(p-p_0)^2/\Delta p^2 - i(p-p_0)x_0\right], \end{aligned} \tag{4.11}$$

where $\phi^i(x,p)$ are the solutions given in Eq.(4.9), $A(p,p_0)$ is the momentum distribution of the WP, centred at $p = p_0$, Δp is its width of the WP in momentum space, where $\Delta x = 2/\Delta p$ is the momentum in coordinate space, and $x_0 < 0$ is the initial position of the WP, which assures that the initial WP is far enough to the left of the barrier. We consider throughout the chapter only a positive momentum distribution, $\Delta p < p_0$.

4.2.2 Convergent MRE

We can represent the transmission amplitude in Eq.(4.8) as a convergent geometric progression, known as the Multiple Reflection Expansion (MRE). The

series converges since $|p-q|<|p+q|$. We can write

$$\begin{aligned} T(p,q) =& \frac{1}{b_{++}a_{+}+b_{+-}a_{-}} \rightarrow \frac{1}{b_{++}a_{+}}\sum_{n=0}\left(\frac{b_{+-}a_{-}}{b_{++}a_{+}}\right)^{n} \\ =& \frac{4qpe^{-ipd}}{(p+q)^2}\sum_{n=0}^{\infty}\frac{(p-q)^{2n}}{(p+q)^{2n}}\exp\left[i(2n+1)qd\right] \equiv \sum_{n=0}^{\infty}T_n(p,q). \end{aligned} \tag{4.12}$$

The reflection amplitude can also be represented as a geometric progression. Using Eqs.(4.12) and (4.10) we have

$$\begin{aligned} R(p,q) =& \frac{\left[(p^2-q^2)e^{-iqd}+(p^2+q^2)e^{iqd}\right]e^{ipd}}{4pq}T(p,q) \\ =& \frac{(p^2-q^2)e^{-2iqd}+(p^2+q^2)}{(p+q)^2e^{-iqd}}\sum_{n=0}^{\infty}\frac{(p-q)^{2n}}{(p+q)^{2n}}\exp\left[2inqd\right] \equiv \sum_{n=0}^{\infty}R_n(p,q). \end{aligned} \tag{4.13}$$

To obtain the MRE of the transmitted WP, we insert Eqs.(4.12) into Eq.(4.9) and obtain $\phi^i(x,p)=\sum_{n=0}^{\infty}\phi_n^i(x,p)$. So, from Eq.(4.11) we get

$$\Psi^T(x,t)=\sum_{n=0}^{\infty}\int dpA(p,p_0)\exp[-iE(p)t]\phi_n^i(p,x) \equiv \sum_{n=0}\Psi_n^T(x,t). \tag{4.14}$$

The reflected WP can be written as a series in a similar manner. Alternatively, we can write the sub-amplitudes of these WPs explicitly to see their physical origin. We consider the case where the potential is wider than the spatial width of the WP, $d>\Delta x$, so that there are travelling WPs inside the barrier.

A WP incident from the left on a potential of width d, shown in Fig. 4.3, is reflected with an amplitude r_l^i and transmitted with an amplitude t_l^i at the left edge. The subindices l/r indicate that the scattering occurs at the left/right edges, and the superindices i/o, that the transmitted part goes inside/outside the barrier. The amplitude of the reflected and transmitted WPs are lower than the incident one. The reflected WP travels away from the potential, while the transmitted one travels inside the potential until it reaches the right edge. There, it is reflected with an amplitude r_r^o and transmitted with amplitude t_r^o. The total amplitude of the WP travelling inside the potential is now $t_l^i r_r^o$, and the total amplitude of the

emerged transmitted one is $t_l^i t_r^o$. The WP inside the potential bounces back to the left, where it is scattered again with amplitudes t_l^o and r_l^o, emitting one WP to the left. The WP inside keeps bouncing, each time reducing its amplitude, while consecutively smaller WPs emerge from the edges of the potential. The process ends when the potential region is emptied.

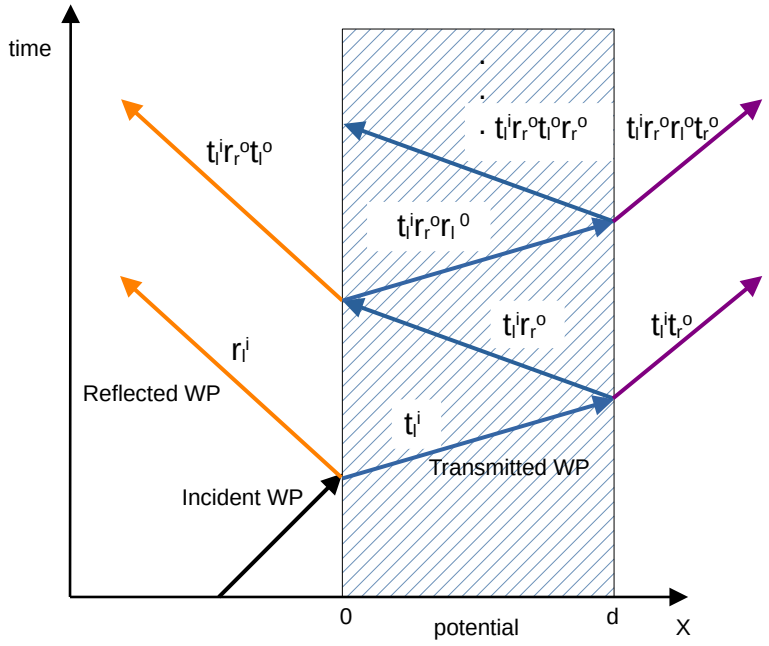

FIGURE 4.3: Schematic of the Multiple Reflection Expansion (MRE). The incident WP splits into transmitted and reflected WPs. The reflected WP moves away from the barrier, while the transmitted one travels through the barrier and bounces off the right edge. The WP inside the barrier keeps bouncing, emitting WPs to the right and to the left of the potential. At each bounce, the reflected and transmitted WPs acquire a complex weight, as appears in Eq.(4.15). These are equivalent to the series of amplitudes in Eq.(4.14).

The emerging transmission and reflection amplitudes can be written as

$$T = \sum_n t_l^i (r_r^o r_l^o)^n t_r^o, \qquad R = r_l^i + \sum_n t_l^i r_r^o (r_l^o r_r^o)^n t_r^o. \tag{4.15}$$

Comparing these expressions with Eqs.(4.12) and (4.13), we can identify $T_n(p,q) = t_l^i (r_r^o r_l^o)^n t_r^o$ and $R_n(p,q) = t_l^i r_r^o (r_l^o r_r^o)^n t_r^o$, since the expansions in Eq.(4.12) and (4.13) are convergent.

4.2.2.1 Non-relativistic convergent MRE

We study first the sub-amplitudes from Eq.(4.14) in a non-relativistic classically allowed scenario of a WP going over a barrier or a well. Thus, the WPs can propagate through the barrier. The Klein-Gordon equation in the non-relativistic regime reduces to the Schrödinger equation. Nevertheless, we can still apply the formalism of the MRE to study both the convergent and divergent solutions, and later compare the relativistic and the non-relativistic solutions. For a momentum distribution $A(p, p_0)$ sharp enough in momentum space, we can approximate the momentum q inside the barrier as

$$q(p) \sim q(p_0) + \partial_p q(p_0)(p - p_0) = q(p_0) + p_0/q_0(p - p_0), \tag{4.16}$$

where p_0 is the mean momentum of the incident particle, and $q_0 \equiv q(p_0)$. Since $\partial_p q(p) > 0$, the group velocity inside the barrier has the same direction as the momentum. Inserting the MRE of the transmission amplitude in Eq.(4.12) into the transmitted WPs of Eq.(4.14) for the region $x > d$ we have

$$\Psi_I^T(x,t) \approx \sum_{n=0}^{\infty} X_n(p_0, q_0)\Psi_0(x - x_n(p_0, q_0), t), \tag{4.17}$$

where

$$\begin{aligned} X_n(p_0, q_0) &= \frac{4p_0q_0}{(p_0+q_0)^2}\frac{(p_0-q_0)^{2n}}{(p_0+q_0)^{2n}}e^{i(2n+1)(q_0-p_0^2/q_0)d} \\ x_n(p_0, q_0) &= d\left[1-(2n+1)p_0/q_0\right]. \end{aligned} \tag{4.18}$$

$X_n(p_0, q_0)$ are the weights of each consecutive transmitted WP, and $x_n(p_0, q_0)$ their corresponding delays. Since the weight of each consecutive WP in the series is smaller than the previous one, $X_{n+1}(p_0, q_0) < X_n(p_0, q_0)$, the series in Eq.(4.12) is convergent. We label the transmitted WPs in Eq.(4.17) as I in order to distinguish from the divergent solution in the following subsection, which we will label as II.

The case for reflection is similar and thus will not be studied here in the same detail as transmission. Although the weights for each consecutive reflected WP

are different than those for transmission, the spatial delay between consecutive WPs and their proportional increase in amplitude is the same. The n-th WP is proportional to a factor $(p_0-q_0)^{2n}/(p_0+q_0)^{2n}$ in both the transmitted and reflected cases. This corresponds to the $(r_l^o r_r^i)^n$ terms in Eq.(4.15) and has the same origin for reflection and transmission.

For a well the WP travels faster in the potential region, $q_0 > p_0$. Thus, the first emerging WP is advanced relative to free propagation, by $x_0 = d(1 - p_0/q_0) > 0$. The rest of the WPs appear delayed an extra $-2dp_0/q_0$ distance. This case is shown in Fig. 4.4. For a barrier the WP slows down, $q_0 < p_0$, and the emerging transmitted WPs are delayed relative to the freely propagating WP, $x_n(p_0, q_0) < 0$.

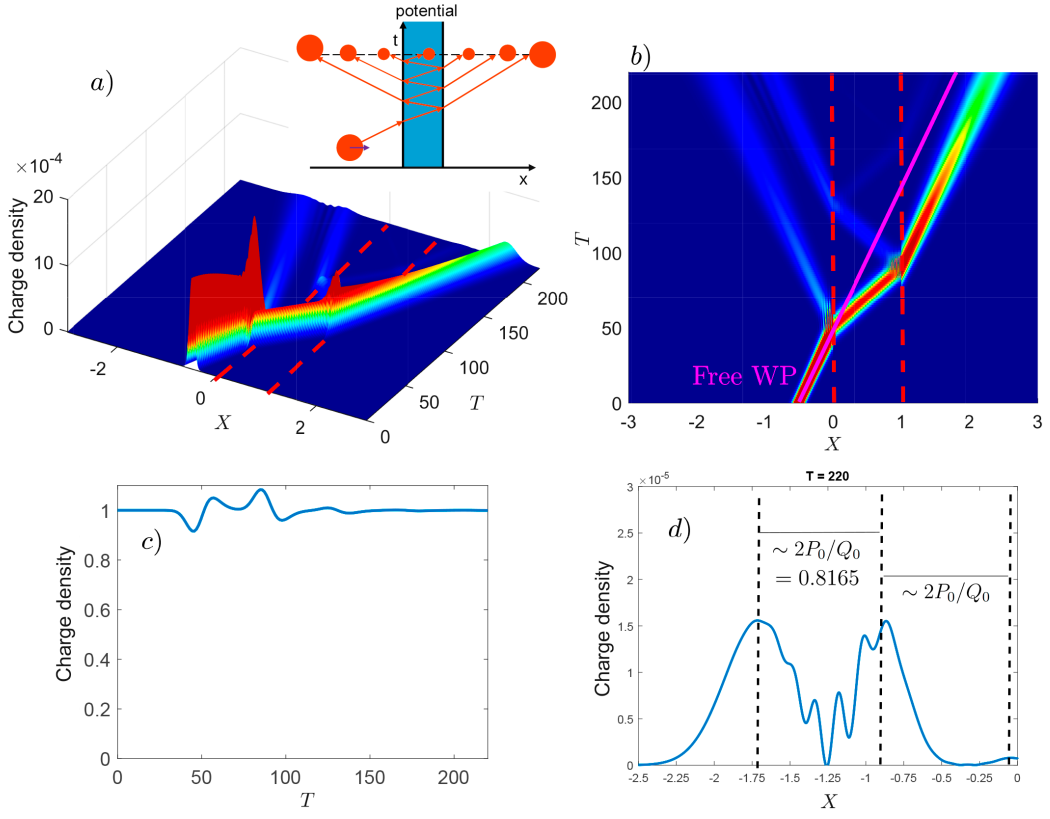

FIGURE 4.4: For a well with $P_0 = 100$, $M = 10^4$, $W/M = -2.5 \times 10^{-4}$ and T from 0 to 220, figures a) and b) show the evolution of a Gaussian WP, and the bounces inside the potential. The first emitted WP at the right of the barrier is advanced relative to a freely propagating WP, whose trajectory is shown in b) with a pink line. The inset in figure a) shows a scheme of the scattering. Figure c) shows the conservation of the charge density through the scattering. The oscillations are due to numerical errors, and could be reduced taking a finer grid for the coordinate X. Figure d) shows the reflected WPs at the final time $T = 220$. The separation between the peaks is related to the bounces inside the barrier, and is equal to $2P_0/Q_0$.

Each new emitted WP is multiplied by a factor $\left(\frac{p_0-q_0}{p_0+q_0}\right)^2 < 1$. As time increases, the probability for the particle to remain inside the barrier decreases, until it escapes. The emitted WPs travel away from the barrier, to the left or to the right. This is therefore a bound and causal solution.

4.2.3 Divergent MRE

A different solution can be obtained, using the fact that $T(p,q)$ is single-valued in the complex q-plane, since we have that $T(p,q) = T(p,-q)$. We can make the change $q \to -q$ in the expansion Eq.(4.12) and still get a solution of the Klein-Gordon equation. This change makes the series to diverge. The transmission amplitude is now

$$\begin{aligned} T(p,q) =& \frac{1}{b_{++}a_{+} + b_{+-}a_{-}} \to \frac{1}{b_{+-}a_{-}} \sum_{n=0} \left(\frac{b_{++}a_{+}}{b_{+-}a_{-}}\right)^n \\ =& \frac{-4qpe^{-ipd}}{(p-q)^2} \sum_{n=0}^{\infty} \frac{(p+q)^{2n}}{(p-q)^{2n}} e^{-i(2n+1)qd} \equiv \sum_{n=0}^{\infty} T_n(p,-q). \end{aligned} \tag{4.19}$$

Proceeding as in the previous section, we study first the non-relativistic case. We write the transmitted particle as a sum of WPs, Eq.(4.17), changing $q \to -q$,

$$\Psi^T_{II}(x,t) \approx \sum_{n=0}^{\infty} X_n(p_0,-q_0)\Psi_0(x - x_n(p_0,-q_0),t), \tag{4.20}$$

with

$$\begin{aligned} X_n(p_0,-q_0) =& \frac{-4p_0q_0}{(p_0-q_0)^2} \frac{(p_0+q_0)^{2n}}{(p_0-q_0)^{2n}} e^{i(2n+1)(-q_0+p_0^2/q_0)d} \\ x_n(p_0,-q_0) =& d\left[1 + (2n+1)p_0/q_0\right]. \end{aligned} \tag{4.21}$$

In this case, each $(n+1)$-th WP in the series has a larger amplitude than the n-th WP, $X_{n+1}(p_0,-q_0) > X_n(p_0,-q_0)$, and is *further away* from the barrier, $x_{n+1}(p_0,-q_0) > x_n(p_0,-q_0)$. Before the arrival of the incident WP, there is a WP propagating inside the barrier, emitting WPs and decreasing its amplitude at each bounce. This is shown in Fig.4.5 (for clarity, see the schematic diagram in Fig.4.5

c)). The continuous emission stops once the incident WP arrives at the left edge of the barrier, is reflected and, in a coherent manner, interferes with the WP inside the barrier, leaving the potential empty. The last emitted WP to the right of the barrier has already left it when the incident particle reaches the potential, at a time $\mu d/q_0$ *before*.

Since there is no limit to the series, $|X_n(p_0, -q_0)| \to \infty$ as $n \to \infty$, the solution is unbound and not normalisable. The case for a divergent scattering solution through a well is shown in Fig.4.5.

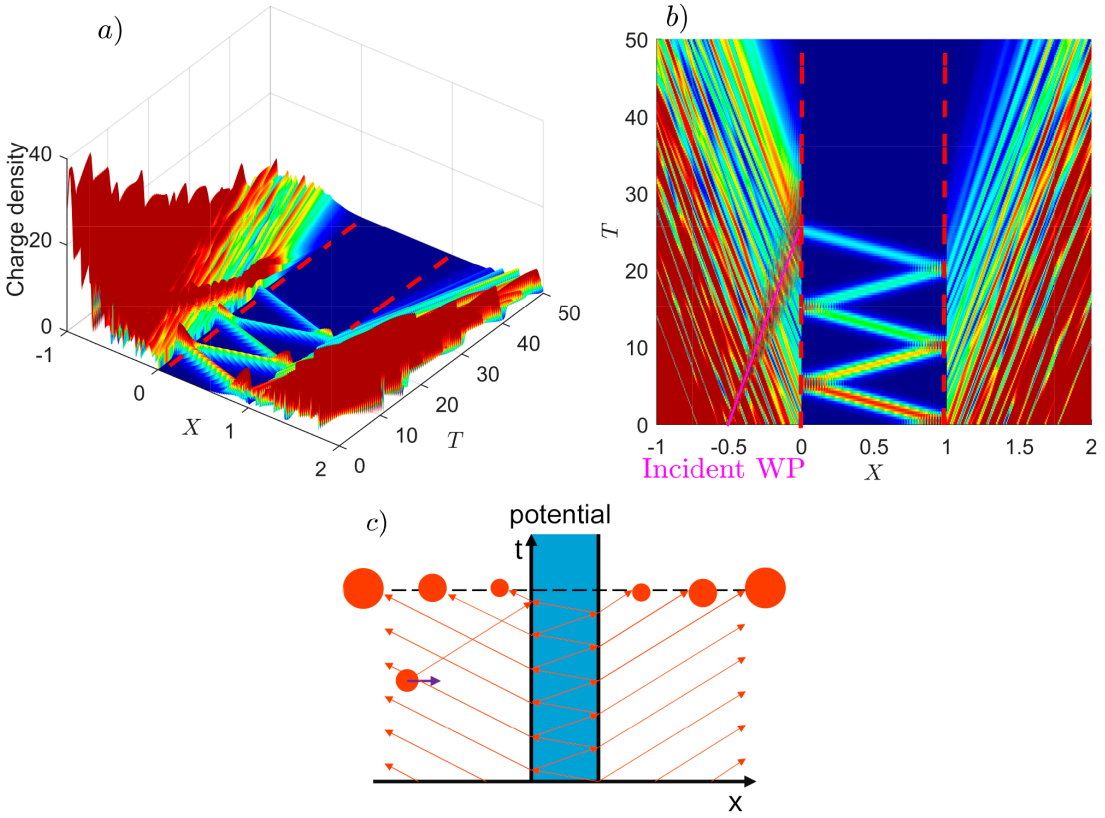

FIGURE 4.5: Divergent scattering for a well with $P_0 = 400$, $M = 2 \times 10^4$, $W/M = -2 \times 10^{-2}$, $X_0 = -0.5$ up to $T = 50$. Before the incident WP reaches the well, there are already WPs in the system, moving away from the well in both directions and also bouncing inside the well. The WPs become smaller each bounce, Eq.(4.21). Once the incident WP reaches the well, the creation of WPs stops.

This solution, although mathematically possible, is not physically meaningful. It describes a WP with an infinite amplitude being "injected" at an infinitely

distant past. Nevertheless, we can combine both solutions to describe physical (causal and bounce) scenarios, as we will show next.

4.2.3.1 Physical non-relativistic solution

The two previous solutions can be combined to obtain a physical solution. We consider the particular case of a single particle whose wave function consists of two spatially separated Gaussian WPs. The first of them starts the propagation inside the well, and the emission starts at the edges of the barrier. After a given number of bounces, the second WP arrives at the left edge of the barrier. This second WP is tuned in such a way that it cancels the bouncing WP inside the potential, as happened in the case of the acausal solution in the previous section. This solution is shown in Fig.4.6 for 1 bounce.

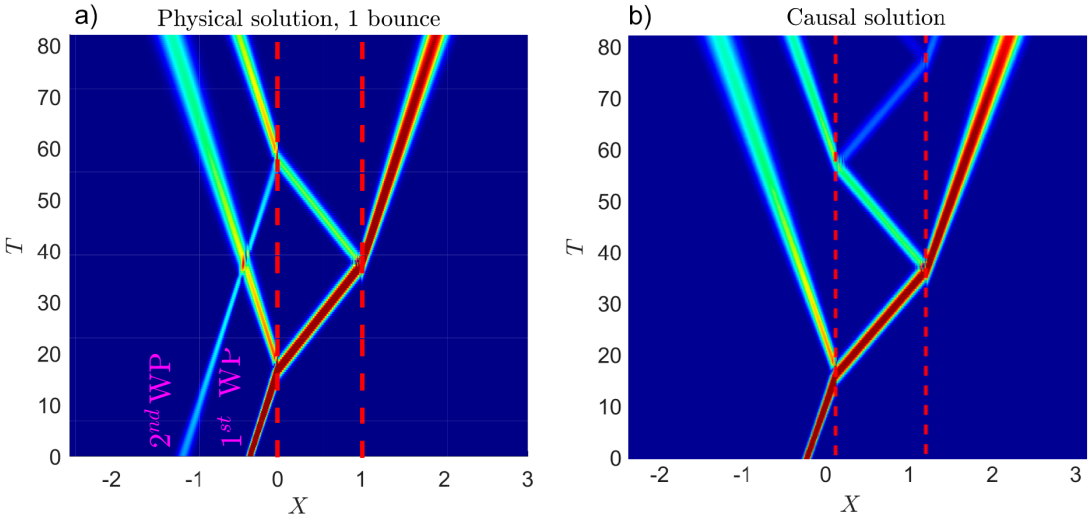

FIGURE 4.6: $P_0 = 600$, $M = 3 \times 10^4$, $W/M = -1 \times 10^{-3}$ and $X_0 = -0.33$. *a)* shows the solution for a second wave packet cancelling the oscillations inside the barrier. *b)* shows how the oscillations would continue inside the barrier without the second WP.

4.2.4 Relativistic bosonic scattering: Supercritical barrier

For a supercritical barrier, with $V_0 > E + \mu c^2$, the momentum inside the barrier is real and allows for WP propagation inside the barrier. We can study the supercritical transmission using the same MRE formalism presented for the non-relativistic scattering.

As we will see, the charge density inside the barrier, given by Eq.(4.2), is negative. We will refer to the WPs propagating with negative charge as antiparticles, since their charge has opposite sign to the incident positively charged particles and they propagate through the second energy continuum. Both the transmitted and the reflected WPs have positive charge density.

The behaviour of the scattering in a supercritical barrier will differ from the non-relativistic case due to the change in the antiparticle's momentum inside the barrier. We can expand it around the mean momentum p_0,

$$q(p) \approx q(p_0) + \partial_p(p - p_0) = q(p_0) - p_0/q_0(p - p_0). \tag{4.22}$$

The group velocity inside the barrier has a sign opposite to the momentum, since $\partial_p q(p) < 0$. As in the previous case, we can construct the convergent and divergent solutions, taking $+q$ or $-q$, respectively.

4.2.4.1 Convergent relativistic solution

Taking the solution for the supercritical scattering with $+q$, the main difference with respect to the non-relativistic scattering is that now $\partial_p q(p) < 0$. This changes the sign of q in the x_n expression. Using the convergent solution of Eq.(4.17), we have a transmitted WP

$$\Psi_I^T(x,t) \approx \sum_{n=0}^{\infty} X_n(p_0, q_0)\Psi_0(x - x_n(p_0, -q_0), t), \tag{4.23}$$

where the weights X_n are given in Eq.(4.18) and the delays x_n are those given in Eq.(4.21). Thus, in the case of transmission through a supercritical barrier, the convergent solution is acausal. The potential region is populated at $t \to \infty$ by a bouncing WP whose amplitude *increases* with each bounce, emitting consecutively larger WPs from the edges. The incident WP terminates the scattering. This is shown in Fig.4.7.

This behaviour can be understood using Feynman's interpretation of the antiparticles as particles travelling *backwards* in time [56]. Within this interpretation,

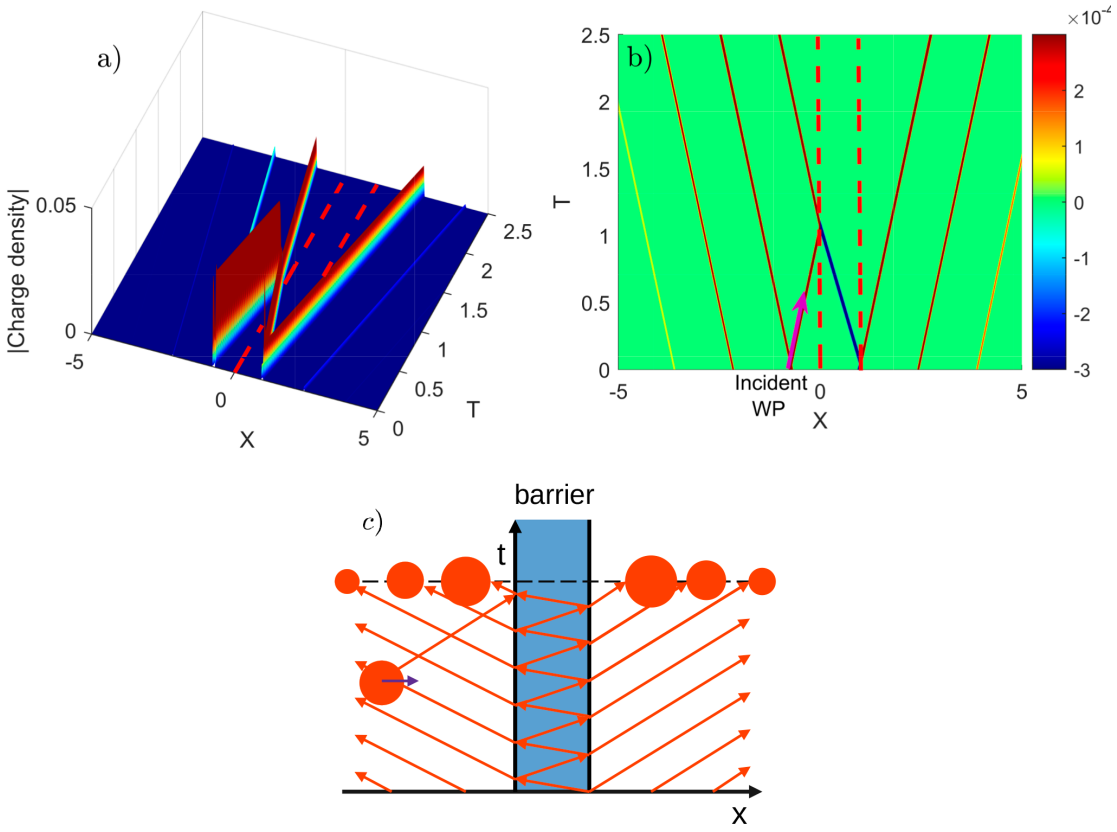

FIGURE 4.7: Convergent and acausal solution for relativistic Klein-Gordon particles, for a Gaussian WP with $P_0 = 10^4$, $M = 10^4$, $W/M = 4\sqrt{2}$, $\Delta P = 100$, $X_0 = -0.75$ and $T = 0$ to 2.5. *a*) absolute value of the charge density, *b*) charge density, where the barrier is marked (red dotted lines), as well as the incident WP (purple solid arrow) and *c*) schematic depiction of the scattering.

the scenario in Fig.4.7 corresponds to a particle that enters the supercritical region in $0 < x < d$ and is scattered *backwards in time*, bouncing at the edges of the barrier. At each bounce it emits increasingly smaller particles *forward in time* as the antiparticle reduces its amplitude.

One can also think of the behaviour at the edges in terms of pair creation or annihilation. Since particles and antiparticles have opposite charges, the total charge is conserved through the scattering. When the antiparticle, injected at a distant past, bounces off the barrier, pairs are created. The antiparticle inside the supercritical barrier increases its amplitude, while increasingly larger particles move away from the barrier. When the incident WP, corresponding to a particle, reaches the barrier, it annihilates the existing antiparticle. At a time t large enough so that the scattering has stopped, only the emitted WPs to the right and left of

the potential remain. Their total charge is equal to the charge of the incident WP. This solution is bound but acausal.

4.2.4.2 Singularity at $E = V_0/2$

For the special case of the super-Klein tunnelling, at $E = V_0/2$, we have that $p_0 = q_0$, so, in Eq.(4.18), only one term of the series, $X_0(p_0, q_0)$, is different from 0. There is only one emitted particle in the region $x > d$. This scenario is shown in Fig.4.8.

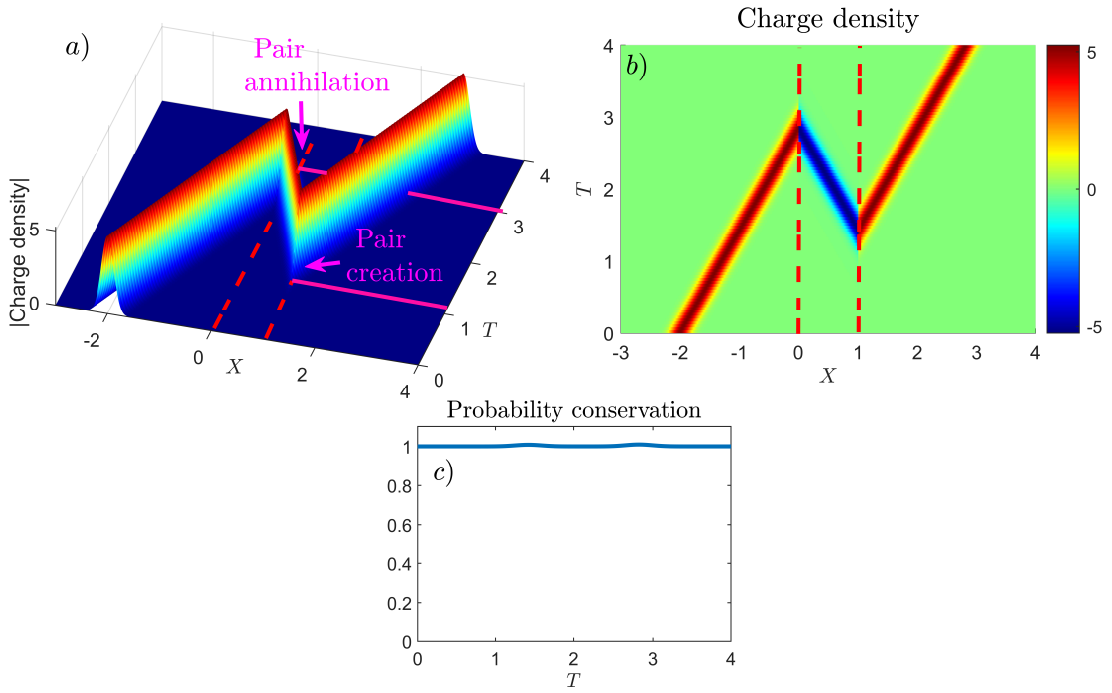

FIGURE 4.8: Bosonic convergent and acausal solution for $M = 5 \times 10^3$, $W/M = 2.2361$, $bM/d = 100$, $\Delta P = 25/3$, $X_0 = -2$ and $E(P_0)/W = 1/2$. Since the antiparticle has negative charge density, the pair creation does not produce any charge, and the charge density is conserved.

For this energy, the weights of the transmitted WPs, given in Eq.(4.21), have a pole. This is due to the sharp edges of the square barrier we are considering, and can be avoided using a smooth one. For the results shown in Fig.4.8, we have used a hyperbolic barrier, $V(x) = V_0/2(\tanh bx - \tanh b(x-d))$, where the parameter b controls the smoothness of the potential. Using this potential one can show that the poles move into the complex plane, as $(p-q)^{-1} \to (p-q+i\delta)^{-1}$, where $\delta = V_0^2/2b$. See Appendix M for details.

Considering Feynman's interpretation, this case corresponds to a single particle transmitted backwards in time from the left edge, and then forward in time from the right edge. Thus, it gains an extra $2d$ distance relative to free propagation, twice the barrier's width. The apparent "negative duration" of the tunnelling is a result of the scattering being acausal, and thus physically impossible.

In terms of pair creation and annihilation, there is a single pair being created at the right edge of the barrier at a time dp_0/μ before the incident WP reaches it, as shown in Fig.4.8. The particle and the antiparticle move forward in time, with the antiparticle encountering and annihilating the incident particle.

4.2.4.3 Divergent relativistic solution

If we take the divergent series, by changing $q \to -q$ in Eq.(4.23), we obtain a causal solution. The transmitted WP is

$$\Psi_{II}^{T}(x,t) \approx \sum_{n=0}^{\infty} X_n(p_0,-q_0)\Psi_0(x - x_n(p_0,q_0),t), \tag{4.24}$$

where again the weights and the delays are given by Eq.(4.18).

In this solution, the creation of pairs is started by the incoming particle, as shown in Fig.4.9. A P-AP pair is created when the bouncing antiparticle reaches the edge of the barrier. This creates a WP outside the barrier and increases the amplitude of the WP inside. Each successive WP has a higher amplitude than the previous one. As can be seen in Fig.4.9*c*), the total charge is conserved, although there is local charge creation outside and inside the potential.

This is not a scattering type solution, as the final state is not a free state. The emission of particles continues as t increases, and both the WP inside the barrier and the travelling WPs outside it grow infinitely. This growth of the probabilities is a sign of the limitations of the single particle approach. In a physical system, the increase in the antiparticle density inside the potential should lead to a decrease in the potential's height [55]. Therefore, the continuous emission thus stops as soon as the potential reaches a value below supercriticality.

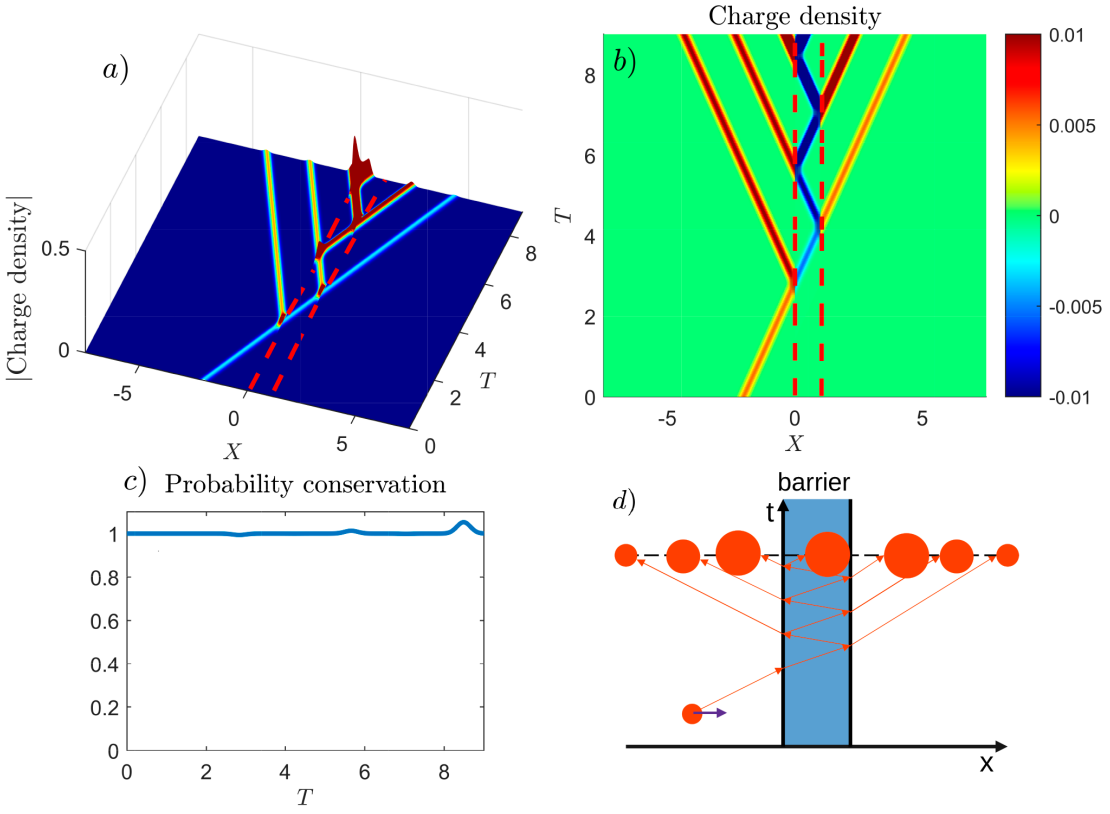

FIGURE 4.9: Bosonic divergent and causal solution for $M = 5 \times 10^3$, $W/M = 2\sqrt{2}$, $bM/d = 2$, $\Delta P = 100/3$, $X_0 = -1$, $E(P_0)/W = 1/2$ and T from 0 to 9. The oscillations appearing in c) are due to numerical errors due to the grid taken in X. The charge is conserved in every pair creation.

4.2.4.4 Physical relativistic solution

As in the non-relativistic case, there is a way to describe a physical solution combining the two previous solutions. We consider a single particle, whose wave function consists of two separated Gaussian WPs, tuned so that the pair production is triggered by the first and, after a number of bounces, stopped by the second, as shown in Fig.4.10.

The first WP triggers the P-AP pair creation in the supercritical barrier. Increasingly higher amplitude WPs are emitted as the WP bounces inside the barrier, increasing in amplitude with each bounce. The emission ends with a P-AP pair annihilation when the second WP reaches the barrier.

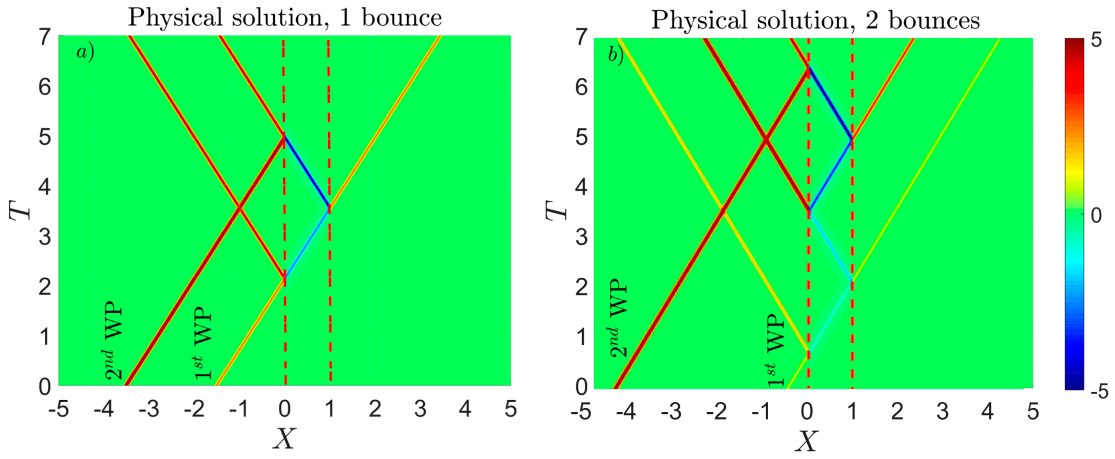

FIGURE 4.10: Physical solution for *a*) one bounce and *b*) three bounces. The first WP starts the creation of the negative charge inside the potential, and the second one, which arrives at a later time, anninilates it, making this solution causal and bound or convergent.

4.3 Fermions

The Dirac equation is the relativistic equation for spin-1/2 particles. In one dimension, it takes the form

$$\hat{H}\Psi_E = E\Psi_E, \tag{4.25}$$

with the Hamiltonian

$$\hat{H} = c\sigma_x(-i\hbar\partial_x) + \sigma_z\mu c^2 + V(x)I, \tag{4.26}$$

where σ_i are the Pauli matrices and $V(x)$ the potential. Generally, a Dirac particle, a solution of Eq.(4.27), is described with a spinor with four components to account for the spin. In the one-dimensional case, the spin has no effect on the dynamics [56] and we can consider a spinor with only two components. Fermions are a solution of ($\hbar = 1$ and $c = 1$)

$$\left[i\partial_t - V\right]\Psi(x,t) = \left[\sigma_x(-i\partial_x) + \sigma_z\mu\right]\Psi(x,t). \tag{4.27}$$

A general positive energy solution of Eq.(4.27) has the form

$$\Psi(x,t) = \begin{pmatrix} 1 \\ \frac{q}{E-V+\mu} \end{pmatrix} e^{iqx-iEt}. \tag{4.28}$$

where $q = \sqrt{(E-V)^2-\mu^2}$ is the momentum inside the potential. In the case of a free particle, $V(x) = 0$, it becomes $p = \sqrt{E^2-\mu^2}$, which is the momentum of the free travelling fermion. The conserved quantity is the total probability [32]. We consider the probability density, which is positive definite, to describe the scattering solutions. In the one-dimensional two-component case studied here, this is

$$\rho = \Psi^*\Psi = \sum_{i=1}^{2} \Psi_i^*\Psi_i. \tag{4.29}$$

For the numerical results of the figures, we will use the same dimensionless units as for the Klein-Gordon case, given in Eq.(4.3).

In the non-relativistic limit, the Dirac equation tends to the Pauli equation which, in the one-dimensional case and in the abscence of magnetic field, reduces to the Schödinger equation. Thus, the non-relativistic solution described in Sections 4.2.2 and 4.2.3 for bosonic particles is also valid for fermions. Therefore, in the current Section we will only focus on the relativistic case, where the differences between the Klein-Gordon and the Dirac scattering do occur.

4.3.1 Transmission amplitude and scattering states

We consider a square potential with $V(x) = V_0$ for $0 < x < d$ and 0 otherwise. For fermions we only require continuity of the wave functions at the edges. We can match the solutions outside and inside the barrier in order to obtain the transmission amplitude and the scattering states. For clarity, we define $K_p \equiv p/(E+m)$ and $K_q \equiv q/(E-V+m)$. Starting with a free wave packet travelling

away from the barrier at $x > d$,

$$x > d: \qquad \begin{pmatrix} 1 \\ K_p \end{pmatrix} e^{ipx}, \tag{4.30}$$

we match it at $x = d$ with two WPs propagating inside the barrier,

$$0 < x < d: \qquad a_+ \begin{pmatrix} 1 \\ K_q \end{pmatrix} e^{iqx/\hbar} + a_- \begin{pmatrix} 1 \\ -K_q \end{pmatrix} e^{-iqx/\hbar} \leftarrow \begin{pmatrix} 1 \\ K_p \end{pmatrix} e^{ipx/\hbar}, \tag{4.31}$$

and apply the same procedure at $x = 0$,

$$\begin{aligned} x < 0: \qquad & b_{++} \begin{pmatrix} 1 \\ K_p \end{pmatrix} e^{ipx} + b_{-+} \begin{pmatrix} 1 \\ -K_p \end{pmatrix} e^{-ipx} \leftarrow \begin{pmatrix} 1 \\ K_q \end{pmatrix} e^{iqx} \\ x < 0: \qquad & b_{+-} \begin{pmatrix} 1 \\ K_p \end{pmatrix} e^{ipx} + b_{--} \begin{pmatrix} 1 \\ -K_p \end{pmatrix} e^{-ipx} \leftarrow \begin{pmatrix} 1 \\ -K_q \end{pmatrix} e^{-iqx}. \end{aligned} \tag{4.32}$$

From Eqs.(4.31) and (4.32) we get the coefficients

$$\begin{aligned} a_+ =& \frac{1}{2}\left(1 + \frac{K_p}{K_q}\right) e^{i(p-q)d}, & a_- =& \frac{1}{2}\left(1 - \frac{K_p}{K_q}\right) e^{i(p+q)d} \\ b_{++} =& \frac{1}{2}\left(1 + \frac{K_q}{K_p}\right) = b_{--}, & b_{-+} =& \frac{1}{2}\left(1 - \frac{K_q}{K_p}\right) = b_{+-}, \end{aligned} \tag{4.33}$$

and the transmission amplitude,

$$T(p,q) = \frac{1}{b_{++}a_+ + b_{+-}a_-} = \frac{4K_pK_qe^{-ipd}}{(K_p+K_q)^2e^{-iqd} - (K_p-K_q)^2e^{iqd}}. \tag{4.34}$$

As we did for bosons, we name the region $x \leq 0$ as 1, $0 \leq x \leq d$ as 2 and $x > d$ as 3. The complete solution of the scattering states in each region is

$$\phi^1(x,p) = R(p,q)\begin{pmatrix}1\\-K_p\end{pmatrix}e^{-ipx} + \begin{pmatrix}1\\K_p\end{pmatrix}e^{ipx}, \qquad x \leq 0, \tag{4.35}$$

$$\phi^2(x,p) = B_+(p)\begin{pmatrix}1\\K_q\end{pmatrix}e^{iqx} + B_-(p)\begin{pmatrix}1\\-K_q\end{pmatrix}e^{-iqx}, \quad 0 \leq x \leq d,$$

$$\phi^3(x,p) = T(p,q)\begin{pmatrix}1\\K_p\end{pmatrix}e^{ipx}, \qquad x > d,$$

with

$$B_\pm(p) = a_\pm T(p,q), \qquad R(p,q) = (b_{-+}a_+ + b_{--}a_-)T(p,q). \tag{4.36}$$

With the scattering states $\phi^i(x,p)$ in Eq.(4.35), we can write the WPs using by Eq.(4.11).

4.3.2 Multiple Reflection Expansion for fermions

As in the bosonic case, the transmission amplitude can be written as a MRE, where each term in the series corresponds to a bounce of a particle inside the barrier. Again, there are two different ways of doing this expansion, taking $+q$

$$\begin{aligned} T(p,q) &= \frac{1}{b_{++}a_+ + b_{+-}a_-} \to \frac{1}{b_{++}a_+}\sum_{n=0}^{\infty}\left(-\frac{b_{+-}a_-}{b_{++}a_+}\right)^n \\ &= \frac{4K_pK_q}{(K_p+K_q)^2}e^{-ipd}\sum_{n=0}^{\infty}\frac{(K_p-K_q)^{2n}}{(K_p+K_q)^{2n}}e^{i(2n+1)qd} \equiv \sum_{n=0}^{\infty}T_n(p,q) \end{aligned} \tag{4.37}$$

and taking $-q$, which, since $K_q(-q) = -K_q(q) \equiv -K_q$, is equivalent to

$$T(p,q) = \frac{1}{b_{++}a_+ + b_{+-}a_-} \to \frac{1}{b_{+-}a_-}\sum_{n=0}^{\infty}\left(-\frac{b_{++}a_+}{b_{+-}a_-}\right)^n \tag{4.38}$$
$$= \frac{-4K_pK_q}{(K_q-K_q)^2}e^{-ipd}\sum_{n=0}^{\infty}\frac{(K_p+K_q)^{2n}}{(K_p-K_q)^{2n}}e^{-i(2n+1)qd} \equiv \sum_{n=0}^{\infty}T_n(p,-q).$$

4.3.3 Relativistic fermionic scattering: Supercritical barrier

We consider a supercritical rectangular barrier, with $V_0 > E + \mu c^2$. Taking a WP narrow enough in momentum space, the momentum inside the barrier can be approximated as in Eq.(4.22). We have that $\partial_p q(p)|_{p=p_0} < 0$, and thus the group velocity inside the barrier has an opposite direction to that of the momentum.

4.3.3.1 Divergent MRE

Using the expansion (4.37), for $+q$, the supercritical fermionic WPs can be written as

$$\Psi_I^T(x,t) \approx \sum_{n=0}^{\infty} X_n(p_0,q_0)\Psi_0(x - x_n(p_0,q_0),t), \tag{4.39}$$

with weights $X_n(p_0,q_0)$ and delays $x_n(p_0,q_0)$ given by

$$X_n(p_0,q_0) = \frac{4K_pK_q}{(K_p+K_q)^2}\frac{(K_p-K_q)^{2n}}{(K_p+K_q)^{2n}}e^{i(2n+1)(q_0-p_0^2/q_0)d}, \tag{4.40}$$
$$x_n(p_0,q_0) = d\left[1-(2n+1)p_0/q_0\right].$$

This solution leads to divergent scattering. From Eq.(4.40) we see that each emitted WP is multiplied by an extra factor $\sim (K_p - K_q)^2/(K_p + K_q)^2$. For the supercritical barrier we are considering, we have that $V_0 > E + \mu$, and thus $K_q = q/(E - V_0 + \mu) < 0$. Since $K_p = p/(E+\mu) > 0$, we have that $(K_p - K_q)^2 >$

$(K_p + K_q)^2$, therefore $X_{n+1}(p_0, q_0) > X_n(p_0, q_0)$ and the expansion diverges. The solution is acausal.

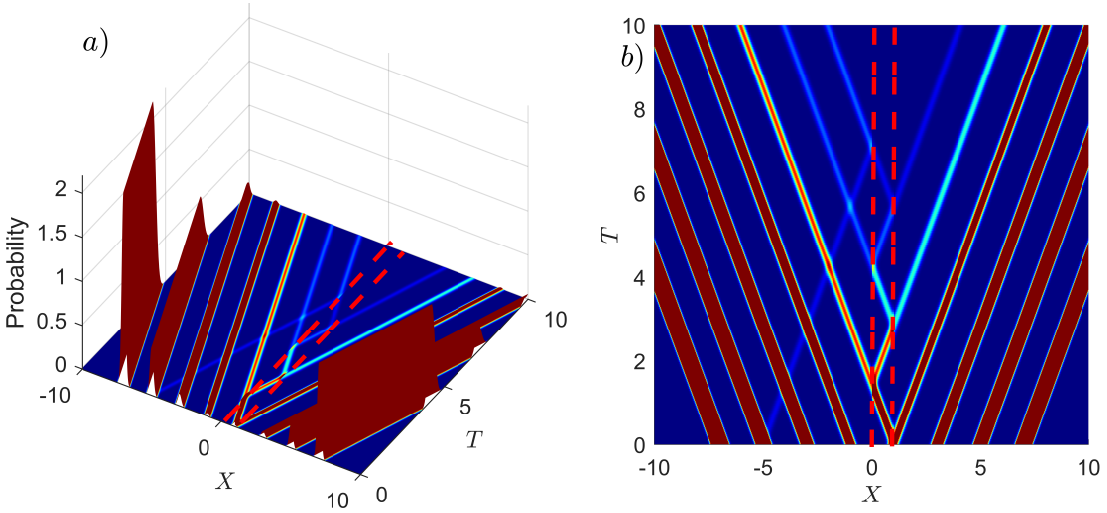

FIGURE 4.11: Relativistic solution of the Dirac equation using $+q$, Eq.(4.39), with $P_0 = 2 \times 10^4$, $M = 2 \times 10^4$, $W/M = 2\sqrt{2}$, $\Delta P = 8$, $X_0 = -5$ and $T = 0$ to 10, which is acausal and divergent.

This behaviour is shown in Fig.4.11 and corresponds to a WP already propagating inside the barrier before the arrival of the incident one. As in the non-relativistic case, we can think of this WP as being "injected" at a time $t \to -\infty$. At each bounce, it reduces its amplitude, and a WP is emitted and travels away from the barrier. The propagation inside the barrier stops when the incident WP reaches it and interferes destructively with it, leaving the barrier empty. The solution is acausal and unbound.

It is worth noting that there is no P-AP pair creation, and that the emission of WPs at each bounce conserves not only the charge but also the probability.

4.3.3.2 Convergent MRE

Taking the expansion for $-q$, Eq.(4.38), the MRE of the transmitted WP is

$$\Psi_{II}^{T} x, t) \approx \sum_{n=0}^{\infty} X_n(p_0, q_0) \Psi_0(x - x_n(p_0, -q_0), t), \tag{4.41}$$

where the weights and the delays are given in Eq.(4.39). This corresponds the convergent solution. The successive weights are $X_{n+1}(p_0, -q_0) < X_n(p_0, -q_0)$, and

the delays correspond to the causal solution, $x_n(p_0, q_0)$, given in Eq.(4.40). This case is shown in Fig.4.12, where the incident WP starts the propagation inside the barrier.

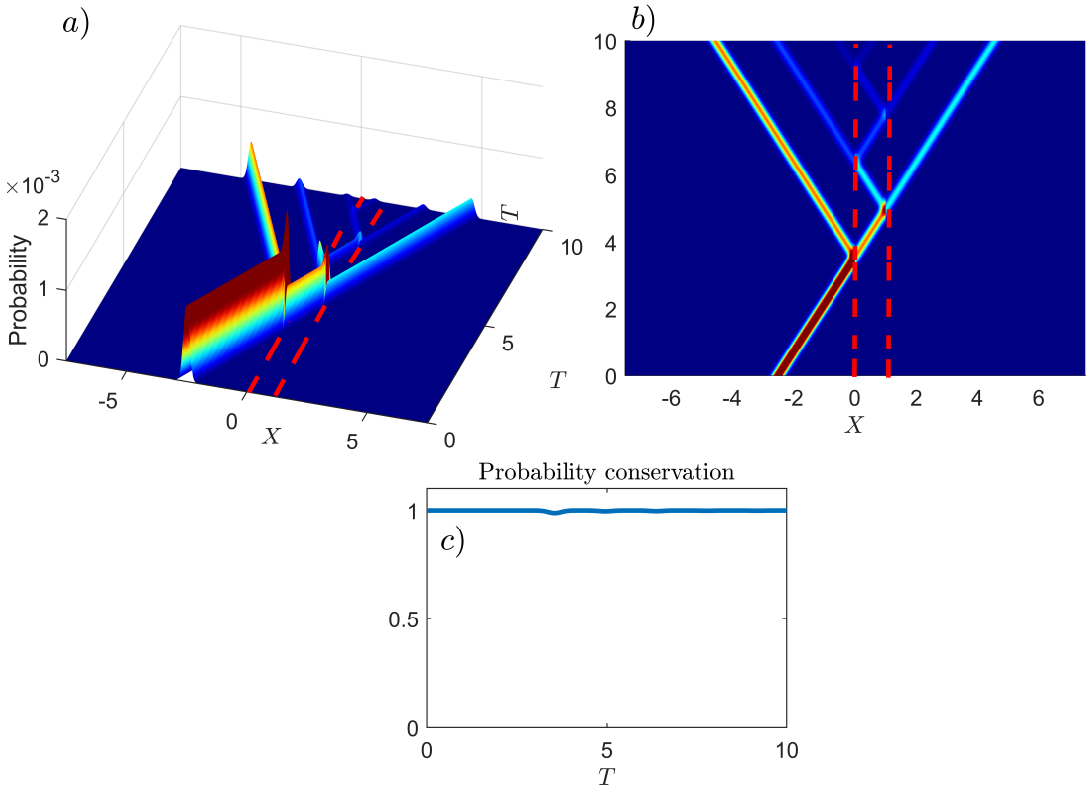

FIGURE 4.12: Relativistic solution of the Dirac equation for $-q$, Eq.(4.41), with $P_0 = 2 \times 10^4$, $M = 2 \times 10^4$, $W/M = 2\sqrt{2}$, $\Delta P = 8$, $X_0 = -2.5$ and $T = 0$ to 10, which is causal and convergent.

The amplitude of the WP inside the barrier is reduced at each bounce, and a WP is emitted to the right or to the left of the barrier. This continues until the barrier is emptied, and there are only WPs outside the barrier region, moving away from it.

4.4 Conclusions and discussion

In this chapter we have studied the scattering through a potential barrier for both bosons, obeying the Klein-Gordon equation, and fermions, obeying the Dirac equation, in non-relativistic and relativistic scenarios. We have used the Multiple Reflection Expansion (MRE), writing the WPs inside and outside the barrier

region in terms of reflection and transmission sub-amplitudes. We can make the change $q \to -q$ in the series and obtain two different solutions for bosons and fermions, making the series to be divergent or convergent [55]. This also changes the types of scattering solutions.

In the non-relativistic limit, with potentials far below supercriticality and non-relativistic velocities, both particles behave in the same way since both obey the Schrödinger equation. The convergent solution is causal, as the scattering is started by the incident particle. This is a scattering type solution which can also be obtained with the S-matrix method, as it describes the scattering between two asymptotically free states. The divergent solution describes a situation where there are bouncing WPs inside the potential *before* the arrival of the incident one. At each bounce a WP is emitted outside the barrier region, with larger amplitudes the further they are from the barrier. The arrival of the incident WP interferes destructively with the one inside the potential, stopping the oscillations.

For a supercritical barrier the scattering enters the Klein regime, where WPs can propagate freely through the barrier. In this regime, bosons and fermions scatter very differently. Again, we can construct two different MREs taking the expansions with $+q$ or $-q$.

4.4.1 Bosonic scattering

For bosons, there is no solution that is both causal and bound. The convergent solution is acausal. It describes WPs already propagating in the barrier *before* the arrival of the incident WP, with their amplitude decreasing with each bounce, and being terminated by the arrival of the incident WP (see Fig.4.7). This scenario can be described in terms of pair creation at the edges of the barrier, caused by the supercritical barrier. Alternatively, the antiparticles can be though of as particles moving *backwards in time* inside the potential [56]. At each bounce of the antiparticle, a particle moving forward in time is emitted, while the antiparticle's amplitude decreases as it moves backwards in time. This process goes on until the probability density is zero inside the barrier.

For the particular case of $E = V_0/2$, only one WP is emitted (see Fig.(4.8)), which is advanced by twice the width of the barrier relative to free propagation. If we derive a tunnelling time from this advance we obtain a "negative duration", which is a consequence of the solution being acausal. Using this interpretation of the antiparticle as a particle moving backwards in time, one can obtain this solution via the S-matrix method, since both the initial and final states are of asymptotically free moving WPs.

The divergent solution is causal, and the arrival of the incident particle starts the P-AP pair creation at the edges of the barrier, causing an increasing emission of particles outside the potential and higher amplitude antiparticles inside it (see Fig.4.9). Since antiparticles have opposite charge, pair creation does not create a net charge, which is conserved through the scattering, unlike the total probability.

4.4.2 Fermionic scattering

This contrasts with the effect of the supercritical barrier on the fermionic scattering, for which the convergent solution remains causal. The WP propagation inside the barrier is started by the incoming particle, and its amplitude decays with each bounce (see Fig.4.12). It is a scattering type solution. If we use the divergent expansion of the WPs, Fig.4.11, we obtain an acausal solution, where each successive WP in the MRE has a higher amplitude than the previous one and is further away from the barrier. These solutions are similar to those obtained for non-relativistic scattering. There is no P-AP pair creation, and both the total charge and the total probability density are conserved through the scattering.

4.4.3 Beyond the one-particle approach: Quantum Field Theory and future perspective

In this chapter we have considered a single-particle approach, for both bosons and fermions. Nevertheless, the solutions for bosonic supercritical scattering that we have studied seem to be compatible with P-AP creation. This pair creation is not present in the MRE solutions for the Dirac equation. In the standard

interpretation of fermionic pair creation, the concept of the Dirac sea is introduced, [32], where all negative energy states are filled with electrons.

In order to describe completely a multi-particle process, such as the P-AP pair creation, one has to rely on QFT. A time-dependent solution is studied in [57]. The solutions of the single-particle approach appear related to the multi-particle solutions, studied for the Klein-Gordon equation in [58], and for the Dirac equation in [59] for step potentials.

The single-particle approach taken in this work shows differences between the supercritical solutions to the Klein-Gordon and the Dirac equations. We believe these differences can be further understood taken a multi-particle QFT approach, where bosonic and fermionic pair creation appears. We intend to continue the present work in this direction.

Conclusions

Conclusions on Part I: non-relativistic scattering

- **Eisenbud-Wigner-Smith times**
  - We have analysed the Eisenbud-Wigner-Smith (EWS) delay, given by the energy derivative of the phase shift. In the limit of a very broad wave packet (WP), we obtain the time delay experienced by the WP from the measurement of the spatial delay.
  - The spatial delay is calculated as the distance between the centres of mass (COM) of the transmitted and the free WPs.
  - In the case of tunnelling, the EWS times are very short, apparently superluminal.
- **Delay distribution and quantum measurements**
  - The transmitted WP can be represented as the sum of freely propagating envelopes, each shifted in space by x', with a complex weight given by the delay distribution, $\eta(p_0, x')$(see Eq.(1.16)), which is the Fourier Transform of the transmission amplitude. This delay distribution contains the available shifts that the interfering envelopes can acquire in a particular potential.
  - The amplitude in Eq.(1.16) for the transmitted WP can be interpreted as a quantum measurement of the spatial delay x', where $G_0(x, t)$ plays the role of the "apparatus function".

- A narrower WP corresponds to an accurate measurement and can "discriminate" between interfering delays, while a wider WP corresponds to inaccurate measurements. The case of an accurate measurement is highly perturbative, and destroys the studied transition (see Fig.3.7).

- *Classically allowed transition:* In the semiclassical limit, the delay distribution, $\eta(p_0, x')$, has a real saddle point, $\tilde{x}'$, in the complex x'-plane. The interference of the shifted envelopes cancels all the envelopes except the one delayed by $\tilde{x}'$, so there is a single delayed envelope, $G_0(x-\tilde{x}', t)$, "selected" by the transition. This (classical) value of x' gives the classical duration of the transition. The delay can be written in terms of the mean velocity of the WP inside and outside the potential (see Eq.(1.11)).

- *Tunnelling:* In the semiclassical limit, the transition is classically forbidden and the saddle point is complex, $\tilde{x}' \equiv \tilde{x}'_1 + i\tilde{x}'_2$. There are two effects that shift the COM of the tunnelled WP. The imaginary part of the delay, $\tilde{x}'_2$, contributes to a momentum filtering effect, increasing the mean momentum of the transmitted WP. When the momentum filtering can be neglected, $\tilde{x}'_1$ accounts for the spatial delay. The classically forbidden region does not contribute to $\tilde{x}'_1$ (see Eq.(1.12)), which explains the apparently instantaneous transmission. No single shift is selected on the x'-axis. Instead, the resulting WP comes from interference via a reshaping mechanism.

- **Reshaping mechanism for tunnelling**

  - In the case of tunnelling, the delay distribution shows fast oscillations along the x'-axis (see Fig. 1.6 *c*)), which results in the suppression of transmission. The reshaping mechanism is such that only the front tails of the envelopes interfere constructively, so that the COM of the tunnelled WP is advanced relative to a freely propagating one. The resulting position of the transmitted WP is not the result of a single real spatial shift, but of the interference of several spatial delays.

- As in the double-slit experiment, the Uncertainty Principle "hides" the information about the path taken by the particle inside the potential [25]. *The spatial delay can be related to the time at which COM arrives at a detector to the right of the barrier, but not to the duration of the transition.*

- **The Eisenbud-Wigner-Smith delay as a weak value**

  - If we neglect the momentum filtering effect, the spatial delay of the tunnelled particle can be calculated as the real part of the first moment of the delay distribution (see Eqs.(1.30) and (1.29)). Even though for a barrier $\eta(p_0, x')$ vanishes for positive x', in the case of tunnelling the resulting shift of the COM is positive.

  - The delay is calculated as an "average" obtained with *amplitudes* instead of *probabilities*. This can be understood as a "weak measurement" of the shifts x' [22], which is designed to perturb the system minimally, and thus do not to destroy the interference. It is a well-known property of quantum measurements that *if interference were not destroyed (...) the quantum theory could be shown to lead to absurd results* [24].

- **A pole representation**

  - The delay distribution and the transmitted WP can be conveniently expressed in terms of the singularities of the transmission amplitude in the complex momentum plane. These singularities, or poles, are related to bound states, which lie on the positive imaginary axis, $\mathrm{Re}(k) = 0$, or to resonant states, which lie on the negative half plane, $\mathrm{Im}(k) < 0$. The contribution of each pole to the delay distribution is a decaying exponential, weighted by the residue of the poles (see Eq.(1.33)). $\eta(p_0, x')$ only has non-zero positive x' contributions for bound states, and non-zero negative x' contributions for resonant states.

- **The Eckart potential**
  - As an example, we have used the Eckart potential [40], barrier or well, and reproduced the results for classically allowed transmission and tunnelling (see Figs. 2.2 and 2.3).
  - We have applied the pole representation to the Eckart potential, and studied the delay distributions obtained. The resonant and bound states are related to a slow-down or a speed-up effect, respectively. The pole representation becomes impractical in the semiclassical case, for very high barriers and deep wells, since the value of the residues becomes prohibitively large.
  - We have studied in more detail the cases of low-energy scattering by shallow wells and low barriers, where a single pole determines the transmission (see Figs. 2.8 and 2.11). This pole corresponds to a bound state in the case of a well, and to virtual state, a long-lived state [39], in the case of a barrier.
- **Zero-range potential**
  - We have compared the results of the EWS delays for a zero-range potential, which is an ultra-quantum case, with those obtained using the Larmor clock. Both approaches agree in the classical limit, but become contradictory in an ultra-quantum scattering scenario [6].
  - *Larmor clock:* This approach measures the net time spent by the particle in the potential. In the limit of the zero-range potential the range of available temporal delays narrows to only $\tau = 0$. Thus, the measured delay is always zero. The accuracy of the meter is irrelevant, since there are no alternative delays.
  - *EWS delay:* As explained before, the quantity measured is the displacement x'. For a zero-range potential, there is still a range of spatial delays available, and thus there is an interference between different delays that produce a shifted transmitted WP. Since the transmission

amplitude has a single pole, $\eta(p_0, x')$ has a simple form, with a single decaying exponential. We have extended the study of the delay distribution to reflection.

Conclusions on Part II: relativistic scattering

- **Multiple Reflection Expansion**
  - We have studied the dynamics of relativistic scattering of WPs through rectangular potentials using the Klein-Gordon and Dirac equations. This is a first quantized, and therefore single-particle approach.
  - The transmission amplitude can be expanded in a convergent geometric series, the Multiple Reflection Expansion (MRE), by writing it as a sum of sub-amplitudes. This leads to a decomposition of the scattering states as a sum of consecutively delayed WPs. Each term in the series has a weight and a phase, related to the spatial delay between consecutive WPs.
- **Convergent and divergent solutions**
  - We can change $q \to -q$ in the MRE of the scattered WPs, and obtain a divergent series, which is still a solution of the equations. Each new WP emitted from the barrier has a larger amplitude than the previous one.
  - *Causality:* The solutions can be causal or acausal. A causal solution is one in which the barrier is initially empty, and the scattering is triggered by the incoming WP. In the acausal solution, even before the initial WP reaches the barrier, there is a WP propagating inside it and emitted WPs on both sides of the barrier.
- **Non-relativistic limit**
  - Both types of particles can be described by the Schrödinger equation in the non-relativistic limit. We have considered classically allowed

transitions. The convergent solution is causal (see Fig. 4.4), while the divergent solution is acausal (see Fig. 4.5).

– The convergent and divergent solutions can be combined to describe a new physical situation. It consists of two incident WPs, tuned so that the first one triggers the oscillations inside the barrier, and the second one stops them (see Fig. 4.6).

- **Supercritical barriers**

  – For relativistic scattering, we are interested in supercritical barriers, $V_0 > E + \mu c^2$, where there are WPs propagating inside the barrier region. For a causal solution, the sign of q in the MRE must be changed.

  – *Bosons:* The divergent solution is causal (see Fig.4.9). The divergence is related to the creation of particle-antiparticle (P-AP) pairs at the edges of the barrier, triggered by the incoming WP. A P-AP creation (or annihilation) satisfies the Klein-Gordon equation and the charge is conserved, although the probability is not. The convergent solution for bosons is acausal (see Fig.4.7).

  For $E = V_0/2$, corresponding to the super-Klein tunnelling [52, 53], there is complete transmission. A single P-AP pair is created at the opposite edge of the barrier before the arrival of the incident WP (see Fig.4.8). When the incident WP reaches the barrier, it annihilates the antiparticle inside it. The transmitted WP is advanced by twice the width of the barrier, resulting in the apparent negative tunnelling time.

  Following Feynman [56], antiparticles can be though of as particles travelling *backwards* in time. A WP incident from the left is scattered backwards in time inside the barrier and, when it reaches the right edge, a particle is scattered forwards in time, while the antiparticle continues to travel backwards in time. In the case of super-Klein tunnelling, there is a single WP that is transmitted backwards in time at the left edge of the barrier and forwards in time at the right edge, without reflection.

– *Fermions:* The causal solution is convergent, and there is no P-AP creation (see Fig.4.12). If we choose the divergent solution instead, we get an acausal scattering (see Fig.4.11). The conserved quantity for fermions is the probability density, the same as for the Schrödinger equation. Thus, the solutions are similar. The conservation of the probability density does not allow for P-AP creation or annihilation, and therefore the charge density is also conserved. For a negatively charged incident WP, as an electron, the WP travelling inside the potential has also negative charge.

– All these solutions, for both particles and in the non-relativistic and relativistic cases, appear summarised in the table below.

q in the MRE	**non-relativistic Schrödinger above the barrier**	**relativistic Klein-Gordon supercritical**	**relativistic Dirac supercritical**
$+q$	convergent/causal	convergent/acausal	divergent/acausal
$-q$	divergent/acausal	divergent/causal	convergent/causal

- **Limitations of the single-particle approach and QFT**

  – The use of the Dirac equation does not lead to P-AP pair production. In the case of the Klein-Gordon equation we have analysed how the causal solution diverges, as pairs are being created at the edge of the supercritical barrier. Both approaches are limited describing pair production, as they are single-particle approaches. To deal properly with multi-particle dynamics, one has to resort to Quantum Field Theory [57–59].

Appendices

Appendix A

A square potential

For a square barrier of width d, $V(x) = V_0$ for $0 < x < d$ and $V(x) = 0$ elsewhere, the transmission amplitude is known (see for example [30]), and has an expression

$$T(k, V) = \frac{4kqe^{-ikd}}{(k+q)^2 e^{-iqd} + (k-q)^2 e^{iqd}}. \tag{A.1}$$

Since this potential does not vary with x, except for the discontinuities at its edges, the semiclassical condition is met everywhere, except at the edges. The semiclassical delays in Eqs. (1.11) and (1.12) are given by

$$\begin{aligned} \tilde{x}' &= \left[1 - p_0/q(x, p_0)\right] d, \\ \tilde{x}'_1 &= d, \\ \tilde{x}'_2 &= -\left[p_0/\left|q(x, p_0)\right|\right] d. \end{aligned} \tag{A.2}$$

The tunnelled particle is advanced exactly the width of the potential, because the whole potential corresponds to the classically forbidden region.

The reason for using different potentials in the following chapters is that the transmission amplitude for the square potential in Eq.(A.1) has no easy analytical solution for the poles k_p, which play a central role in the pole representation

explained in Section 1.8. Contrary to this case, the poles appear easily in the case of the Eckart potential and the zero-range potential, used in the following chapters. The pole representation allows for an analytical exact expression in Eq.(1.33).

Appendix B

The steepest descent method

The steepest descent method[60] is an approximation for highly oscillatory integrals with the form $I = \int e^{i\lambda f(x)} g(x) dx$, where $\lambda \to \infty$. The main contribution comes from a small region around the maximum of $f(x)$, at the stationary point x_0, defined as $f'(x_0) = 0$. Far from that point, the rapid oscillations, much faster than the change in $g(x)$, tend to cancel each other. Only the region around the stationary point, where the frequency of these oscillations decreases, contribute to the final integral with the value of $g(x)$ at the point x_0. We expand the phase around that point and keep up to the second order term. When this function is complex, this stationary point x_0 becomes a saddle point. The integral, evaluating the remaining Gaussian integral after the expansion, is $I \approx e^{i\lambda f(x_0)} g(x_0) \sqrt{2\pi/\lambda |f''(x_0)|}$.

We can apply this method to evaluate the integral for the delay distribution Eq.(1.17),

$$\eta(p_0, x') = \frac{\exp(-ip_0 x')}{2\pi} \int_{-\infty}^{\infty} \exp\left[i\Phi(k, V) + ikx'\right] dk, \tag{B.1}$$

where $\Phi(k, V)$ is the semiclassical phase of the transmission amplitude given in Eq.(1.8) and we identify $g(x) = 1$, $f(x) = \Phi(k, V) + kx'$ and $\lambda = 1/\hbar$. The condition for the semiclassical approximation that we are using is that the actions, in this case, $f(x)$, are much larger than $\hbar$, so we can use the steepest descent

method. The stationary momentum, $\tilde{k}$, which is a function of x', must verify

$$\partial_k \left[\Phi(k,V) + kx'\right]|_{k=\tilde{k}(x')} = \left.\frac{\partial\Phi(k,V)}{\partial k}\right|_{k=\tilde{k}(x')} + x' = 0. \tag{B.2}$$

With this, we can solve Eq.(B.1)

$$\eta(p_0,x') \approx \left(2\pi/\left|\partial_k^2\Phi(k,V)|_{k=\tilde{k}(x')}\right|\right)^{-1/2} \exp\left[-ip_0x' + i\Phi(\tilde{k}(x'),V) + i\tilde{k}(x')x'\right]. \tag{B.3}$$

and use this result to evaluate the integral for the transmitted WP, $\Psi^T(x,t)$ in Eq.(1.16), again with the steepest descent method. For simplicity we name $\Theta = -p_0x' + \Phi(\tilde{k}(x'),V) + \tilde{k}(x')x'$ and get the condition for the stationary point

$$\begin{aligned}\partial_{x'}\Theta = \partial_{x'}\left[\Phi(\tilde{k}(x')) + \tilde{k}(x')x' - p_0x'\right]\Big|_{x'=\tilde{x}'} = \\ = \frac{\partial\Phi(\tilde{k}(x'),V)}{\partial k}\frac{\partial\tilde{k}(x')}{\partial x'} + \tilde{x'}\frac{\partial\tilde{k}(\tilde{x'})}{\partial x'} + \tilde{k}(x') - p_0 = \\ = \frac{\partial\tilde{k}(x')}{\partial x'}\left[\left.\frac{\partial\Phi(k,V)}{\partial k}\right|_{k=\tilde{k}(x')} + \tilde{x'}\right] + \tilde{k}(\tilde{x'}) - p_0 = 0.\end{aligned} \tag{B.4}$$

The term in brackets is 0 directly from Eq.(1.24). For the second derivative of the phase, which appears as a prefactor after evaluating the Gaussian integral, we have that

$$\frac{\partial^2\Theta}{\partial x'^2} = \frac{\partial}{\partial x'}\left[\tilde{k}(\tilde{x'}) - p_0\right] = \frac{\partial\tilde{k}(x')}{\partial x'}. \tag{B.5}$$

We can differentiate the term in bracket in Eq.(B.4) with respect to x', which is zero, and obtain

$$\frac{\partial}{\partial x'}\left[\left.\frac{\partial\Phi(k,V)}{\partial k}\right|_{k=\tilde{k}(x')} + x' = 0\right] = \left.\frac{\partial^2\Phi(k,V)}{\partial k^2}\right|_{k=\tilde{k}'(x')}\frac{\partial\tilde{k}(x')}{\partial x'} + 1 = 0, \tag{B.6}$$

from where, combining it with Eq.(B.5), we get that

$$\frac{\partial^2\Theta}{\partial x'^2} = \left[-\frac{\partial^2\Phi(k,V)}{\partial k^2}\bigg|_{k=\tilde{k}(x')} \right]^{-1}, \tag{B.7}$$

which cancels out the second derivative of the prefactor in Eq.(B.3). Finally, the transmitted WP is the same as the one in Eq.(1.14).

Appendix C

Superimposed oscillations at the stationary point of $\eta(p_0, x')$

Knowing that the FT of the transmission amplitude, $\exp(ip_0x')\eta(p_0, x')$, is a real function, from Eq.(B.3), we can write

$$\begin{aligned}\eta(p_0, x') \sim \exp\left[-ip_0x'\right] \cos\left[i\Phi(\tilde{k}(x'), V) + i\tilde{k}(x')x'\right] = \\ = \left[\cos(-ip_0x') + i\sin(-ip_0x')\right] \cos\left[i\Phi(\tilde{k}(x'), V) + i\tilde{k}(x')x'\right].\end{aligned} \tag{C.1}$$

The real part of Eq.(C.1), plotted in Fig.1.6, is

$$\begin{aligned}\mathrm{Re}\left[\eta(p_0, x')\right] \sim & \cos\left(-ip_0x'\right) \cos\left[i\Phi(\tilde{k}(x'), V) + i\tilde{k}(x')x'\right] = \\ = & \frac{1}{2}\Big\{\cos\left[-ip_0x' + i\Phi(\tilde{k}(x'), V) + i\tilde{k}(x')x'\right] + \\ & + \cos\left[-ip_0x' - i\Phi(\tilde{k}(x'), V) - i\tilde{k}(x')x'\right]\Big\}.\end{aligned} \tag{C.2}$$

Only the oscillations of the first cosine in Eq.(C.2) cancel at the stationary point given by Eq.(1.26), but not the ones coming from the second cosine, which is the responsible of the superimposed oscillations in Fig.1.6. The imaginary part of $\eta(p_0, x')$ can be done equivalently, and has also superimposed oscillations.

Appendix D

Approximation of the delay for wide WPs

Inserting the expansion $G_0(x-x',t) \approx G_0(x,t) - \partial_x G_0(x,t)x'$ into Eq.(1.16) we have

$$\Psi^T(x,t) = \exp\left[ip_0x - iE(p_0)t\right]\left[G_0(x,t)\int \eta(p_0,x')dx' - \partial_x G_0(x,t)\int x'\eta(p_0,x')dx'\right] \tag{D.1}$$

$$\equiv \exp\left[ip_0x - iE(p_0)t\right]\left[G_0 I - G_0' J\right],$$

where $G_0' = \partial_x G_0(x,t)$, $I = \int \eta(p_0,x')dx'$ and $J = \int x'\eta(p_0,x')dx'$. From there,

$$|\Psi^T(x,t)|^2 \approx |G_0|^2|I|^2 + |G_0'|^2|J|^2 - G_0 G_0'^* I J^* - G_0^* G_0' I^* J. \tag{D.2}$$

In order to compute the delay of the particle, Eq.(1.5), for a large enough time so that the particle is far enough to the right of the barrier, we take as the COM of the freely propagating particle

$$x^0_{COM}(x,t) = v_0 t, \tag{D.3}$$

where $v_0 = p/\mu$ is the mean velocity of the free particle. For the COM of the tunnelled particle we have

$$x^T_{COM}(x,t) = \frac{\int x|\Psi^T(x,t)|^2 dx}{\int |\Psi^T(x,t)|^2 dx}. \tag{D.4}$$

The denominator can be approximated considering that $\int G_0'(x,t)dx \ll 1$, so we end up with only one term,

$$\int |\Psi^T(x,t)|^2 dx \approx \int |G_0|^2 |I|^2 dx = |I|^2, \tag{D.5}$$

where we have used that $|G_0|^2$ is normalised over x.

We will compute the numerator of Eq.(D.4) by inserting the expansion in Eq.(D.2) into it,

$$\begin{aligned}\int x|\Psi^T(x,t)|^2 dx = &\int x|G_0|^2 dx|I|^2 + \int x|G_0'|^2 dx|J|^2 \\ &- \int xG_0 G_0'^* I J^* dx - \int xG_0^* G_0' I^* J dx.\end{aligned} \tag{D.6}$$

The first term is directly $\int x|G_0|^2 dx|I|^2 \approx v_0 t|I|^2$, which with the denominator in Eq.(D.5) cancels the position of the COM of the freely propagating WP in Eq.(D.3). For the second term we have that $\int x|G_0'|^2 dx \approx 0$. We can expand the remaining terms,

$$\begin{aligned}&- \int xG_0 G_0'^* I J^* dx - \int xG_0^* G_0' I^* J dx = \\ &- (1/2)\int xG_0 G_0'^* I J^* dx - (1/2)\int xG_0^* G_0' I^* J dx - \\ &- (1/2)\int xG_0 G_0'^* I J^* dx - (1/2)\int xG_0^* G_0' I^* J dx + \\ &+ (1/2)\int xG_0 G_0'^* I^* J dx + (1/2)\int xG_0^* G_0' I J^* dx + \\ &+ (1/2)\int xG_0 G_0'^* I^* J dx + (1/2)\int xG_0^* G_0' I J^* dx,\end{aligned} \tag{D.7}$$

where the last four terms add up to 0.

Grouping the first two and the fifth and sixth terms, we have

$$\begin{aligned} &-(1/2)\int xG_0G_0'^*IJ^*dx-(1/2)\int xG_0^*G_0'I^*Jdx+ \\ &+(1/2)\int xG_0G_0'^*I^*Jdx+(1/2)\int xG_0^*G_0'IJ^*dx= \\ &-(1/2)(I^*J-IJ^*)\left(\int xG_0'G_0^*dx-\int xG_0G_0'^*dx\right). \end{aligned} \tag{D.8}$$

We divide this solution in Eq.(D.8) by Eq.(D.5), writing this last result as $|I|^2=II^*$, and get

$$\begin{aligned} &-(1/2)\frac{I^*J-IJ^*}{II^*}\left[\int xG_0'G_0^*dx-\left(\int xG_0^*G_0'dx\right)^*\right]= \\ &=(1/2)\left(\frac{J}{I}-\frac{J^*}{I^*}\right)\times(2i)\mathrm{Im}\left[\int xG_0'G_0^*dx\right]= \\ &=2\mathrm{Im}\left[\overline{x'}\right]\mathrm{Im}\left[\int xG_0^*G_0'dx\right], \end{aligned} \tag{D.9}$$

since $J/I=\overline{x}'$ is the first moment of the amplitude distribution of the delays, Eq.(1.30). The rest of the terms give

$$\begin{aligned} (II^*)^{-1}\,[&-(1/2)\int xG_0G_0'^*IJ^*dx-(1/2)\int xG_0^*G_0'I^*Jdx \\ &+(1/2)\int xG_0G_0'^*I^*Jdx+(1/2)\int xG_0^*G_0'IJ^*dx\Big]= \\ &-2\mathrm{Re}\left[\overline{x'}\right]\mathrm{Re}\left[\int xG_0^*G_0'dx\right]. \end{aligned} \tag{D.10}$$

We can develop further the last term, taking into account that

$$\begin{aligned} |G_0|^{2\prime}&=G_0^*G_0'+G_0'^*G_0, \\ \mathrm{Re}\left[\int xG_0^*G_0dx\right.&=(1/2)\int x(G_0^*G_0'+G_0'^*G_0)=(1/2)\left.\int x|G_0|^{2\prime}\right]. \end{aligned} \tag{D.11}$$

Integrating it by parts we get

$$(1/2)\int x|G_0|^{2\prime}=(1/2)\left[x|G_0|^2\big|_{-\infty}^{\infty}-\int|G_0|^2dx\right]=-1/2. \tag{D.12}$$

Inserting Eq.(D.12) into Eq.(D.10) we have that $-2\mathrm{Re}[\overline{x}'] \times (-2) = \mathrm{Re}[\overline{x}']$, the real part of the first moment of the delay distribution. This result and Eq.(D.9) gives the delay in Eq.(1.29).

Appendix E

Momentum filtering

The integral in the second term of Eq.(1.29), using that $\partial_x G_0 = \left[-2(x - p_0 t/\mu - x_0)/\Delta x_t^2\right] G_0$, can be rewritten as

$$\begin{aligned} &\mathrm{Im}\left[\int x G_0^* \partial_x G_0 dx\right] = \mathrm{Im}\left[-\frac{2}{\Delta x_t^2}\int x G_0^*(x - p_0 t\mu - x_0) G_0 dx\right] = \\ =&\mathrm{Im}\left[-\frac{2}{\Delta x_t^2}\int x(x - p_0 t/\mu - x_0)|G_0|^2\, dx\right] = \\ =&\mathrm{Im}\left[-\frac{2}{\Delta x_t^2}\int x^2|G_0|^2\, dx + \frac{2}{\Delta x_t^2}(p_0 t/\mu + x_0)\int x|G_0|^2\, dx\right]. \end{aligned} \tag{E.1}$$

The last integral is directly the position of the COM of the WP at a time t, $\int x|G_0|^2\, dx = (p_0 t/\mu + x_0)$. The first integral is, making a change of basis $x \to x - p_0 t/\mu - x_0$,

$$\begin{aligned} \int x^2|G_0|^2\, dx =& \sqrt{\frac{2}{\pi}}\frac{1}{|\Delta x_t|}\int (x + p_0 t\mu + x_0)^2 \exp\left(-2x^2/|\Delta x_t|^2\right) dx \\ =& \sqrt{\frac{2}{\pi}}\frac{1}{|\Delta x_t|}\left[\int x^2 \exp\left(-2x^2/|\Delta x_t|^2\right) dx\right. \\ &+ 2(p_0 t/\mu + x_0)\int x \exp\left(-2x^2/|\Delta x_t|^2\right) dx \\ &\left. + \left(p_0 t/\mu + x_0\right)^2 \int \exp\left(-2x^2/|\Delta x_t|^2\right) dx\right]. \end{aligned} \tag{E.2}$$

The second integral in Eq.(E.2) is directly 0, as the Gaussian is centered around $x = 0$. The last one, with the prefactor, is equal to 1 since G_0 is normalized. For the first one we have

$$\sqrt{\frac{2}{\pi}}\frac{1}{|\Delta x_t|}\int x^2 \exp\left(-2x^2/|\Delta x_t|^2\right) dx = \sqrt{\frac{2}{\pi}}\frac{1}{|\Delta x_t|}\sqrt{\pi}\frac{|\Delta x_t|^3}{2^{5/2}} = \frac{|\Delta x_t|^2}{4}. \tag{E.3}$$

Inserting Eqs.(E.2) and (E.3) into Eq.(E.1) we have

$$\begin{aligned}
&\mathrm{Im}\left[\int x G_0^* \partial_x G_0 dx\right] = \\
=&\mathrm{Im}\left[-\frac{2}{\Delta x_t^2}\left\{\frac{|\Delta x_t|^2}{4} - \left(p_0 t/\mu + x_0\right)^2 + \left(p_0 t/\mu + x_0\right)^2\right\}\right] = -|\Delta x_t|^2\,\mathrm{Im}\left[\frac{1}{2\Delta x_t^2}\right] = \\
=&-\frac{\Delta x^4 + 4t^2/\mu^2}{\Delta x^2}\frac{-t/\mu}{\Delta x^4 + 4t^2/\mu^2} = \frac{1}{\Delta x^2 \mu}t = \frac{\Delta p^2}{4\mu}t.
\end{aligned} \tag{E.4}$$

Going back to Eq.(1.29), multiplying the result in Eq.(E.4) by $2\mathrm{Im}\left[\overline{x}'\right]$ gives $\mathrm{Im}\left[\overline{x}'\right]\Delta p^2 t/(2\mu) = \delta v_0 t$. We can identify $\mathrm{Im}\left[\overline{x}'\right]$ with the imaginary part of the complex delay, $\tilde{x}_2'$ in Eq.(1.12).

Appendix F

Approximation for the residues

For large z we approximate $\Gamma(z)$ as [61]

$$\Gamma(z) \approx z^{z-1/2} e^{-z} \sqrt{2\pi} \tag{F.1}$$

which is valid for $\left|\arg(z)\right| < \pi$. In the case of wells, this approximation will not be valid for the non-bound state poles, since z is real and negative. Nevertheless, generally we will only need the bound state poles, which can be calculated exactly.

We can also approximate the $1/n!$ factor appearing in Eq.(2.8), using that, for large n, $\Gamma(z+1) = n!$, so, from Eq.(F.1),

$$n! \approx \sqrt{2\pi n} \left(\frac{n}{e}\right)^n . \tag{F.2}$$

Each Γ function in Eq.(2.2) may take an extremelly high value, so Matlab is not able to compute them. Still, we can rewrite the Γ's in an expoential form, using $z^{z-1/2} = \exp[(z-1/2)\ln(z)]$ and considering that $-ik_p^1(n)/\alpha = -n+s$. For

the approximation of $\text{Res}\Big[T(k), k_p^1(n)\Big]$ we obtain

$$\begin{aligned}\text{Res}\left[T(k), k_p^1(n)\right] \approx & \frac{\alpha}{-i}\frac{(-1)^n}{2\pi\sqrt{n}}\exp[(-n+2s-1/2)\ln(-n+2s+1) \\ & -(-n+s-1/2)\ln(-n+s) \\ & -(-n+s+1/2)\ln(1-n+s)-n\ln(n)].\end{aligned} \tag{F.3}$$

All terms with e^{-z} give $e^{n-2s-1-n+s+1-n+s} = e^{-n}$, which cancels the e^n term from the factorial in Eq.(F.2).

Applying the same approximation for $\text{Res}\Big[T(k), k_p^2(n)\Big]$, and using in this case that $-ik_p^2(n)/\alpha = -n-s-1$, we obtain

$$\begin{aligned}\text{Res}\left[T(k), k_p^2(n)\right] \approx & \frac{\alpha}{-i}\frac{(-1)^n}{2\pi\sqrt{n}}\exp([-n-2s-3/2)\ln(-n-2s-1) \\ & -(-n-s-3/2)\ln(-n-s-1) \\ & -(-n-s-1/2)\ln(-n-s)-n\ln(n)],\end{aligned} \tag{F.4}$$

which can equivalently be computed using that $\text{Res}\Big[T(k), k_p^1(n)\Big] = -\text{Res}^*\Big[T(k), k_p^1(n)\Big]$.

For the resonant states of a well, which had $z<0$, we can use the relation

$$\Gamma(1-z)\Gamma(z) = \frac{\pi}{\sin(\pi z)}, \tag{F.5}$$

sice $1-z>0$, and we can again use the approximation in Eq.(F.1). The final expressions for the first kind of residues are

$$\begin{aligned}\text{Res}\left[T(k), k_p^1(n)\right] \approx & \frac{\alpha}{-i}\frac{(-1)^n}{\pi\sqrt{2\pi n}}\frac{\sin[\pi(-n+s)]\sin[\pi(-n+s+1)]}{\sin[\pi(-n+2s+1)]} \\ & \times\exp[(n-s+1/2)\ln(1+n-s) \\ & +(n-s-1/2)\ln(n-s) \\ & -(n-2s-1/2)\ln(n-2s)-1-n\ln(n)],\end{aligned} \tag{F.6}$$

and for the second kind

$$\begin{aligned}\operatorname{Res}\left[T(k), k_p^2(n)\right] \approx & \frac{\alpha}{-i}\frac{(-1)^n}{\pi\sqrt{2\pi n}}\frac{\sin[\pi(-n-s-1)]\sin[\pi(-n-s)]}{\sin[\pi(-n-2s-1)]} \\ & \times \exp[(n+s+3/2)\ln(n+s+2) \\ & + (n+s+1/2)\ln(n+s+1) \\ & - (n+2s+3/2)\ln(n+2s+2) - 1 - n\ln(n)].\end{aligned} \tag{F.7}$$

Appendix G

Perfect transmission for integer s

We can expand the transmission amplitude in Eq.(2.2) for integer s using $\Gamma(z+1) = z\Gamma(z)$ and $\Gamma(z-1) = (z-1)^{-1}\Gamma(z)$.

The Γ functions in the numerator are expanded as

$$\begin{aligned}\Gamma(-ip/\alpha - s) =&(-1)^{-s}(ip/\alpha + s)^{-1} \times ... \times (ip/\alpha + 1)^{-1}\Gamma(-ip/\alpha) \\ \Gamma(-ip/\alpha + s + 1) =&(-ip/\alpha + s) \times ... \times (-ip/\alpha + 1)(-ip/\alpha)\Gamma(-ip/\alpha).\end{aligned} \tag{G.1}$$

The denominator becomes

$$\Gamma(-ip/\alpha)\Gamma(1 - ip/\alpha) = (-ip/\alpha)\Gamma^2(-ip/\alpha). \tag{G.2}$$

Everything together gives

$$\begin{aligned}T(p,V) =&(-1)^s \frac{(-ip/\alpha + s) \times ... \times (-ip/\alpha + 1)(-ip/\alpha)}{(ip/\alpha + s) \times ... \times (ip/\alpha + 1)(-ip/\alpha)} = \\ =&(-1)^s \frac{(-ip/\alpha + s) \times ... \times (-ip/\alpha + 1)}{(ip/\alpha + s) \times ... \times (ip/\alpha + 1)} \equiv (-1)^s \frac{K}{K^*},\end{aligned} \tag{G.3}$$

and from it we find

$$|T(p,V)| = \left|\frac{K}{K^*}\right| = 1. \tag{G.4}$$

Therefore, for integer s, as a new bound state enters the well, the potential is transparent for all incident momenta. There is perfect transmission, as the transmitted particle is only affected by a phase.

Appendix H

Residues for double poles

Since we have $(-i/\alpha)(k_n^{II} - k_n^I) = 2s + 1$, the residue for a double pole will be proportional to the product of two Gammas separated by $2s + 1$. Using the Cauchy integration formula for double poles this is

$$\text{Res}(\Gamma(z)\Gamma(z-2s-1), z=-n) = \lim_{z\to -n} \frac{\partial}{\partial z}[(z+n)^2\Gamma(z)\Gamma(z-2s-1)]. \quad \text{(H.1)}$$

This equation can be solved taking into account that $2s$ is an integer. Thus, we can use that $\Gamma(z+n+1) = z(z+1)...(z+n-1)\Gamma(z)$. Using also that $\partial/\partial z\Gamma(z=1) = -\gamma(1) \approx -0.5772$, where $\gamma(1)$ is the Euler-Mascheroni constant, we expand Eq. (H.1) as

$$\begin{aligned}
&\text{Res}(\Gamma(z)\Gamma(z-2s-1), z=-n) = \quad \text{(H.2)}\\
&= \lim_{z\to -n} \frac{\partial}{\partial z} \frac{\Gamma^2(z+n+1)}{[z(z+1)...(z+n-1)]^2(z-2s-1)...(z-1)}\\
&= \frac{-2\Gamma(1)\gamma(1)[-n...(-1)]^2[(-n-2s-1)...(-n-1)]}{[-n(-n+1)...(1)]^4[(-n-2s-1)...(-n-1)]^2}\\
&\quad - \Gamma^2(1)2[-n...(-1)]\times\\
&\quad \times \frac{[(-n+1)...(-1)+...+-n...(-1)]\times[(-n-2s-1)...(-n-1)]}{[-n(-n+1)...(1)]^4[(-n-2s-1)...(-n-1)]^2}\\
&\quad - \Gamma^2(1)[(-n(-n+1)...(-1))]^2\times\\
&\quad \times \frac{[(-n-2s-2)...(-n-1)+...+(-n-2s-1)...(-n-2)]}{[-n(-n+1)...(1)]^4[(-n-2s-1)...(-n-1)]^2}.
\end{aligned}$$

The first term of H.2 is

$$\begin{aligned}&\frac{-2\Gamma(1)\gamma(1)[-n(-n+1)...(1)]^2[(-n-2s-1)...(-n-1)]}{[-n(-n+1)...(1)]^4[(-n-2s-1)...(-n-1)]^2}\\ =&\frac{-2\gamma(1)}{n!^2[(-n-2s-1)...(-n-1)]}=\frac{-2\gamma(1)}{n!(n+2s+1)!}.\end{aligned} \tag{H.3}$$

The second term contains terms as

$$\begin{aligned}&\frac{-\Gamma^2(1)2[-n(-n+1)...(1)]\times[(-n+1)...(1)][(-n-2s-1)...(-n-1)]}{[-n(-n+1)...(1)]^4[(-n-2s-1)...(-n-1)]^2}\\ =&\frac{-\Gamma^2(1)2\times[(-n+1)...(1)]}{[-n(-n+1)...(1)]^3[(-n-2s-1)...(-n-1)]}\times\frac{-n}{-n}\\ =&\frac{-1}{(-n)n!(n+2s+1)!}=\frac{1}{n}\frac{1}{n!(n+2s+1)!},\end{aligned} \tag{H.4}$$

and equivalently for the rest of the terms. The following terms will be $1/(n-1)1/[n!(n+2s+1)!]$, $1/(n-2)1/[n!(n+2s+1)!]$ and so on.

The last part is similar. Taking the first term as before

$$\begin{aligned}&\frac{-[-n...(-1)]^2\times[(-n-2s-2)...(-n-1)]}{[-n...(-1)]^4[(-n-2s-1)...(-n-1)]^2}\times\frac{-n-2s-1}{-n-2s-1}=\\ &=\frac{1}{n+2s+1}\frac{1}{n!(n+2s+1)!},\end{aligned} \tag{H.5}$$

and similarly for the rest of the terms. The final result of Eq.(H.2) is

$$\mathrm{Res}(\Gamma(z)\Gamma(z-2s-1),z=-n)=\frac{2}{n!(n+2s+1)!}\left(\sum_{k=1}^{k=n}\frac{1}{k}+\sum_{k=n+1}^{k=n+2s+1}\frac{1}{2k}-\gamma(1)\right). \tag{H.6}$$

Finally, the residue is

$$\begin{aligned}\mathrm{Res}(T(k),n) = &-\alpha^2 \frac{2}{n!(n+2s+1)!}\left(\sum_{k=1}^{k=n}\frac{1}{k}+\sum_{k=n+1}^{k=n+2s+1}\frac{1}{2k}-\gamma(1)\right) \\ &\times \frac{1}{\Gamma(-ik_p^1(2s+1)/\alpha)\Gamma(-ik_p^1(2s+1)/\alpha+1)}.\end{aligned} \tag{H.7}$$

Appendix I

Limit of the residues for $n \to \infty$

We can compute the asymptotic limit of the residues for $n \to \infty$ from Eqs.(F.3) and (F.4) evaluating the limit of everything inside the exponentials as

$$\lim_{n\to\infty} \frac{(-n+s)^{n-s+1/2}(1-n+s)^{n-s-1/2}}{(-n+2s+1)^{n-2s-1/2}n^n} = \frac{(-n)^{n-s+1/2}e^{-s}(-n)^{n-s-1/2}e^{-s-1}}{(-n)^{n-2s-1/2}e^{-2s-1}n^n} = \\ = \frac{(-n)^{n-s+1/2}(-n)^{n-s-1/2}}{(-n)^{n-2s-1/2}n^n}, \tag{I.1}$$

where we have used $(-n+s)^{n-s+1/2} = (-n)^{n-s+1/2}(1-s/n)^n(1-s/n)^{-s+1/2}$ and that $\lim_{n\to\infty}(1-s/n)^n = e^{-s}$. The second term for large n is $(1-s/n)^{-s+1/2} \approx 1$. From the last result,

$$\frac{(-n)^{n-s+1/2}(-n)^{n-s-1/2}}{(-n)^{n-2s-1/2}n^n} = \left(\frac{(-n)(-n)}{(-n)n}\right)^n \frac{(-n)^{-s+1/2}(-n)^{-s-1/2}}{(-n)^{-2s-1/2}} = \\ = (-1)^n(-n)^{1/2} = i(-1)^n\sqrt{n}. \tag{I.2}$$

Inserting Eq.(K.2) into Eq.(F.3) we have

$$\lim_{n\to\infty} \text{Res}\left[T(k), k_p^1(n)\right] = -\frac{\alpha}{2\pi}. \tag{I.3}$$

Equivalently, we have that $\text{Res}\left[T(k), k_p^2(n)\right] = \alpha/2\pi$.

Appendix J

Error functions for zero-range potentials

The integrals for $\Psi^{T,R}(x,t)$ in Eqs. (3.25) and (3.31) can also be expressed as error functions for a Gaussian envelope $G(x-x'\mp pt) = \left(\frac{2\Delta_x^2}{\pi\Delta_{x_t}^4(t)}\right)^{1/4}\exp\left[-(x\mp x_0-x'\mp pt)^2/\Delta_{x_t}^2(t)\right]$, where $\Delta_{x_t} = \Delta_x\sqrt{1+2it/\Delta_x^2}$ is the time-dependent complex width accounting for the spreading of the WP over time. We will use

$$\int_{-\infty}^{0}\exp(-a_Tx^2+b_Tx)dx = \exp(b_T^2/4a_T)\sqrt{\pi}\mathrm{erfc}(b_T/2\sqrt{a_T})/2\sqrt{a_T}, \tag{J.1}$$

where $\mathrm{erfc}(z) = 1-\mathrm{erf}(z) = 1-2/\sqrt{\pi}\int_0^z e^{-t^2}dt$ is the complementary error function.

The final expressions for the transmitted and reflected particles are

$$\Psi^{T,R}(x,t) = C_{T,R}\exp(b_{T,R}^2/4a_{T,R})\sqrt{\pi} \times \ \mathrm{erfc}(b_{T,R}/2\sqrt{a_{T,R}})/2\sqrt{a_{T,R}}, \tag{J.2}$$

$$\text{with } C_{T,R} = -\,\Omega \left(\frac{2\Delta_x^2}{\pi\Delta_{x_t}^4(t)}\right)^{1/4}$$

$$\exp\{-(1/\Delta_{x_t}^2(t)) \times \left[(x \mp x_0)^2 \mp 2pt(x \mp x_0) + (pt)^2)\right]\},$$

$$a_{T,R} = 1/\Delta_{x_t}^2(t),$$

$$b_{T,R} = \left[2\left(x \mp x_0 \mp pt\right)/\Delta_{x_t}^2(t) \mp ip + \Omega\right],$$

where in $\mp$, the minus sign corresponds to the transmission coefficients and the plus sign to the reflection ones.

Appendix K

COM delays and momentum filtering for $\Delta x \to 0$

For a WP with a general expression $\Psi(x) = \int F(k)\exp(ikx)dk$, where $F(k)$ is the momentum distribution for the free case, transmission or reflection, the position of its COM is $\langle x\rangle = \int x|\Psi(x)|^2dx/\int|\Psi(x)|^2dx$. We use that $x\Psi(x,t) = -i\int F(k)\partial_k\left[\exp(ikx)\right] = i\int\exp(ikx)\partial_k F(k)dk$ and find

$$\langle x\rangle = -\frac{\int \mathrm{Im}\left[F^*(k)\partial_k F(k)\right]dk}{\int|F(k)|^2dk}. \tag{K.1}$$

For the three WPs we are analysing, the amplitude we evaluate is, for the freely propagating one, $F_0(k) = A(k)$, for the transmitted one $F_T(k) = A(k)T(k,V)$ and for the reflected one $F_R(k) = A(k)R(k,V)$. Using these amplitudes we obtain the delay in Eq.(K.1) as

$$\begin{aligned}\langle x\rangle_0 =& x_0 + \langle v(k)\rangle_0 t, \\ \langle x\rangle_{T,R} =& \pm x_0 \pm \langle v(k)\rangle_{T,R} t \mp \langle\partial_k\Phi_{T,R}(k,V)\rangle_{T,R},\end{aligned} \tag{K.2}$$

where $\langle f(k)\rangle_{0,T,R} \equiv \int f(k)|F_{0,T,R}(k)|^2dk/\int|F_{0,T,R}(k)|^2dk$, the velocity is $v(k) = \partial_k E(k)$, $T(k,V) = |T(k,V)|\exp[i\Phi_T(k,V)]$ and $R(k,V) = |R(k,V)|\exp[i\Phi_R(k,V)]$.

In the limit $\Delta x \to \infty$, we have that $\lim_{\Delta x \to \infty} \langle f(k) \rangle = f(k)$, and we recover the delays from Eqs.(3.21) and (3.34).

We can use the term corresponding to the velocity in Eq.(3.38) to compute the momentum filtering in the case $E(k) = k^2/2\mu$. We compare the velocity of the transmitted WP with p_0/μ. The increase in the momentum of the transmitted WP is thus

$$\langle \delta p_0^T \rangle = \langle v_T(k) - p_0/\mu \rangle = \langle \partial_k |T(k, V)| \rangle \, \Delta k^2/2\mu. \tag{K.3}$$

We can calculate equivalently the momentum filtering of the reflected WP. In the limit $\Delta x \to \infty$, we have that $\langle \delta p_T \rangle = \delta p_T$.

Appendix L

Expansion in scattering states

For a particle incident from the left, the left scattering states are

$$\Phi_l(k,x) = \langle x \rangle \, \Phi_l(k) = \begin{cases} \dfrac{1}{\sqrt{2\pi}} \left[e^{ikx} + R(k) e^{-ikx} \right], & \text{x<0} \\ \dfrac{1}{\sqrt{2\pi}} T(k) e^{ikx}, & \text{x>0.} \end{cases} \tag{L.1}$$

The right scattering states are obtained as $\Phi_r(k,x) = \Phi_l(k,-x)$. We start with a WP state as

$$G(k',p) = \langle k' | G(p) \rangle = A(k',p) e^{-ik'x_0}, \tag{L.2}$$

where k' is the momentum, $A(k',p)$ is the momentum distribution, centered around $k'=p$, and with $x_0 < 0$, so it is initially at the left of the barrier. We can expand this state in the scattering states of Eq.(L.1), projecting on the initial states for $x < 0$, letting the time increase with the time evolution operator, which for this case is just $e^{iE(k)t}$, and projecting it finally on the states to the right or left of the

barrier, after the scattering has occurred. Doing so, we get

$$\begin{aligned} G(x>0,p,t) =& \int dk \left\langle \Phi_r(k) \right\rangle G(p) e^{-iE(k)t} \left\langle x>0 \right\rangle \Phi_r(k) + \\ &+ \int dk \left\langle x>0 \right| \left\langle \Phi_l(k) \right\rangle G(p) e^{-iE(k)t} \left\langle x>0 \right\rangle \Phi_l(k) \\ =& \int dk \left[\int \int dk' dx \left\langle \Phi_r(k) \right\rangle x \left\langle x \right\rangle k' \left\langle k' \right\rangle G(p) e^{-iE(k)t} \Phi_r(k, x>0) \right. \\ &\left. + \int \int dk' dx \left\langle \Phi_l(k) \right\rangle x \left\langle x \right\rangle k' \left\langle k' \right\rangle G(p) e^{-iE(k)t} \Phi_l(k, x>0) \right], \end{aligned} \tag{L.3}$$

with $\langle x|k' \rangle = (1/\sqrt{2\pi}) e^{ik'x}$.

Starting with the initial projection on the right scattering states, we have

$$\begin{aligned} &\int \int dk' dx \left\langle \Phi_r(k) \right\rangle x \left\langle x \right\rangle k' \left\langle k' \right\rangle G(p) = \\ &= \frac{1}{2\pi} \int \int dk' dx \left[e^{-ikx} + R^*(k) e^{ikx} \right] e^{ik'x} A(k', p) e^{-ik'x_0)} \\ &= \frac{1}{2\pi} \left[\int \int dk' dx A(k', p) e^{-ik'x_0} e^{i(k'-k)x} dx \right. \\ &\left. + \int \int dk' dx A(k', p) R^*(k) e^{-ik'x_0} e^{i(k'+k)x} \right]. \end{aligned} \tag{L.4}$$

Using that $\frac{1}{2\pi} \int e^{i(k' \pm k)x} dx = \delta(k' \pm k)$ we write

$$\begin{aligned} &\int dk' A(k', p) e^{-ik'x_0} \delta(k'-k) + \int dk' A(k', p) R^*(k) e^{-ik'x_0} \delta(k'+k) \\ =& A(k, p) e^{-ikx_0} + A(-k, p) R^*(k) e^{ikx_0}. \end{aligned} \tag{L.5}$$

Equivalently, projecting on the right scattering states gives

$$\int \int dk' dx \left\langle \Phi_l(k) \right\rangle x \left\langle x \right\rangle k' \left\langle k' \right\rangle G(p) = \int \int dk' dx T^*(k) e^{ikx} e^{ik'x} A(k', p) e^{-ik'x_0} \tag{L.6}$$

$$= \int T^*(k) A(k', p) \delta(k'+k) e^{-ik'x_0} dk = A(-k, p) T^*(k) e^{ikx_0}.$$

The complete expansion is, then,

$$G(x>0,p,t) = \int_0^\infty \left[A(k,p)e^{-ikx_0} + A(-k,p)R^*(k)e^{ikx_0}\right] e^{-iE(k)t}T(k)e^{ikx}dk + \int_0^\infty A(-k,p)T^*(k)e^{ikx_0}e^{-iE(k)t}\left[R(k)e^{ikx} + e^{-ikx}\right]dk, \tag{L.7}$$

where the integrals over the momentum are taken from 0 to ∞ as we are interested in the states from Eq.(L.1) that, coming from the left, travel to the right and reach the potential with e^{ikx}, and $\Phi_l(k, x>0) = T(k)e^{ikx}$ and $\Phi_r(k, x>0) = R(k)e^{ikx} + e^{-ikx}$.

The cross terms of the transmission and reflection amplitudes cancel each other, as $R(k)T^*(k) = -R^*(k)T(k)$. In the remaining term with $T^*(k)$ we can make a change of variable as $k \to -k$, using that $T^*(-k) = T(k)$ and $E(-k) = (-k)^2/2m = E(k)$. We are left with

$$\begin{aligned} G(x>0,p,t) &= \int_0^\infty A(k,p)T(k)e^{ik(x-x_0)}e^{-iE(k)t}dk - \\ &\int_0^{-\infty} A(k,p)T(k)e^{ik(x-x_0)}e^{-iE(k)t}dk \\ &= \int_{-\infty}^\infty A(k,p)T(k)e^{ik(x-x_0)-iE(k)t}dk. \end{aligned} \tag{L.8}$$

This is the usual transmitted WP expression, where in this case we have not made any assumption about the shape of the envelope $A(k,p)$. This also applies to the case of a particle wide enough in momentum space so it has positive and negative momentum contributions, and, due to the spreading, partly runs away from the barrier.

We can make the same expansion for the scattered particle at $x<0$, which gives

$$G(x<0,p,t) = \int_{-\infty}^\infty A(k,p)\left[e^{ik(x-x_0)} + R(k)e^{-ik(x+x_0)}\right]e^{-iE(k)t}dk, \tag{L.9}$$

where again the expression applies for any shape of $A(k,p)$.

Appendix M

A smooth potential for Klein-Gordon particles

For a smooth step potential with the form $V(x) = a \tanh bx$, an incident plane wave will be reflected and transmitted as [62]

$$\begin{aligned} \Phi_{inc}(x) &= Ae^{2ib\nu x} \\ \Phi_{ref}(x) &= Be^{-2ib\nu x} \\ \Phi_{trans}(x) &= e^{2ib\mu x} \end{aligned} \tag{M.1}$$

where

$$A = \frac{\Gamma(1-2i\mu)\Gamma(-2i\nu)}{\Gamma(-i\nu+\lambda-i\mu)\Gamma(1-i\nu-\lambda-i\mu)}, \qquad B = \frac{\Gamma(1-2i\mu)\Gamma(2i\nu)}{\Gamma(i\nu-\lambda-i\mu)\Gamma(1+i\nu-\lambda-i\mu)} \tag{M.2}$$

and

$$\nu = \frac{\sqrt{(E+a)^2-m^2}}{2b}, \qquad \mu = \frac{\sqrt{(E-a)^2-m^2}}{2b}, \qquad \lambda = \frac{b+\sqrt{b^2-4a^2}}{2b}. \tag{M.3}$$

For a smooth barrier we take $V(x) = V_0/2(\tanh bx - \tanh b(x-d))$, where the solution in $x = 0$ and $x = d$ is given by the scattering coefficients in Eq.(M.1). For the matching at $x = d$ one has to take the complex conjugate of the plane waves. Using $p = 2b\nu$, $q = 2b\mu$, $V_0/2 = a$ and the solution from Eqs.(4.5) and (4.6), the coefficients for scattering are

$$
\begin{aligned}
a_+ &= \frac{\Gamma(1-ip/b)\Gamma(-iq/b)}{\Gamma(-iq/2b+\lambda-ip/2b)\Gamma(1-iq/2b-\lambda-ip/2b)} e^{i(p-q)d} \\
a_- &= \frac{\Gamma(1-ip/b)\Gamma(iq/b)}{\Gamma(iq/2b+\lambda-ip/2b)\Gamma(1+iq/2b-\lambda-ip/2b)} e^{i(p+q)d}, \\
b_{++} &= \frac{\Gamma(1-iq/b)\Gamma(-ip/b)}{\Gamma(-ip/2b+\lambda-iq/2b)\Gamma(1-ip/2b-\lambda-iq/2b)} \\
b_{-+} &= \frac{\Gamma(1-iq/b)\Gamma(ip/b)}{\Gamma(ip/2b+\lambda-iq/2b)\Gamma(1+ip/2b-\lambda-iq/2b)} \\
b_{+-} &= \frac{\Gamma(1+iq/b)\Gamma(ip/b)}{\Gamma(ip/2b+\lambda+iq/2b)\Gamma(1+ip/2b-\lambda+iq/2b)} \\
b_{--} &= \frac{\Gamma(1+iq/b)\Gamma(-ip/b)}{\Gamma(-ip/2b+\lambda+iq/2b)\Gamma(1-ip/2b-\lambda+iq/2b)}.
\end{aligned}
\tag{M.4}
$$

The same convergent and divergent expansions used for the square barrier are valid here (see Eqs.(4.12) and (4.19)).

In the limit $b \to \infty$, the coefficients tend to the solutions obtained for the square potential. We use that for large b we have that $\lambda \to 1$. For the Gamma functions, we can approximate $\Gamma(1+(z\to 0)) \to 1$ and $\frac{1}{\Gamma(z\to 0)} \to z$. Using these expressions we can take, as an example, the hyperbolic coefficient a_+, Eq.(4), and compute its limit

$$
\begin{aligned}
a_{+,hyperbolic} &= \frac{\Gamma(1-ip/b)\Gamma(-iq/b)}{\Gamma(-iq/2b+\lambda-ip/2b)\Gamma(1-iq/2b-\lambda-ip/2b)} e^{i(p-q)d} \to \\
&\to \frac{1\times\frac{1}{-iq/b}}{1\times\frac{1}{-iq/2b-ip/2b}} e^{i(p-q)d} = \frac{-q/2-p/2}{-q} e^{i(p-q)d} = \\
&= \frac{1}{2}(1+\frac{p}{q}) e^{i(p-q)d} = a_{+,square},
\end{aligned}
\tag{M.5}
$$

where we have recovered the coefficient obtained for the square potential, Eq.(4.7). The rest of the coefficients can be calculated equivalently.

The transmission amplitude, using that $1-\lambda \approx V_0^2/2b$ and the coefficients from Eq.(M.4), is

$$T_{smooth}(p,-q) = \frac{\Gamma(iq/b - ip/b + \lambda)\Gamma(iq/b - ip/b + 1 - \lambda)}{\Gamma(1 + 2iq/b)\Gamma(-2ip/b)}. \tag{M.6}$$

Approximating for large b we get

$$\lim_{b\to\infty} T_{smooth}(p,-q) = \frac{2p}{p - q + i\delta}, \quad \delta = V_0^2/2b, \tag{M.7}$$

which moves the pole to the complex plane, making it avoidable for carrying out the WP integration.

Bibliography

[1] A. S. Landsman and U. Keller, "*Attosecond science and the tunnelling time problem*", Physics Reports **547**, 1–24 (2015).

[2] N. Camus, E. Yakaboylu, L. Fechner, M. Klaiber, M. Laux, Y. Mi, K. Z. Hatsagortsyan, T. Pfeifer, C. H. Keitel, and R. Moshammer, "*Experimental Evidence for Quantum Tunneling Time*", Phys. Rev. Lett. **119**, 023201 (2017).

[3] U. S. Sainadh, H. Xu, X. Wang, A. Atia-Tul-Noor, W. C. Wallace, N. Douguet, A. Bray, I. Ivanov, K. Bartschat, A. Kheifets, R. T. Sang, and I. V. Litvinyuk, "*Attosecond angular streaking and tunnelling time in atomic hydrogen*", Nature **568**, 75–77 (2019).

[4] W. Pauli, *Handbuch der Physik*, volume 24. 1933.

[5] G. Muga, R. S. Mayato, and I. Egusquiza, *Time in quantum mechanics*, volume 734. Springer Science & Business Media, 2007.

[6] E. Hauge and J. Stoevneng, "*Tunneling times: a critical review*", Rev. Mod. Phys. **61**, 917 .

[7] G. E. Field, "*On the status of quantum tunnelling time*", Euro Jnl Phil Sci **12**, 57 (2022).

[8] L. Eisenbud, *The formal properties of nuclear collisions*. Princeton University, 1948.

[9] E. P. Wigner, "*Lower limit for the energy derivative of the scattering phase shift*", Physical Review **98**, 145 (1955).

[10] F. T. Smith, "*Lifetime Matrix in Collision Theory*", Phys. Rev. **118**, 349–356 (1960).

[11] L. A. MacColl, "*Note on the Transmission and Reflection of Wave Packets by Potential Barriers*", Phys. Rev. **40**, 621–626 (1932).

[12] R. S. Dumont, T. Rivlin, and E. Pollak, "*The relativistic tunneling flight time may be superluminal, but it does not imply superluminal signaling*", New J. Phys. **22**, 093060 (2020).

[13] S. D. Leo, "*A study of transit times in Dirac tunneling*", J. Phys. A: Math. Theor. **46**, 155306 (2013).

[14] V. Petrillo and D. Janner, "*Relativistic analysis of a wave packet interacting with a quantum-mechanical barrier*", Phys. Rev. A **67**, 012110 (2003).

[15] R. Ramos, D. Spierings, I. Racicot, and A. M. Steinberg, "*Measurement of the time spent by a tunnelling atom within the barrier region*", Nature **583**, 529–532 (2020).

[16] C. R. Leavens, "*Bohm trajectory and Feynman path approaches to the "Tunneling time problem"*", Found Phys **25**, 229–268 (1995).

[17] R. P. Feynman, A. R. Hibbs, and D. F. Styer, *Quantum mechanics and path integrals*. Courier Corporation, 2010.

[18] D. Sokolovski, "*Salecker-Wigner-Peres clock, Feynman paths, and a tunneling time that should not exist*", Physical Review A **96**, 022120 (2017).

[19] D. Sokolovski and L. M. Baskin, "*Traversal time in quantum scattering*", Phys. Rev. A **36**, 4604–4611 (1987).

[20] A. M. Steinberg, "*How Much Time Does a Tunneling Particle Spend in the Barrier Region?*", Phys. Rev. Lett. **74**, 2405–2409 (1995).

[21] T. Zimmermann, S. Mishra, B. R. Doran, D. F. Gordon, and A. S. Landsman, "*Tunneling Time and Weak Measurement in Strong Field Ionization*", Phys. Rev. Lett. **116**, 233603 (2016).

[22] D. Sokolovski, "*Weak measurements measure probability amplitudes (and very little else)*", Physics Letters A **380**, 1593–1599 (2016).

[23] D. Sokolovski, "*Weak values, "negative probability," and the uncertainty principle*", Phys. Rev. A **76**, 042125 (2007).

[24] D. Bohm, *Quantum theory*. Dover Publications, 1951. page 600.

[25] R. P. Feynman, R. B. Leighton, and M. Sands, "*The feynman lectures on physics; vol. III*", American Journal of Physics **33**, 750–752 (1989).

[26] G. Diener, "*Superluminal group velocities and information transfer*", Physics Letters A **223**, 327–331 (1996).

[27] J. Petersen and E. Pollak, "*Tunneling flight time, chemistry, and special relativity*", The Journal of Physical Chemistry Letters **8**, 4017–4022 (2017).

[28] D. Sokolovski, "*Why does relativity allow quantum tunnelling to 'take no time'?*", Proceedings of the Royal Society of London. Series A: Mathematical, Physical and Engineering Sciences **460**, 499–506 (2004).

[29] D. Sokolovski and J. Connor, "*Quantum interference and determination of the traversal time*", Physical Review A **47**, 4677 (1993).

[30] D. Sokolovski and E. Akhmatskaya, "*No time at the end of the tunnel*", Commun Phys **1**, 1–9 (2018).

[31] D. Sokolovski and E. Akhmatskaya, "*Tunnelling times, Larmor clock, and the elephant in the room*", Sci Rep **11**, 10040 (2021).

[32] W. Greiner, *Relativistic Quantum Mechanics. Wave Equations*. Springer, Berlin, Heidelberg, 2000.

[33] B. Thaller, *The Dirac Equation*. Springer, Berlin, Heidelberg, 1992.

[34] D. Sokolovski and E. Akhmatskaya, "*'Superluminal paradox' in wave packet propagation and its quantum mechanical resolution*", Annals of Physics **339**, 307–327 (2013).

[35] D. Sokolovski, "*Causality, apparent "superluminality," and reshaping in barrier penetration*", Phys. Rev. A **81**, 042115 (2010).

[36] D. M. Brink, *Semi-classical methods for nucleus-nucleus scattering.* 1989.

[37] D. Sokolovski, "*Residence Time of a Two-Level Quantum System*", Proceedings: Mathematical, Physical and Engineering Sciences **460**, 1505–1517 (2004).

[38] Y. Aharonov, D. Z. Albert, and L. Vaidman, "*How the result of a measurement of a component of the spin of a spin-1/2 particle can turn out to be 100*", Phys. Rev. Lett. **60**, 1351–1354 (1988).

[39] A. I. Baz, Y. B. Zel'dovich, and A. M. Perelomov, *Scattering, reactions and decay in nonrelativistic quantum mechanics.* Jerusalem, Israel Program for Scientific Translation, 1969.

[40] L. D. Landau and E. M. Lifshitz, *Quantum mechanics: non-relativistic theory*, volume 3. Pergamon Press, 1977.

[41] M. Abramowitz and I. A. Stegun, *Handbook of Mathematical Functions with Formulas, Graphs, and Mathematical Tables.* U.S. Government Printing Office, 1948.

[42] B. A. I and Y. Fiz Sov. J. Nucl. Phys **4**, (1966).

[43] R. Landauer and T. Martin, "*Barrier interaction time in tunneling*", Rev. Mod. Phys. **66**, 217–228 (1994).

[44] D. Sokolovski, "*Path integral approach to space-time probabilities: A theory without pitfalls but with strict rules*", Phys. Rev. D **87**, 076001 (2013).

[45] J. v. Neumann, *Mathematical Foundations of Quantum Mechanics.* Princeton University Press, 1955.

[46] D. Sokolovski, S. Brouard, and J. N. L. Connor, "*Traversal-time wave-function analysis of resonance and nonresonance tunneling*", Phys. Rev. A **50**, 1240–1256 (1994).

[47] H. A. Fertig, "*Path decomposition and the traversal-time distribution in quantum tunneling*", Phys. Rev. B **47**, 1346–1358 (1993).

[48] J. M. Deutch and F. E. Low, "*Barrier Penetration and Superluminal Velocity*", Annals of Physics **228**, 184–202 (1993).

[49] B. R. Holstein, "*Klein's paradox*", American Journal of Physics **66**, 507–512 (1998).

[50] A. Calogeracos and N. Dombey, "*History and physics of the Klein paradox*", Contemporary Physics **40**, 313–321 (1999).

[51] O. Klein, "*Die Reflexion von Elektronen an einem Potentialsprung nach der relativistischen Dynamik von Dirac*", Z. Physik **53**, 157–165 (1929).

[52] K. Kim, "*Super-Klein tunneling of Klein-Gordon particles*", Results in Physics **12**, 1391–1394 (2019).

[53] F. Nieto-Guadarrama and J. Villavicencio, "*Zitterbewegung and Klein-tunneling phenomena for transient quantum waves*", Phys. Rev. A **101**, 042104 (2020).

[54] M. J. Thomson and B. H. J. McKellar, "*The solution of the Dirac equation for a high square barrier*", American Journal of Physics **59**, 340–346 (1991).

[55] S. De Leo and P. P. Rotelli, "*Barrier paradox in the Klein zone*", Phys. Rev. A **73**, 042107 (2006).

[56] R. P. Feynman, *Quantum electrodynamics: a lecture note and reprint volume.*

[57] T. Cheng, Q. Su, and R. Grobe, "*Introductory review on quantum field theory with space–time resolution*", Contemporary Physics **51**, 315–330 (2010).

[58] R. E. Wagner, M. R. Ware, Q. Su, and R. Grobe, "*Bosonic analog of the Klein paradox*", Phys. Rev. A **81**, 024101 (2010).

[59] P. Krekora, Q. Su, and R. Grobe, "*Klein paradox with spin-resolved electrons and positrons*", Phys. Rev. A **72**, 064103 (2005).

[60] M. Fedoryuk, "*Encyclopedia of Mathematics; Chapter Saddle Point Method*", 1994.

[61] I. S. Gradshteyn and I. M. Ryzhik, *Table of integrals, series, and products*. Academic press, 2007.

[62] C. Rojas, "*Scattering of a scalar relativistic particle by the hyperbolic tangent potential*", Can. J. Phys. **93**, 85–88 (2015).

Measuring the traversal time of a tunnelled wave packet through a potential region leads to an apparent superluminal transmission. The reason behind this paradoxical result lies in the reshaping mechanism the particle experiences in the barrier, since no single trajectory has been taken by the wave packet through the potential.

Alternative definitions of the traversal time, as the Eisenbud-Wigner-Smith delay or the Larmor clock, are instructions of how to perform a measurement, which, in a quantum case, do not coincide. The use of relativistic scattering does not get rid of this apparent superluminal effect, and in fact introduces new strange results, as negative tunnelling times.

eman ta zabal zazu

del Universidad País Vasco

Euskal Herriko Unibertsitatea

EHU QC

EHU Quantum Center